Study of organic semiconductor / ferromagnet interfaces by spin-polarized electron scattering and photoemission

Fatima Zohra Djeghloul

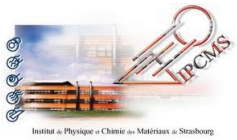

UNIVERSITE DE STRASBOURG

Institut De Physique et Chimie Des Matériaux De Strasbourg (IPCMS)

THÈSE DE DOCTORAT

presenté par

Fatima Zohra Djeghloul

pour obtenir le grade de

Docteur de l'université de Strasbourg

Domaine/Spécialité: **Sciences, Technologies, Santé/Physique**

Study of organic semiconductor/ferromagnet interfaces by spin-polarized electron scattering and photoemission

Soutenue publiquement le 26 Novembre 2013

Membres du Jury:

Directeur de Thése	:	Wolfgang Weber
Rapporteur Externe	:	Henri-Jean Drouhin
Rapporteur Externe	:	Markus Donath
Rapporteur Interne	:	Bernard Doudin

I dedicate this thesis to my mother
To who I owe being who I am,

"If we knew what it was we were doing, it would not be called research, would it?"
Albert Einstein

Résumé

L'électronique de spin utilisant des matériaux organiques est un domaine de recherche émergeant à l'interface entre la spintronique et l'électronique organique/moléculaire [1]. Ces matériaux possèdent un avantage majeur: les éléments légers (C, O, H, N) dont les molécules sont composées présentent une interaction spin-orbite très faible et mènent donc à des temps de relaxation de spin très longs.

Pour mieux comprendre le transport de spin à travers l'interface entre un film organique et un substrat ferromagnétique nous étudions le mouvement du spin d'électrons quand ils sont réfléchis par un film organique déposé sur une surface ferromagnétique. Notre expérience se distingue d'autres expériences utilisant des électrons polarisés en spin par le fait que la polarisation $\mathbf{P}_0$ des électrons incidents est perpendiculaire par rapport à l'aimantation $\mathbf{M}$ du matériau ferromagnétique [2,3]. C'est seulement dans cette configuration initiale non collinaire que le mouvement du spin peut être observé. Le mouvement du spin consiste en deux sous-mouvement, à savoir une précession d'un angle ε autour de l'aimantation $\mathbf{M}$ et une rotation d'un angle ϕ soit dans la direction parallèle à $\mathbf{M}$ soit antiparallèle à $\mathbf{M}$ (voir encart dans la Fig. 1).

Le principe de l'expérience est montré dans la Fig. 1. Un cristal de GaAs sert de source d'électrons polarisés en spin. Le faisceau polarisé frappe l'échantillon sous un angle de 45° par rapport à la normale de la surface. Les électrons réfléchis traversent ensuite une grille retardatrice qui ne laisse passer que des électrons élastiques. Ces électrons sont ensuite accélérés à une énergie de 100 keV pour la mesure de leur polarisation dans un détecteur de spin.

La Fig. 2 montre l'angle de précession ε en fonction de l'épaisseur de phthalocyanine (Pc) pour des électrons d'une énergie E-E_F = 9 eV. Trois différents régimes d'épaisseur peuvent être identifiés. Le premier régime s'étend de zéro à 0.2 monocouche (ML) où ε reste constante. Dans le deuxième régime, qui va de 0.2 à 0.6 ML, ε montre une très forte diminution. Finalement, epsilon s'annule pour des épaisseurs supérieures à 0.6 ML. Nous soulignons que ce comportement est vu avec des petites différences pour toutes les énergies étudiées (de 7 à 50 eV). On pourrait donc penser que cet effondrement du signal magnétique est du à une disparation du magnétisme dans le film de Co induite par la présence des molécules de Pc. Cependant, des mesures de la

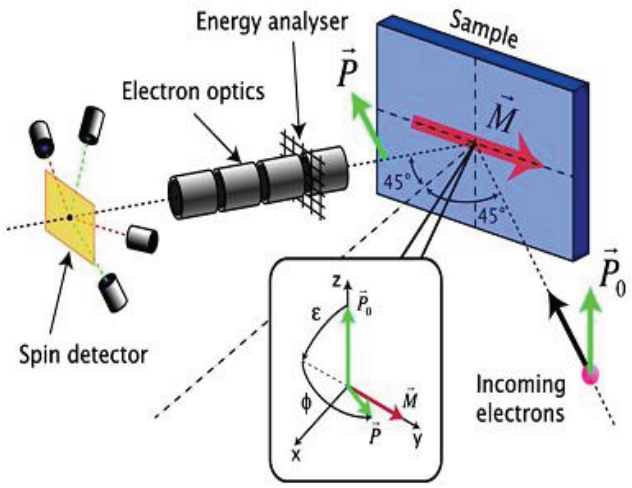

Figure 1: L'expérience consiste en une source d'électrons polarisés en spin, un échantillon qui est aimanté d'une façon rémanente, une grille retardatrice pour l'analyse d'énergie et un détecteur de spin. Les deux mouvements de spin, à savoir la précession d'angle ε et la rotation d'angle ϕ sont présentés dans l'encart.

polarisation de spin des électrons secondaires, effectués sur le même système, montrent clairement que l'aimantation n'est pas significativement modifiée par le film de Pc.

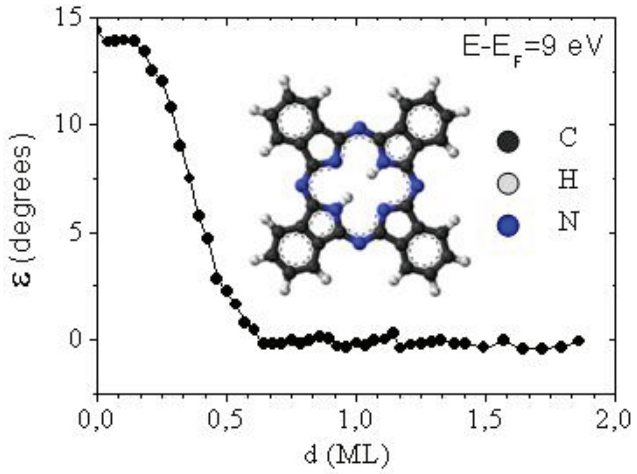

Figure 2: L'angle de précession ε en fonction de l'épaisseur de H_2Pc pour des électrons d'une énergie primaire de 9 eV. L'encart montre la molécule de H_2Pc.

Nos expériences sur les films de CoPc déposés sur un autre ferromagnétique, à savoir le Fe(001) ont montré que le choix du substrat ferromagnétique

n'a pas d'importance pour l'existence de cet effet. Ce qui est encore beaucoup plus étonnant est l'observation qu'on trouve le même type de comportement même si les molécules sont séparées du film de Co par une couche d'Au. Cela montre qu'une interaction directe des molécules avec le ferromagnétique n'a aucune importance pour l'observation de l'effet.

Dans le but de trouver la cause de cet effet, nous avons varié aussi le type de molécule organique. Dans un premier temps d'autres molécules de Pc ont été essayées (CoPc, FePc et MnPc). Quelque soit l'atome central de la molécule, le comportement est très similaire. Puis, Pc a été remplacé par d'autres molécules aromatiques telles que PTCDA et Coronene. Cependant, le même comportement global a pu être observé. Nous avons aussi essayé des molécules non-aromatiques telles que Pentacontane ($C_{50}H_{102}$) ainsi que des molécules sans hydrogène telles que C_{60}. Finalement, nous avons évaporé des atomes de carbone pour former une couche de graphite amorphe. Encore une fois, le même type de comportement est observé.

Pour le moment aucune idée sur l'origine de cet effet très surprenant des molécules organiques sur le mouvement du spin ne peut être présentée.

Dans ma deuxième partie de thèse, nous avons effectué des expériences de photoémission polarisée en spin à la ligne de lumière "Cassiopée" du synchrotron "Soleil" sur des films de MnPc et H_2Pc déposés sur une surface ferromagnétique de Co(001). Le but était d'étudier les propriétés polarisées en spin de l'interface entre le film organique et le substrat ferromagnétique.

Nous présentons dans la Fig. 3 les spectres pour les deux canaux de spin ainsi que la polarisation du spin P pour le système MnPc (xML)/Co(001) (x = 0, 1.3, 2.6, 3.9 et 5.2). On trouve que le dépôt de MnPc induit une modification importante de la polarisation de spin proche du niveau de Fermi. Dans la gamme d'énergie de liaison de 0.2-0.3 eV on remarque un changement de signe à cause du dépôt. Alors, nous déduisons que le dépôt de MnPc conduit non seulement à une suppression de la polarisation négative du Co, mais contribue également à une polarisation positive. La densité d'états sur les sites de Co étant plus importante que celle sur les sites de Mn, de N et de C, cette contribution positive de la polarisation due aux molécules doit être substantielle.

Pour obtenir le signal de photoémission qui vient seulement de l'interface organique/ferromagnétique nous avons dévéloppé une procédure particulière de soustraction, dont sa validité a été vérifiée. Figure 4 montre les spectres

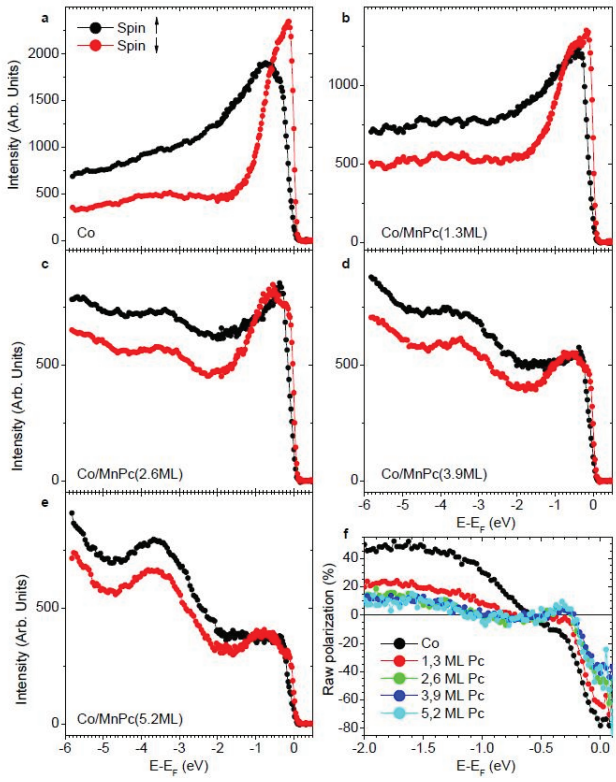

Figure 3: (a-e) Spectres de photoémission résolue en spin (spin up: symboles noirs, spin down: symboles rouges) du système MnPc/Co(001) pour cinq différentes épaisseurs de MnPc et (f) la polarisation de spin en fonction de l'énergie de liaison. L'énergie des photons est de 20 eV.

de différence obtenus à partir de cette procédure. De cette analyse, nous pouvons donc affirmer que la polarisation de spin à température ambiante à E_F des deux premières couches de MnPc adsorbés sur le Co(001) est très importantes et approche $+80\% \pm 10\%$. Nous notons que d'autres expériences du type photoémission résolue en spin sur des systèmes similaires ont été faites récemment par d'autres groupes [4, 5]. Alors que ces mesures montrent également l'existence des états induits par la présence des molécules de Pc, ces derniers ne possèdent que de très faible polarisation.

Afin de vèrifier ces résultats expérimentaux, des calculs théoriques sur des interfaces du type Pc/Co ont été effectués. Ces calculs ont montré l'existence des états d'interface polarisés en spin due à l'hybridation des bandes électroniques.

Une étude en fonction de l'énergie de photon nous renseigne sur deux as-

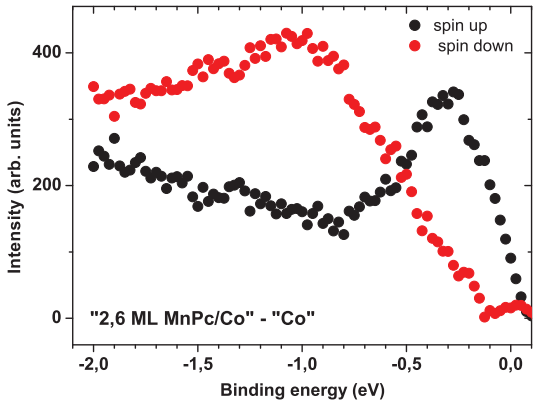

Figure 4: Spectres de différence. Les spectres du film de Co pur ont été soustraits des spectres du système 2.6 ML MnPc/Co(001) en utilisant un facteur approprié.

pects de ces états électroniques. Premièrement, ils ne montrent pas de dispersion de leur position d'énergie. Cela prouve qu'il s'agit des états d'interface, c.à.d. des états électroniques localisés à l'interface organique/ferromagnétique. Deuxièmement, une mesure en énergie de photon plus élevée (100 eV) montre que ces états d'interface sont majoritairement du caractère C ou N 2p.

Finalement, la comparaison des données obtenues avec MnPc et H_2Pc montre qu'il n'y a pas de différences significatives entre les spectres de différence résolus en spin. Cette observation prouve clairement que l'ion central Mn^{2+} dans la molécule MnPc ne joue pas un rôle important dans la formation des états d'interface polarisés en spin.

Acknowledgement

This thesis represents the work of nearly three years of my life, and as it is with most things, it would simply not have been possible without all the people around me, not even close. It is my great pleasure to express my special gratitude to the following people.

First of all, I would like to express my sincere gratitude to my supervisor Prof. Wolfgang Weber for giving me the opportunity to perform this challenging research in his group. I would like to thank him for many enlightening discussions, continuous encouragement and his kind guidance to achieve my thesis. However, I would specially like to thank him for treating me as a colleague and taking my ideas seriously, even at the beginning of my thesis when I barely knew what I was talking about half of the time (still the case occasionally). This gave me the confidence to keep trying out my own ideas.

I will take this opportunity to thank the members of the jury: Henri-Jean Drouhin, Markus Donath and Bernard Doudin who accepted to review this work. I want also to thank the director of the IPCMS who gave me the permission to perform this work at the IPCMS. I am also thankful to the members of the department DSI for their help in accomplishing this thesis. My sincere thanks go to "Le Ministère de l'enseignement Supérieur et de la Recherche Scientifique d'Algérie" (MESRS) for granting me the financial support, thus giving me the opportunity for achieving my thesis.

I am indebted to all the great professors in France and Algeria (especially at the University of Sétif) who helped me along my studies. I particulary mention Mustapha Maamache, Philippe Turek, Abdelkader Bourzami, Lahcene Krache, and Fatima Setifi.

It is difficult to overestimate my appreciation for my colleagues Dr. Ali Hallal and Dr. Puja Dey, who helped me very much in the electron-spin motion measurements and with them I had many fruitful discussions.

The experiments at synchrotron SOLEIL were supported by a number of persons. I am very grateful to Amina Taleb-Ibrahimi for providing me with a lot of helpful advice and to Patrick Lefèvre's efforts in teaching me the fundamental principles of photoemission spectroscopy and how to perform this type of experiment.

I am thankful to Martin Bowen, Samy Boukari, Fabrice Scheurer, Loïc Joly, Vincent Davesne, and Manuel Gruber for their cooperation during the

synchrotron experiments not only in the daytime but also at midnight and early in the morning, and for kindly helping me to enjoy my stay at SOLEIL.

I am very thankful for the fruitful collaboration we had with R. Bertacco and his coworkers from Milan, Italy, who performed the spin-resolved inverse photoemission experiments. I would like to acknowledge the technical support provided by Jacek Arabski (purification of molecules) and Bernard Muller (mechanical workshop). I also acknowledge all the help I have gotten from theorists here at the IPCMS and elsewhere, especially from Mébarek Alouani, Fatima Ibrahim, Saqib Javaid, and Ali Jaafar.

Thanks to all my office colleagues who provided a comfortable environment.

I owe special thanks to everyone of my friends for the good moments that we shared together: Mohamad Hamieh, Thibaut Berdot, Saber Gueddida, Ahmed Maghraoui, Ferdaous Ben Romdhane, Filip Schleicher, Hadeer El-Dakhakhni, Sara Mahiddine, Dorria Fatnassi, Amina Neggache, Hashim M. Jabbar, Assil Bouzid and Mohamad Assaad Mawass.

I would also like to thank my Algerian friends in Strasbourg and in Algeria. Life has been a great fun, thanks to Chams El-din Kihel, Sofian Tachi, Ilhem Ben Sehil, Rima Merkach, Rofia Mazaach, Lobna Arab, Riadh Bourzami, Khalif Benzid, Abdelmounaim Chetout, Youcef Messai, Farida Azouz, Tefaha Khberara, Bilal Allouche, Athmane Boulaouade, Fahim Tighemin, Mohamed Djouadi, Chamssou Belabed, Soumia Zaiou,Ahlem Khberara... I would like to thank my best friend Khlissa Merahi. Thanks for all of your support, and for lifting my spirits always.

I am thankful to my parents, my uncles and all my family. They have encouraged me nearly every day of my entire life and helped me through so many problems and challenges. I want to thank my mom for encouraging me, helping me stay organized, and always fighting for the best for me. Sometimes having an Algerian mother willing to go all the way for her children comes in handy. I want to thank my uncles Ferhat and Smaail Saadi for their confidence and supporting me all the time especially through the difficulties. I'd like to thank my grandparents for being always a wonderful, at least to me, intellectual model with great compassion and humanity, and an extraordinary mind. I'd also like to thank my sisters Houda and Nadjela. It is so nice to have you both as good friends now that we are finally grown up.

Last but not least, a deep thank from my heart to my husband Majed,

who stood next to me and supported me in the happy and sad moments and for everything he has done to help me get through the last 3 years. I'd like also to thank my family in-law for their help and interest.

Contents

List of Figures

Chapter 1

Introduction

Since its discovery by J.J. Thomson more than one hundred years ago, the electron has become fundamental to modern technology. There are two fields of technology at the moment which use the electron for their operation, conventional electronics and spintronics. While spintronics [6, 7] deals with the control and the manipulation of the spin of the electron, conventional electronics manipulates its charge by an electric field without taking into account the spin degree of freedom. So, spintronics is a promising field in the information technology because spintronics devices allow for the efficient control on the motion of electrons by acting on their spin through magnetic means. Most importantly, it has the advantage of high storage capacity, high integration density and increased processing speed over conventional electronic devices.

The first steps in spintronics were done thirty years ago with the discovery of the giant magnetoresistance (GMR). In 1986, Grünberg and coworkers reported the antiferromagnetic coupling of Fe in Fe/Cr/Fe trilayers [8], where magnetoresistance ratio was observed to be several % [9]. In 1988, Fert and coworkers discovered a magnetoresistance of $\approx 40\%$ by using antiferromagnetically coupled Fe/Cr multilayers [10]. Because of its enormous amplitude this magnetoresistance effect has been named "giant magnetoresistance (GMR)". These discoveries have been awarded with the physics Nobel prize in 2007. Similar GMR-effects have been observed later for many metallic systems, in which ferromagnetic layers are always separated by a nonmagnetic metallic spacer layer. Already in 1975 experiments were performed in which instead of the metallic spacer layers insulating layers were studied. In these magnetic tunnel junctions (MTJs) very significant tunneling magnetoresistance (TMR) values were discovered by Julliére [11]. Magnetic tunnel junctions regained interest only in 1995 by experiments with amorphous barrier materials performed by Moodera and coworkers [12] and Miyzaki and coworkers [13]. In 2004, MgO(001) single crystalline films were introduced in TMR devices as a tunneling barrier, which made possible the coherent spin tunneling in a

Fe/MgO/Fe system [14, 15]. Currently, experimental TMR values of about 600% at room temperature are obtained in Fe/MgO/Fe MTJs [16].

Since 1999, scientists are trying to marry spintronics with molecular electronics by replacing the inorganic spacer layers for instance in MTJs by organic layers. In fact, organic spintronics, when compared to its inorganic counterpart, offers many advantages. From the application point of view, organic materials open the way to cheap, low-weight, mechanically flexible, chemically interactive, and bottom-up fabricated electronics. Furthermore, more efficient and innovative devices may be produced due to the long spin coherence time and spin-flip length, thanks to the weak spin-orbit coupling for light elements such as hydrogen, carbon, and nitrogen. Model vertical magneto-resistive devices have been produced using ferromagnetic metals or half-metals [17] as ferromagnetic electrodes and evaporated small molecules as tunnel barriers. Typically a few 10% of tunnel magnetoresistance has been obtained at low temperatures and a few % at room temperature. These results show the interesting efficiency of spin transfer through organic materials.

1.1 Motivation and Outline

The objective of my work is to understand the electronic and magnetic interactions at the interface between an organic semiconductor and a ferromagnetic metal. In fact, the study of the spin properties of metal-organic interfaces has recently received considerable attention [1, 18–20] because of the prospect of developing a new generation of spin devices. From the fundamental point of view a lot of interesting physics takes place at the interface between ferromagnets and molecules [21, 22]. Effects ranging from ferromagnetic coupling between a molecule's transition metal site and the ferromagnet [20], to metallic [23], spin-polarized states induced on the molecule by the interface's chemical bonds [24] have been subsumed in a recent analysis by Sanvito *et al.* [25] as signatures of a spinterface that can craft spin-polarized transport [24, 26].

Despite these very promising features, however, a more complete understanding of the spinterface properties, in particular the spin transport through the molecular layer, needs the knowledge of (1) how incident spin-polarized electrons are influenced when interacting with the molecular layer and (2) the knowledge of the molecule-induced electronic band structure at the interface.

This is exactly the goal of the present study. The first point is treated by performing spin-polarized electron scattering experiments on very different spinterfaces, consisting of different ferromagnetic metals as well as of different organic layers. The second point is treated by performing spin-resolved photoemission spectroscopy measurements on several prototypical spinterfaces.

The thesis is divided into five chapters. Chapter 2 describes the different theoretical concepts necessary for an understanding of both the spin-polarized electron scattering experiments and the spin-resolved photoemission experiments. The experimental set-ups as well as the preparation and characterization of the studied samples are presented in chapter 3. Chapter 4 and 5 show the results and discussion of the spin-polarized electron scattering experiments and the spin-resolved photoemission experiments, respectively.

Part I

Theoretical concepts and experimental set-ups

Chapter 2

Spin and Electron-spin motion

Contents

2.1 The spin and its mathematical formulation

An electron with an orbital angular momentum $\boldsymbol{L}$ possesses a magnetic dipole moment $\boldsymbol{\mu}$ given by the relation:

$$\boldsymbol{\mu_L} = \frac{-e}{2m} g_L \boldsymbol{L} \tag{2.1}$$

where g_L the gyromagnetic ratio for the orbital motion is 1. Because of this magnetic moment an electron interacts with a magnetic field. So, it is expected that an electron with an orbital angular momentum equal to zero ($l = 0$) will not interact with a magnetic field. However, in 1922, Stern and Gerlach [27,28] conducted an experiment, whose results were quite unexpected. In this experiment, a beam of Ag atoms with vanishing orbital angular momentum passed through an inhomogeneous magnetic field. Because of the vanishing orbital angular momentum they did not expect any deviation of the Ag-beam. However, they found a separation of the Ag-beam into two beams after having passed the inhomogenous magnetic field region. In 1925, Goudsmit and Uhlenbeck [29] suggested that an electron has, in addition to its orbital angular

momentum $\boldsymbol{L}$, an additional intrinsic angular momentum $\boldsymbol{S}$ called spin. Supposing that the spin of an electron can take only two values, an explanation for the Stern-Gerlach experiment has been found.

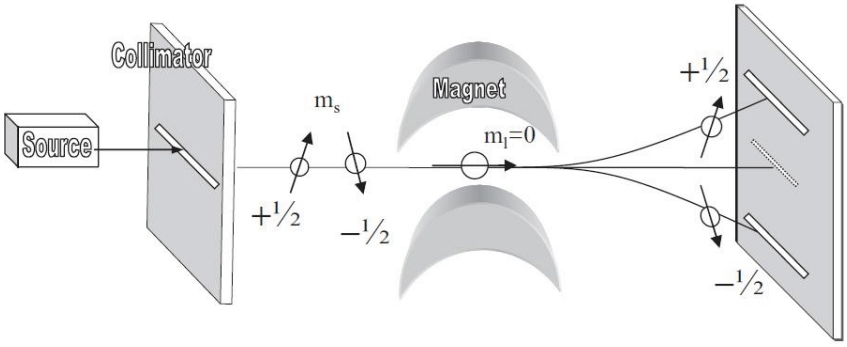

Figure 2.1: Schematics of the Stern-Gerlach experiment.

The spin is described by the operator $\boldsymbol{S}$, which has three components S_x, S_y and S_z. Similarly to the orbital angular momentum, they obey the same commutation relations [30]:

$$[S_i, S_j] = i\hbar\varepsilon_{ijk}S_k \tag{2.2}$$

where ε_{ijk} is the Levi-Civita symbol. It follows that the eigenvectors of S^2 and S_z are, respectively:

$$\boldsymbol{S^2}|s,m\rangle = \hbar^2 s(s+1)|s,m\rangle \tag{2.3}$$

$$\boldsymbol{S_z}|s,m\rangle = \hbar m|s,m\rangle \tag{2.4}$$

In the case of electrons the dimensionality of the spin space is 2. One can take as an orthonormal basis $|\uparrow\rangle, |\downarrow\rangle$ the common eigen-kets of $\boldsymbol{S^2}$ and $\boldsymbol{S_z}$ which verify the following conditions:

$$\begin{cases} \boldsymbol{S}^2|\uparrow\rangle = \frac{3}{4}\hbar^2|\uparrow\rangle \\ \boldsymbol{S}^2|\downarrow\rangle = \frac{3}{4}\hbar^2|\downarrow\rangle \\ \boldsymbol{S}_z|\uparrow\rangle = \frac{+1}{2}\hbar|\uparrow\rangle \\ \boldsymbol{S}_z|\downarrow\rangle = \frac{-1}{2}\hbar|\downarrow\rangle \end{cases} \tag{2.5}$$

with

$$\begin{cases} \langle\uparrow|\downarrow\rangle = 0 \\ \langle\uparrow|\uparrow\rangle = \langle\downarrow|\downarrow\rangle = 1 \end{cases} \tag{2.6}$$

The spinor basis states of a general spin wavefunction of a single electron are defined as follows:

$$\chi_\uparrow = |\uparrow\rangle = \begin{pmatrix} 1 \\ 0 \end{pmatrix} \tag{2.7}$$

$$\chi_\downarrow = |\downarrow\rangle = \begin{pmatrix} 0 \\ 1 \end{pmatrix} \tag{2.8}$$

The spin operator $\boldsymbol{S}$ can be defined by the Pauli matrices $\boldsymbol{\sigma} = \frac{2}{\hbar}\boldsymbol{S}$, which only affect the spin state:

$$\sigma_x = \begin{pmatrix} 0 & 1 \\ 1 & 0 \end{pmatrix}; \sigma_y = \begin{pmatrix} 0 & -i \\ i & 0 \end{pmatrix}; \sigma_z = \begin{pmatrix} 1 & 0 \\ 0 & -1 \end{pmatrix}. \tag{2.9}$$

2.2 Spin polarization

2.2.1 Pure spin state

An electron beam is said to be polarized if there exists a direction for which the two possible spin states are not equally populated. If all spins have the same direction, they are represented by a pure spin state. In such a case, the electron spin is described by a linear combination of the two basis spinors as follows:

$$\chi = a_1 \begin{pmatrix} 1 \\ 0 \end{pmatrix} + a_2 \begin{pmatrix} 0 \\ 1 \end{pmatrix} = \begin{pmatrix} a_1 \\ a_2 \end{pmatrix}. \tag{2.10}$$

By definition, we have $\chi^* = (a_1^*, a_2^*)$ and therefore $\chi^*\chi = a_1^* a_1 + a_2^* a_2$ with the normalization condition $\chi^*\chi = 1$. Taking the angles θ and φ as shown in Fig. 2.2, the spin function χ is specified by $a_1 = \cos\frac{\theta}{2}$ and $a_2 = \sin\frac{\theta}{2}e^{i\varphi}$. For more explanation we refer to the book by Kessler [31].

In order to see the physical significance of the angles θ and φ, we define the components of the polarization vector as the expectation values of the Pauli spin operators:

$$\boldsymbol{P} = \langle\boldsymbol{\sigma}\rangle = \langle\chi|\boldsymbol{\sigma}|\chi\rangle \tag{2.11}$$

Thus, the three dimensional polarization vector $\boldsymbol{P}$ is given by:

$$P_x = a_1^* a_2 + a_2^* a_1 = \sin\theta\cos\varphi \tag{2.12}$$

$$P_y = i(a_2^* a_1 - a_1^* a_2) = \sin\theta\sin\varphi \tag{2.13}$$

$$P_z = |a_1|^2 - |a_2|^2 = \cos\theta. \tag{2.14}$$

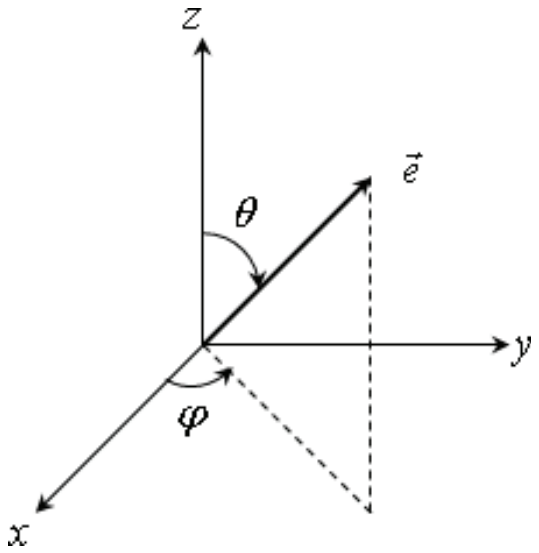

Figure 2.2: Spin direction.

From these equations we obtain the degree of polarization by:

$$P = \sqrt{P_x^2 + P_y^2 + P_z^2} \tag{2.15}$$

We generalize the definition of the polarization if the state $\chi = \begin{pmatrix} a_1 \\ a_2 \end{pmatrix}$ is not normalized by:

$$\boldsymbol{P} = \frac{\langle \chi | \boldsymbol{\sigma} | \chi \rangle}{\langle \chi | \chi \rangle}. \tag{2.16}$$

2.2.2 Partially polarized electron beam

Until now only pure spin states were considered, i.e. states for which there exists a defined direction of the spins. Now, let us consider a partially polarized electron beam which is a statistical mixture of spin states. In this case, the polarization of the total system is the average of the polarization vectors $\boldsymbol{P}^{(n)}$ of the individual systems which are in a pure spin state $\chi^{(n)}$:

$$\boldsymbol{P} = \sum_n w^{(n)} \boldsymbol{P}^{(n)} = \sum_n \omega^{(n)} \frac{\langle \chi^{(n)} | \boldsymbol{\sigma} | \chi^{(n)} \rangle}{\langle \chi^{(n)} | \chi^{(n)} \rangle}, \tag{2.17}$$

where the factors $\omega^{(n)}$ take into account the relative weight of the states $\chi^{(n)}$:

$$\omega^{(n)} = \frac{N^{(n)}}{\sum_n N^{(n)}} \tag{2.18}$$

with $N^{(n)}$ the number of electrons in the state $\chi^{(n)}$.

To simplify the polarization vector in equation 2.17, we choose the direction of the polarization vector to be along the z-direction. In this case the polarization is given by $P = \frac{N_\uparrow - N_\downarrow}{N_\uparrow + N_\downarrow}$, where $N_\uparrow$ and $N_\downarrow$ are the number of electrons having a spin value of $\hbar/2$ and $-\hbar/2$, respectively.

An electron beam with an arbitrary polarization can therefore be considered to be made up of a totally polarized fraction and an unpolarized fraction which are mixed in the ratio $P/(1-P)$.

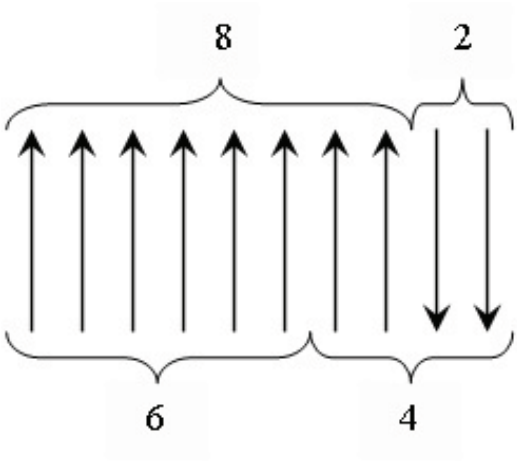

Figure 2.3: Partially polarized beam.

Let us for example consider an ensemble of 100 electrons, that has 80 electrons with spin in the z-direction and 20 electrons with a spin in the -z-direction. With $N_\uparrow = 80$ and $N_\downarrow = 20$ we have:

$$P = \frac{N_\uparrow - N_\downarrow}{N_\uparrow + N_\downarrow} = \frac{80 - 20}{80 + 20} = 0.6 = 60\% \tag{2.19}$$

This case can also be expressed by saying that 60% of the beam is totally polarized and 40% is unpolarized (see Fig. 2.3).

2.3 Electron-spin motion

In the following the spin polarization vector $\mathbf{P}_0$ of the incident electrons is perpendicularly oriented with respect to the magnetization $\mathbf{M}$ of the ferromagnetic film. We note that in the following the direction of $\mathbf{M}$ is defined

to be that of the majority-spin electrons. For simplicity, we consider in this chapter a completely polarized electron beam, i.e. $P_0 = 1$.

In the particular spin configuration, which we consider here, the spin is a coherent superposition of a majority-spin and a minority-spin state. If $\mathbf{P}_0$ is along the x-axis and $\mathbf{M}$ along the z-axis, these two spin states are represented by a (1,0) and a (0,1) spinor, respectively, and the initial spin configuration reads:

$$\chi_0 \sim \begin{pmatrix} 1 \\ 0 \end{pmatrix} + \begin{pmatrix} 0 \\ 1 \end{pmatrix}.$$

The two partial waves have an arbitrary but identical phase prior to reflection at the surface of the ferromagnetic material. However, since the reflection process depends on the spin, the amplitudes of the two spin wave functions are different after reflection, and the total spin wave function will be:

$$\chi \sim |r^{\uparrow}|e^{i\theta^{\uparrow}} \begin{pmatrix} 1 \\ 0 \end{pmatrix} + |r^{\downarrow}|e^{i\theta^{\downarrow}} \begin{pmatrix} 0 \\ 1 \end{pmatrix}$$

with $|r^{\uparrow,\downarrow}|$ the module of the spin-dependent reflection amplitudes and $\theta^{\uparrow,\downarrow}$ the corresponding reflection phases.

The expectation values of the Pauli matrices yield the spin polarization vector $\mathbf{P}$ of the electron beam after reflection:

$$\mathbf{P} = \frac{<\chi|\sigma|\chi>}{<\chi|\chi>} = \begin{pmatrix} |r^{\uparrow}||r^{\downarrow}|\cos\left(\theta^{\downarrow} - \theta^{\uparrow}\right) \\ |r^{\uparrow}||r^{\downarrow}|\sin\left(\theta^{\downarrow} - \theta^{\uparrow}\right) \\ \left(|r^{\uparrow}|^2 - |r^{\downarrow}|^2\right)\left(|r^{\uparrow}|^2 + |r^{\downarrow}|^2\right)^{-1} \end{pmatrix}.$$

By introducing the intensity asymmetry

$$A = \frac{|r^{\uparrow}|^2 - |r^{\downarrow}|^2}{|r^{\uparrow}|^2 + |r^{\downarrow}|^2}$$

and the angle

$$\varepsilon = \theta^{\downarrow} - \theta^{\uparrow}$$

the spin polarization vector becomes:

$$\mathbf{P} = \begin{pmatrix} \sqrt{1 - A^2}\cos\varepsilon \\ \sqrt{1 - A^2}\sin\varepsilon \\ A \end{pmatrix}.$$

This corresponds to a precession of the polarization vector around the magnetization direction by an angle ε and simultaneously a rotation by an angle ϕ in the plane spanned by **P** and **M** (see Fig. 2.4):

$$\phi = \arctan\left(\frac{A}{\sqrt{1-A^2}}\right).$$

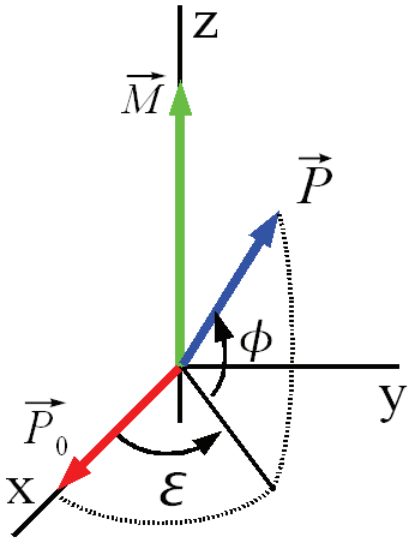

Figure 2.4: Illustration of the two types of motion of the spin-polarization vector. The initial spin polarization $\mathbf{P}_0$ precesses around the magnetization **M** by an angle ε and rotates simultaneously in the plane **P-M** by an angle ϕ.

2.4 Fundamentals of photoemission

Photoemission spectroscopy (PES) is used to investigate the occupied electronic band structure in solids [32, 33]. This method is based on the photoeffect, which was discovered by Hertz and Hallwachs in 1887 and explained 1905 by Einstein by introducing the concept of the photon.

For the interpretation of the photoemission process which is sketched in Fig. 2.5, a phenomenological model called the three-step model is often used [34]. In this model, the photoemission process is divided into three distinct and independent steps:

1. Optical excitation of the electron in the bulk.

2. Travel of the excited electron to the surface.

3. Escape of the photoelectron into vacuum.

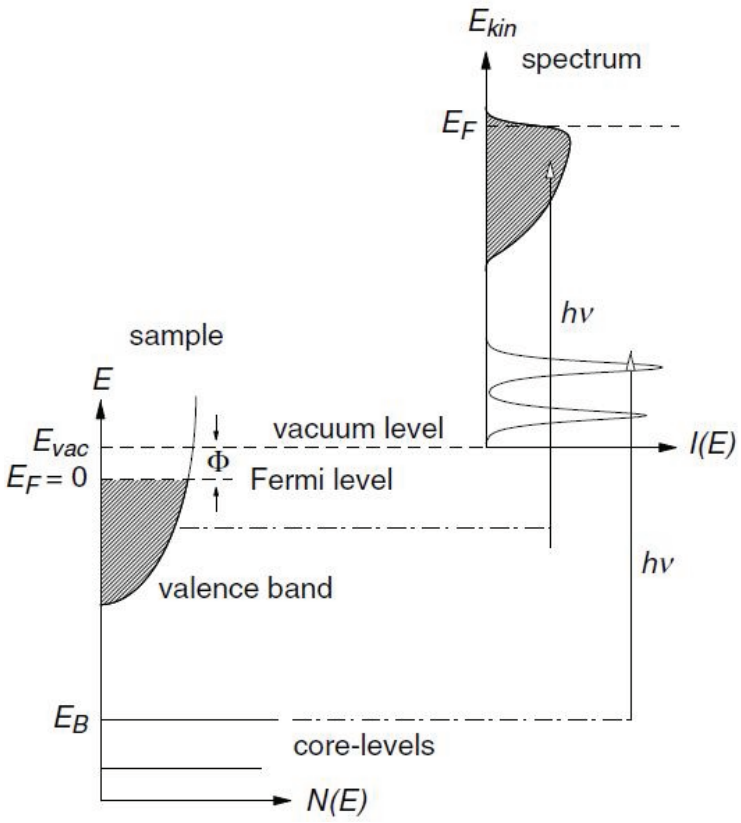

Figure 2.5: Schematic diagram of the principle of photoemission spectroscopy. It shows the relation between the energy levels in a solid and the energy distribution of the emitted electrons produced by photons of energy $h\upsilon$.

In the first step, photoionization takes place, i.e. an electron occupying an initial electronic state is excited into an unoccupied final state through absorption of a photon. The second step can be described in terms of an effective mean free path which is proportional to the probability that the excited electron will reach the surface without scattering. Finally, the electron overcomes the work function and escapes through the surface into the vacuum where it is detected. Within this last process, the momentum perpendicular to the surface is not conserved, and the electron is refracted in a similar manner to that of light at the interface between two materials. The parallel component of the momentum, however, is still conserved (analogous to Snell's law for

light). The consideration of energy conservation [28] leads to an expression for the kinetic energy E_{kin} of the photoemitted electron:

$$E_{kin} = h\upsilon - \Phi - E_B \tag{2.20}$$

where E_{kin} is measured with respect to the vacuum level E_{vac}, Φ is the work function of the sample, and E_B is the binding energy relative to the Fermi level E_F.

Because of the conservation of the parallel momentum [35] one can write:

$$k_{//} = \sqrt{\frac{2m}{\hbar^2} E_{kin}} \cdot \sin\vartheta \tag{2.21}$$

where $k_{//}$ is the parallel wave vector of the initial state and ϑ is the polar emission angle (see Fig. 2.6). E_{kin}, Φ and ϑ can all be measured directly from the experiment. Therefore, the energy and the in-plane wave vector of the electronic state before photoemission can be determined from eqs (2.20) and (2.21).

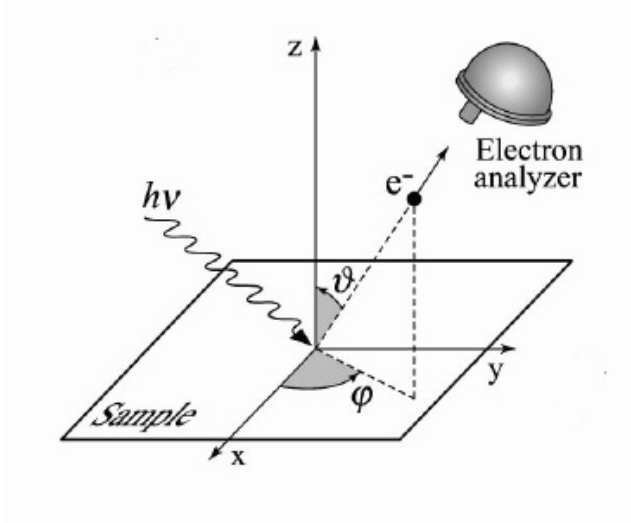

Figure 2.6: Geometry of an PES experiment in which the emission direction of the photoelectron is specified by the polar angle ϑ and the azimuthal angle φ.

According to Fermi's golden rule, the transition probability w_{fi} for an optical excitation between the N-electron ground state Ψ_i^N and the possible final states Ψ_f^N is given by [36]:

$$w_{fi} \propto |\langle \Psi_f^N | \boldsymbol{A} \cdot \boldsymbol{p} | \Psi_i^N \rangle|^2 \delta(E_f^N - E_i^N - h\upsilon) \tag{2.22}$$

where E_i^N and E_f^N are the initial- and final-state energies of the N-particle system, respectively. The term $\boldsymbol{A} \cdot \boldsymbol{p}$ is called the direct transition term which takes into account the interaction between the photon and the electron, where $\boldsymbol{p}$ is the electron momentum operator and $\boldsymbol{A}$ the electromagnetic vector potential.

The equation 2.22 simplifies within the sudden approximation, which assumes that the electron is instantaneously removed by photoexcitation. In this case, the wave function of the final state can be written as:

$$\Psi_f^N \sim \phi_f^k \Psi_f^{N-1} \tag{2.23}$$

where ϕ_f^k is the wave function of the photoelectron and Ψ_f^{N-1} is the final state wave function of the $(N-1)$ electrons left behind, which can be chosen as an excited state with eigenfunction Ψ_s^{N-1} and energy E_s^{N-1}. The total transition probability is then given by the sum over all possible excited states s. By using the same notation, the initial state Ψ_i^N can also be factorized into a one-electron wavefunction ϕ_i^k and a Ψ_i^{N-1}-electron wavefunction of the remaining $(N-1)$ electrons:

$$\Psi_i^N \sim \phi_i^k \Psi_i^{N-1} \tag{2.24}$$

To calculate the total photoemission intensity I we use the relation $I = \sum_{f,i} w_{fi}$ and the equations (2.24, 2.23). We thus obtain [37]:

$$I \propto \sum_{f,i} |M_{f,i}|^2 \sum_s |C_{s,i}|^2 \delta(E_{kin} + E_s^{N-1} - E_i^N - h\upsilon) \tag{2.25}$$

with $|C_{s,i}|^2 = |\langle \Psi_s^{N-1} | \Psi_i^{N-1} \rangle|^2$ and $M_{f,i} = \langle \Phi_f^k | \boldsymbol{A} \cdot \boldsymbol{p} | \Phi_i^k \rangle$. We used here Ψ_s^{N-1} instead of Ψ_f^{N-1} because this term takes into account all the possible excited states, as discussed above. Finally, it should be mentioned that a more complete description of the photoemission process can be obtained within the Green function formalism (see reviews [37, 38] for more information).

Chapter 3

Experimental techniques, sample preparation and characterization

Contents

3.1 Spin-motion experiments

In order to investigate the spin motion of electrons upon reflection from a ferromagnet, a spin-polarized electron scattering experiment in ultra-high vacuum has been set up. It is schematically shown in Fig. 3.1. A free spin-polarized electron beam is produced by optically pumping of GaAs with circularly polarized light. The electron beam impinges on a ferromagnetic film at an angle of 45° with respect to the sample surface. The electrons elastically reflected at 45° and after having traversed a retardation grid for energy analysis are accelerated to an energy of 100 keV to measure their spin polarization by a spin detector.

In the following I will describe the two essential components of the experimental set-up, namely the spin-polarized electron source and the spin detector.

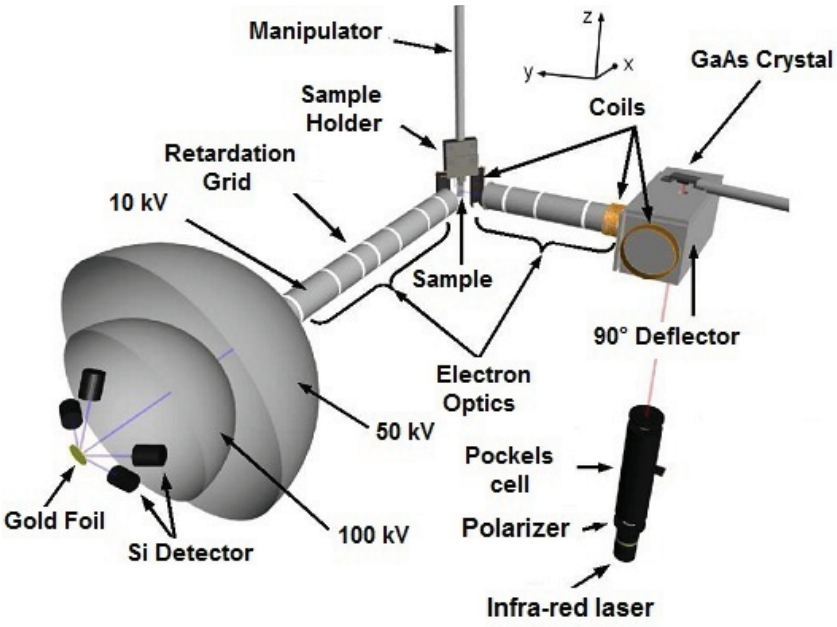

Figure 3.1: Schematics of the experiment. This figure does not show the source chamber or the means of evaporation and characterization within the main chamber.

A detailed description of the other parts of the experimental set-up can be found in [39, 40]

3.1.1 Spin-polarized electron source

As spin-polarized electron source a GaAs crystal is used. GaAs is a direct band gap semiconductor with a minimum band separation of 1.52 eV at room temperature near the center of the Brillouin zone as shown in Fig. 3.2(a) [41, 42]. Due to spin-orbit interaction the valence band is divided into a four-fold degenerated $P_{\frac{3}{2}}$-level and a two-fold degenerated $P_{\frac{1}{2}}$-level, which have a separation of $\triangle = 0.34$ eV. The four-fold degenerated $P_{\frac{3}{2}}$-level contains two "heavy hole (hh)" levels with $m_j = \pm\frac{3}{2}$ and two "light hole (lh)" levels with $m_j = \pm\frac{1}{2}$. The electrons of the conduction band are in the state $4S_{\frac{1}{2}}$ which is two-fold degenerated. The selection rules for photoemission ($\triangle l = \pm 1, \triangle m = \pm 1, 0$) allow both the electronic transition from $4P_{\frac{3}{2}}$ states to $4S_{\frac{1}{2}}$ states and from $4P_{\frac{1}{2}}$ states to $4S_{\frac{1}{2}}$ states.

In order to produce a polarized electron beam, the GaAs has first to be activated. The activation consists in a deposition of Cs and oxygen onto

the GaAs crystal. In this way the work function of the GaAs surface can be significantly lowered such that electrons, which are optically excited into the conduction band can leave the crystal. The details of this activation procedure are described in [42,43]. In a second step we send onto the activated GaAs crystal a beam of right circularly polarized light ($+\sigma$) (photons have a magnetic moment $m = +1$, solid line in Fig. 3.2(b)). The only allowed transitions between the states of the valence band and those of the conduction band are then:

$$\begin{cases} 4P_{\frac{3}{2}}\left(m_j = \frac{-3}{2}\right) \rightarrow 4S_{\frac{1}{2}}\left(m_j = \frac{-1}{2}\right) \\ 4P_{\frac{3}{2}}\left(m_j = \frac{-1}{2}\right) \rightarrow 4S_{\frac{1}{2}}\left(m_j = \frac{+1}{2}\right) \end{cases} \tag{3.1}$$

For left circularly polarized light ($-\sigma$) (photons have a magnetic moment $m = -1$, dotted line in Fig. 3.2(b)) the only allowed transitions are:

$$\begin{cases} 4P_{\frac{3}{2}}\left(m_j = \frac{+3}{2}\right) \rightarrow 4S_{\frac{1}{2}}\left(m_j = \frac{+1}{2}\right) \\ 4P_{\frac{3}{2}}\left(m_j = \frac{+1}{2}\right) \rightarrow 4S_{\frac{1}{2}}\left(m_j = \frac{-1}{2}\right) \end{cases} \tag{3.2}$$

The transition probabilities related to the levels can be calculated from the wave functions of the initial and final states and are indicated in circles in Fig. 3.2(b). With a light energy of 1.42 eV, i.e. avoiding the excitation of electrons in the state $P_{1/2}$, the degree of polarization is found to be $P = (3-1)/(3+1) = 50\%$. Experimentally, one reaches approximately a polarization of 25%. This is explained by the strong diffusion of the excited electrons before being ejected into the vacuum. As these diffusion processes are in general not spin conserving, the polarization of the emitted electrons is smaller. By switching from right-to left-circularly polarized light for the photoexcitation of the spin-polarized electrons, the direction of the initial spin polarization can be inverted.

The emitted electrons from the GaAs source will traverse an electron optics (see Fig. 3.1) which consists essentially of electrostatic elements. In this way the trajectory of the electrons can be changed without changing the direction of the electron spin. The first part consists of a Herzog plate (E_p) accelerating the electrons from the surface of the GaAs crystal to the 90°-deflector (K_i and K_a). It provides a polarization perpendicular to the magnetization of the sample. At the deflector end, electrons are focused onto the sample with the aid of three electrostatic lenses (L1, L2 and L3). Finally, the electron beam has a diameter of about 1 mm when it reaches the surface of the sample. Coils are placed around the electron optics to compensate the influence of the

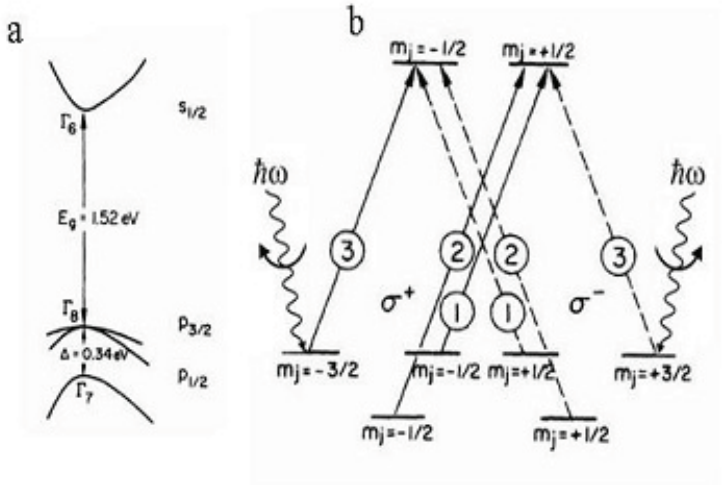

Figure 3.2: Spin-polarized photoemission from GaAs. (a) The energy bands of GaAs at the center of the Brillouin zone showing the band gap energy E_g and the spin-orbit splitting of the valence bands $\triangle$. (b) The allowed transitions between m_j sublevels for circularly polarized light σ^+ (solid line) and σ^- (dotted line), with relative transition probabilities given by the numbers in circles [41].

Earth's magnetic field on the spin polarization direction. So, by applying a combination of electric and magnetic fields to the electron beam, the initial spin polarization P_0 can be rotated into any desired space direction. An unpolarized electron beam as well can be produced by applying linearly polarized light.

3.1.2 Spin detector

The spin detectors which are used in our spin-motion set-up as well as in the spin-resolved photoemission set-up, which is described later, are based on the so-called Mott scattering. What is Mott scattering? Let us consider an electron beam of fairly high energy (100 keV for the detector used in the spin-motion experiments and 30 keV for that of the photoemission experiments), which will be scattered by a thin foil consisting of a heavy metal such as Au, i.e. the target material shows a strong spin-orbit interaction. When an electron is scattered by a Au atom two interactions have to be considered, the Coulomb interaction V_C, which is independent of the electron spin, and the spin-orbit interaction $V_{so} \propto \boldsymbol{L}\cdot\boldsymbol{S}$ with $\boldsymbol{L}$ and $\boldsymbol{S}$ the orbital and the spin angular momentum vector of the scattered electron, respectively. Let us suppose that

the spin is perpendicular to the scattering plane. In this case the scattering of an electron to the right has not the same probability as the scattering to the left. This becomes clear when we consider the orientation of $\boldsymbol{L}$ in these two cases. In fact, they are opposed to each other such that the scalar product $\boldsymbol{L}\cdot\boldsymbol{S}$ and thus the spin-orbit interaction changes sign. Consequently, the total scattering amplitude, being determined by the sum $V_C + V_{so}$ (see Fig. 3.3), and thus the probability for a scattering to the right will be different from a scattering to the left.

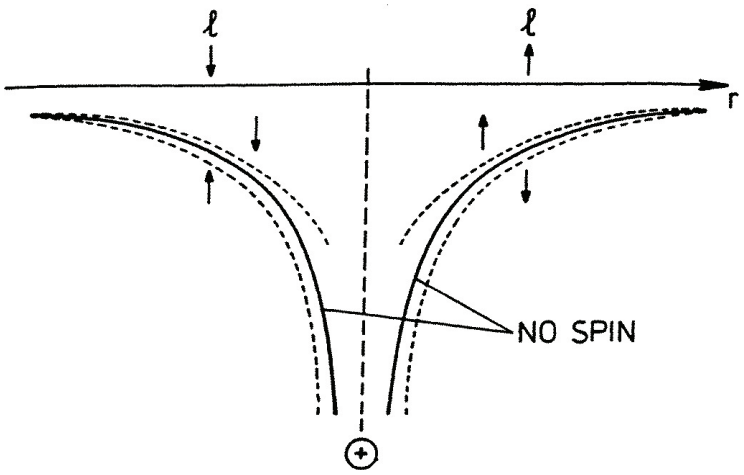

Figure 3.3: Spin-dependent scattering from a gold foil arising due to spin-orbit interaction. Potential curves with (dashed) and without (solid) spin-orbit interaction are shown [31].

We thus obtain a left-right scattering asymmetry:

$$A = \frac{N_r - N_l}{N_r + N_l} \tag{3.3}$$

with N_r and N_l the number of electrons scattered to the right and to the left, respectively. This asymmetry is proportional to the spin polarization of the electron beam normal to the scattering plane P_n. With a proportionality constant S_{eff} called the effective Sherman factor we get:

$$A = S_{eff} P_n. \tag{3.4}$$

In our spin detectors we place two detectors at exactly the same scattering angle of 120° to the right and to left of the Au target to count the number of the scattered electrons. The two detectors to the left and to the right are placed in the horizontal plane, so that they give us only the vertical component

of the polarization. By placing two detectors in the vertical plane in the same way, we can measure the horizontal component of the polarization. In any experiment, however, there is always an artificial asymmetry due to the fact that the detectors are not identical (different efficiencies) and that the electron beam might be misaligned. In order to eliminate this artificial asymmetry, we measure not only the scattered intensities when the incident polarization is $\boldsymbol{P}$ but also when it is $-\boldsymbol{P}$. For a polarization $\boldsymbol{P}$ (indicated by $\uparrow$) we have

$$N_l^{\uparrow} = nNE_l\Omega_l I[1 + P_n S_{eff}] \tag{3.5}$$

$$N_r^{\uparrow} = nNE_r\Omega_r I[1 - P_n S_{eff}] \tag{3.6}$$

with n the number of incident electrons, N the number of Au atoms per unit area, $\Omega_{l,r}$ and $E_{l,r}$ the solid angles and the detector efficiencies for the left and right detector, respectively, and I the differential cross section.

For a polarization $-\boldsymbol{P}$ (indicated by $\downarrow$) we have:

$$N_l^{\downarrow} = n^{'}N^{'}E_l\Omega_l I[1 - P_n S_{eff}] \tag{3.7}$$

$$N_r^{\downarrow} = n^{'}N^{'}E_r\Omega_r I[1 + P_n S_{eff}] \tag{3.8}$$

where the primes indicate that the number of incident electrons and the effective target thickness can be different. We now obtain the intensities N_l and N_r in the following way:

$$N_r = \sqrt{N_r^{\uparrow}N_l^{\downarrow}} = \sqrt{nn'NN'E_lE_r\Omega_l\Omega_r}I[1 - P_n S_{eff}] \tag{3.9}$$

$$N_l = \sqrt{N_r^{\downarrow}N_l^{\uparrow}} = \sqrt{nn'NN'E_lE_r\Omega_l\Omega_r}I[1 + P_n S_{eff}] \tag{3.10}$$

By putting these expressions for N_l and N_r into the above asymmetry expression we obtain an asymmetry which does not include anymore any artificial asymmetry coming from different detector efficiencies and/or a misalignment of the incident electron beam.

We note that the spin detector for our spin-motion experiments is sensitive only to the components P_x and P_z of the polarization vector. That is the reason why later only these components will be discussed and exploited. From the previous discussion the component P_x is given by:

$$P_x = \frac{1}{S_{eff}} \frac{\sqrt{N_l^{\uparrow}N_r^{\downarrow}} - \sqrt{N_l^{\downarrow}N_r^{\uparrow}}}{\sqrt{N_l^{\uparrow}N_r^{\downarrow}} + \sqrt{N_l^{\downarrow}N_r^{\uparrow}}} \tag{3.11}$$

To get the component P_z, we must measure the intensities in the "top" (t) and "bottom" (b) detectors:

$$P_z = \frac{1}{S_{eff}} \frac{\sqrt{N_t^{\uparrow} N_b^{\downarrow}} - \sqrt{N_t^{\downarrow} N_b^{\uparrow}}}{\sqrt{N_t^{\uparrow} N_b^{\downarrow}} + \sqrt{N_t^{\downarrow} N_b^{\uparrow}}} \tag{3.12}$$

Now, we consider the configuration of our experiment, which corresponds to an electron beam polarized along the x-axis, initially propagating along the z-direction, and a magnetization which is in the (yz)-plane at an angle of 45° with respect to the (xz)-plane. We use the following convention for the vector polarization obtained in the configuration $(\boldsymbol{M\sigma})$: $\boldsymbol{P}(\boldsymbol{M\sigma})$ where $M = +$ if the magnetization is in the direction defined in Figure 3.4, and $\sigma = +$ if the polarization vector is in the x-direction.

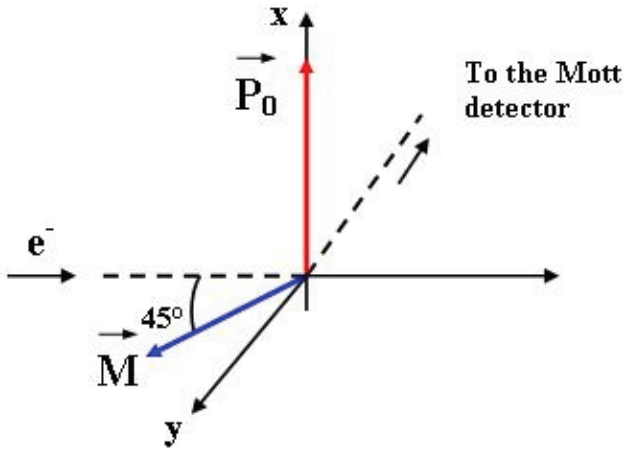

Figure 3.4: Configuration of the initial polarization $\boldsymbol{P_0}$ and $\boldsymbol{M}$ the magnetization in our experiment.

For the configuration $(M\sigma) = (++)$ we get:

$$\boldsymbol{P}(++) = \begin{cases} P_0\sqrt{1-A^2}\cos\varepsilon \\ \frac{1}{\sqrt{2}}(A + P_0\sqrt{1-A^2}\sin\varepsilon) \\ \frac{1}{\sqrt{2}}(A - P_0\sqrt{1-A^2}\sin\varepsilon) \end{cases} \tag{3.13}$$

After reversing only the direction of the initial spin polarization we get:

$$\boldsymbol{P}(+-) = \begin{cases} -P_0\sqrt{1-A^2}\cos\varepsilon \\ \frac{1}{\sqrt{2}}(A - P_0\sqrt{1-A^2}\sin\varepsilon) \\ \frac{1}{\sqrt{2}}(A + P_0\sqrt{1-A^2}\sin\varepsilon) \end{cases} \tag{3.14}$$

After reversing only the direction of the magnetization we get:

$$\boldsymbol{P}(-+) = \begin{cases} +P_0\sqrt{1-A^2}\cos\varepsilon \\ \frac{1}{\sqrt{2}}(-A - P_0\sqrt{1-A^2}\sin\varepsilon) \\ \frac{1}{\sqrt{2}}(-A + P_0\sqrt{1-A^2}\sin\varepsilon) \end{cases} \tag{3.15}$$

After reversing both the direction of the initial polarization and of the magnetization one obtains:

$$\boldsymbol{P}(--) = \begin{cases} -P_0\sqrt{1-A^2}\cos\varepsilon \\ \frac{1}{\sqrt{2}}(-A + P_0\sqrt{1-A^2}\sin\varepsilon) \\ \frac{1}{\sqrt{2}}(-A - P_0\sqrt{1-A^2}\sin\varepsilon) \end{cases} \tag{3.16}$$

By taking the equations 3.11, 3.12 and other identifications which are discussed in detail by Logan Tati-Bismaths in his thesis [40], we are able to write the expression of the polarization $P_x^{(1),(2)}$ and $P_z^{(1),(2)}$, where (1) and (2) designate one of the four configurations $(\pm M, \pm\sigma)$:

$$P_x^{(1),(2)} = \frac{1}{S_{eff}} \frac{\sqrt{N_l^{(1)} N_r^{(2)}} - \sqrt{N_l^{(2)} N_r^{(1)}}}{\sqrt{N_l^{(1)} N_r^{(2)}} + \sqrt{N_l^{(2)} N_r^{(1)}}} \tag{3.17}$$

$$P_z^{(1),(2)} = \frac{1}{S_{eff}} \frac{\sqrt{N_t^{(1)} N_b^{(2)}} - \sqrt{N_t^{(2)} N_b^{(1)}}}{\sqrt{N_t^{(1)} N_b^{(2)}} + \sqrt{N_t^{(2)} N_b^{(1)}}} \tag{3.18}$$

From these equations we are able to find the asymmetry, the initial polarization P_0 and the precession angle ε by using the combination of different polarizations:

$$A = \frac{1}{\sqrt{2}}(P_z^{(--),(+-)} + P_z^{(-+),(++)}) \tag{3.19}$$

$$P_0 = \sqrt{\frac{\frac{1}{4}(P_x^{(++),(--)} + P_x^{(-+),(+-)}) + \frac{1}{2}(P_z^{(-+),(++)} - P_z^{(--),(+-)})}{1 - A^2}} \tag{3.20}$$

$$\varepsilon = \sin^{-1}\left(\frac{\frac{1}{\sqrt{2}}(P_z^{(-+),(++)} - P_z^{(--),(+-)})}{P_0\sqrt{1-A^2}}\right) \tag{3.21}$$

3.2 The spin-resolved photoemission experiment

The photoemission experiments have been performed at the synchrotron SOLEIL in Paris. Using synchrotron radiation offers the possibility of covering a wide spectral range, from the visible to the x-ray region, with an intense and highly polarized continuous spectrum. In addition, there are other important advantages such as variable polarization, high brightness, and small photon spots.

The measurements were carried out in an ultra-high vacuum system by using a hemispherical energy analyzer. Figure 3.5 shows the generic configuration of a spin-resolved photoemission experiment. A high-intensity photon beam is produced by an undulator which is located in the storage ring. This beam is monochromatized by a grating monochromator at a desired energy, and then it is focused onto the sample.

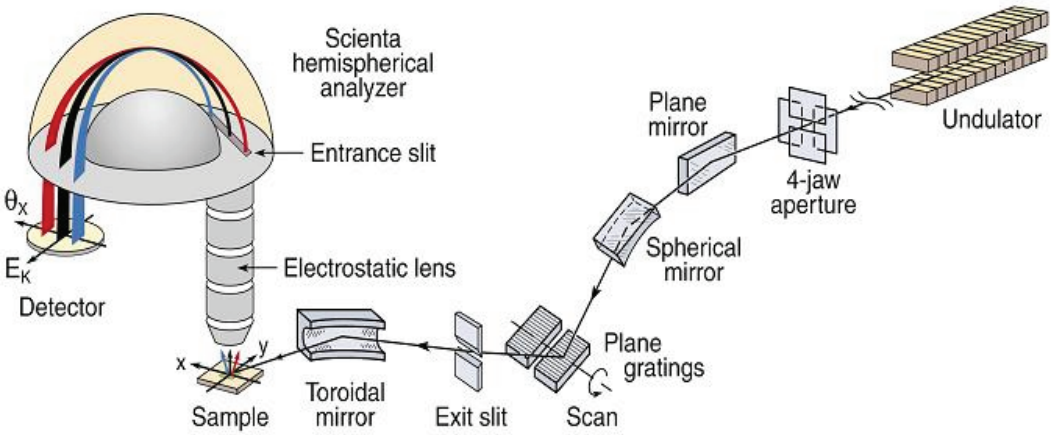

Figure 3.5: Generic beamline equipped with a plane grating monochromator and a Scienta electron spectrometer.

The photoemitted electrons are then collected in normal emission by the energy analyzer, where the kinetic energy of the electrons is determined. We note here, that the hemispherical analyzer is the most commonly used instrument in PES at the present time.

As electron detectors channeltrons are mostly used. However, to improve the detection efficiency a multi-channel detection system with a micro-channel plate (MCP) instead of a single channeltron is used. In this system each

channel detects electrons with different pass energies. Our spin-resolved photoemission experiments were undertaken at the Cassiopee beamline. This experiment is equipped with a Scienta SES2002 electron analyzer which uses a MCP as detector. But the analyzer used in our experiment was modified by the Scienta company to include a Mott spin detector for spin analysis. A part of the electron beam is sent to the classical Scienta 2D detector, while the rest enters the spin detector through a transfer optics. The angular acceptance of the analyzer is about $\pm 8°$.

3.3 Samples

3.3.1 For the electron-spin motion experiments

In the first step of the sample preparation different ferromagnetic films (Co and Fe) have been deposited on different single crystalline substrates (Cu(001), Ag(001), and Pt(001)) at room temperature from a rod heated by electron beam bombardment. Prior to deposition, the single crystalline substrate was cleaned by several cycles of Ar-ion sputtering and annealing at 800 K. The film systems Co/Cu(001) and Fe/Ag(001) have been extensively investigated in the past (see for instance Refs. [44–47] for Co/Cu(001) and Refs. [48–52] for Fe/Ag(001)). For the film system Fe/Pt(001), on the other hand, there have been only few studies [53].

While Co films on Cu(001) are in-plane magnetized for all thicknesses Fe films on Ag(001) and on Pt(001) exhibit an reorientation transition of the magnetization from out-of-plane to in-plane for thicknesses of 4 ML [54] and 2.2 ML [53], respectively. In all cases films of 15 ML thickness are deposited such that the magnetization of all ferromagnetic films lies in-plane.

In the second step of the sample preparation we deposit different organic molecules or amorphous carbon onto the ferromagnetic film at room temperature. The organic molecules are evaporated by radiative heating while carbon films are evaporated by electron beam bombardment and the evaporation rate is controlled by a quartz microbalance. In the electron scattering experiments the molecular or carbon films are grown as follows: at a typical growth rate of 1 ML/10 min we make a deposition during 15 s. This is followed by a measurement that takes several minutes. Then, the procedure is repeated. As a result, the effective deposition rate is much slower than 1

ML/10 min. The molecules studied are (see Fig. 3.6): unsubstituted phthalocyanine (H_2Pc; $C_{32}H_{16}N_8H_2$), metal-substituted Pcs (CoPc, FePc, MnPc), 3,4,9,10-perylene tetracarboxylic dianhydride (PTCDA; $C_{24}H_8O_6$), coronene ($C_{24}H_{12}$), the alkane pentacontane ($C_{50}H_{102}$), and C_{60}. For the purpose of comparison we evaporated also amorphous carbon.

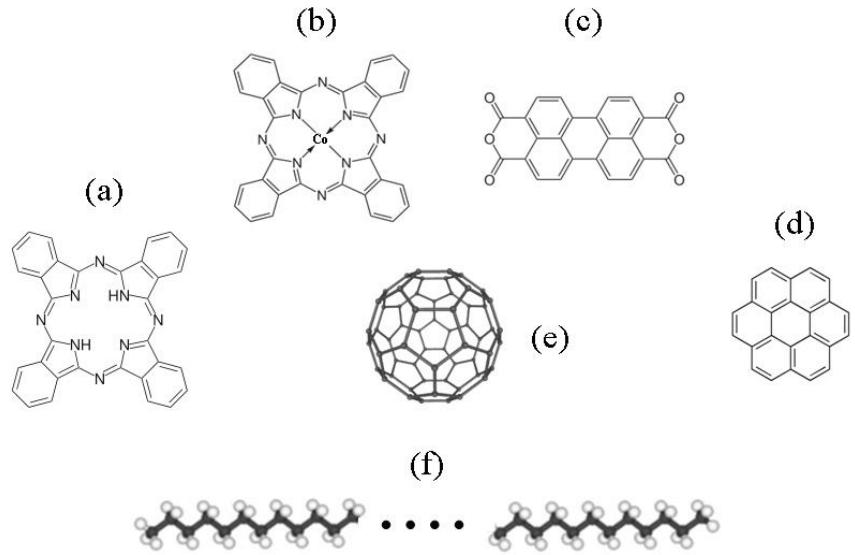

Figure 3.6: Molecule of (a) H_2Pc, (b) metal-substituted Pc (here CoPc), (c) PTCDA, (d) coronene, (e) C_{60}, and (f) pentacontane.

In certain cases where we have chosen Co(001) as ferromagnetic film we deposited an intermediate layer of Au on top of the Co film in order to separate the molecules from the latter. In this way we are able to distinguish effects which are induced by a direct contact of the molecules with the ferromagnetic surface from those which are not induced by a direct contact. For the characterization of the growth and the structure of the Au(111) films on top of Co(001), we refer the reader to the work on electron-spin motion in Au films on Co(001) performed in our group [55]. The advantage of Au for the present study is the fact that it exhibits at low electron energies a very large inelastic mean free path (IMFP) [55]. This enables us to observe still a significant spin-motion signal from the Au/Co interface even for Au thicknesses as large as 15 ML.

In the following two crucial questions will be addressed: (1) Are we really depositing intact molecules? (2) How do we determine the thickness of the

organic layers?

The first question has been addressed by studying exemplarily the system CoPc/Cu(001) by low-energy electron diffraction (LEED). LEED experiments at low coverages (see Fig. 3.7 (left) for 0.6 ML CoPc on Cu(001)) show already evidence of some ordering of the molecules on Cu(001) at room temperature with a typical liquid-like first-order ring around the substrate (0,0) LEED spot and a fourfold-shaped second-order structure. This indicates strong nearest-neighbor ordering of the molecules but only weak long-range order.

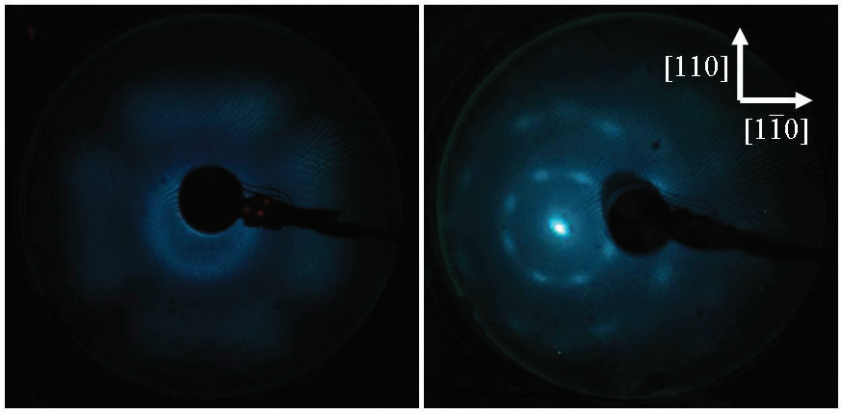

Figure 3.7: (left) LEED image of 0.6 ML CoPc on Cu(001) taken at 14.5 eV. (right) LEED image of 2 ML CoPc on Cu(001) taken in off-center position such that the (0,0) beam appears to the left. The electron energy is 16.5 eV. The crystallographic axes of the Cu(001)-crystal are indicated.

For thicker CoPc films of 2 ML thickness the long-range ordering of the molecules on the Cu(001) surface becomes clear (see Fig. 3.7 (right) for 2 ML CoPc on Cu(001)). Both first and second order spots are visible (third order spots can be vaguely perceived) which indicates a very good long-range ordering. Very similar LEED images have been observed for CuPc on Cu(001) by Buchholz *et al.* [56]. The central message is therefore that we are indeed dealing with intact Pc molecules on the surface as any disintegration of the Pc molecules would lead to a completely different LEED image. Moreover, the Pc molecules are immune to damage by the incident electron beam as the LEED image was stable for periods of hours under the LEED electron beam, not only at low energies but also at much higher energies (150 eV). Thus, we can exclude any damage by our spin-polarized electron beam, as, first, the electron energies are usually much lower than typical LEED energies and,

second, the beam current in the spin-motion experiments is in the nA-range while that of a LEED experiment is typically in the μA-range.

What is the thickness of the organic layers? to calibrate the organic layer thickness we exploit the fact that in most measurements reflectivity maxima appear that turn out to be at a thickness of 1 ML. In fact, the presence of islands for a non-integer coverage leads to a disordered surface such that diffuse electron scattering is enhanced. Consequently, the intensity of the specular elastic peak is reduced and becomes only maximum for a completed ML, for which the number of islands is minimum.

We note that intensity maxima can also be due to a quantum-well effect. In this case they can appear at any thickness depending on the electronic band structure of the overlayer material. A quantum-well origin of at least most of the maxima observed in our experiments with the organic layers can, however, be excluded. In most experiments the reflectivity maxima for a given system appear always at the same deposition time (keeping the evaporation rate constant) independent of the primary electron energy. However, the thickness position of quantum-well induced reflectivity maxima vary in general very strongly with the electron energy [55, 57].

Combined measurements of the electron reflectivity and the Auger signal as a function of the organic layer deposition time allowed us to calibrate the thickness independently. For the particular case of CoPc on Co(001) a calibration using the reflectivity maximum, which is supposed to be at 1 ML coverage, results in IMFP values of 1.5 ± 0.15 nm and 3.3 ± 0.4 nm for electrons with kinetic energies of 277 eV (carbon Auger peak) and 782 eV (high energetic Auger Co peak), respectively. These IMFP values are close to those given in the literature for many planar organic molecules. We refer here for instance to the theoretical work by Tanuma *et al.* [58] and the experimental work by Laibinis *et al.* [59] in which measurements of the IMFP in self-assembled monolayers of n-alkanethiols on different metallic substrates have been performed. Both theory and experiment give quite similar values to those obtained in our experiments, namely 1.5 nm and 2.7 nm for electrons of 277 eV and 782 eV kinetic energy, respectively. Similar Auger experiments with the other planar molecules (PTCDA, coronene, pentacontane) studied in the present work give similar values. This proves that our calibration method based on the reflectivity maxima which appear in most cases at 1 ML coverage (in certain cases an additional maximum at 0.5 ML is identified) is correct.

We note that all studied planar molecules have similar interlayer distances of about 0.35 nm.

Another independent check of the coverage is made in the case of CoPc/Co(001) and MnPc/Cu(001) by measuring the work function change of the substrate as a function of the organic layer coverage (see paragraph "Is the breakdown due to a "mirror"-effect?" in chapter 4). As the main changes of the interface dipole usually appear during the deposition of the first monolayer, we expect a saturation for larger coverages. Indeed, the calibration of the organic layer thickness based on the reflectivity maxima is consistent with this fact.

In the case of C_{60} layers we tried another way to independently calibrate the thickness. While the first layer of C_{60} is chemisorbed on metallic surfaces [60–62] and therefore relatively strongly bonded, further layers are only weakly bonded via the van-der-Waals interaction. Consequently the first C_{60} layer has a sublimation temperature that is substantially higher than that of the C_{60} molecules in subsequent layers (450 K) [63]. In order to obtain exactly 1 ML of C_{60} we performed the experiment in the following way: In a first step we evaporated at room temperature a thick C_{60} film. In a second step we heated the system at 600 K. We note that much higher temperatures above 760 K are necessary to lead to a fragmentation of C_{60}-molecules into graphite [63]. During heating we observed the Auger signal and realized after 10 min a dramatic decrease of the ratio of the Auger signals of C and Co, indicating the sublimation of C_{60} layers and therefore a reduction of the C_{60} coverage. As further heating during 30 min did not change anymore the Auger ratio we have strong reasons to believe that we obtained in this way a stable ML of C_{60}. Knowing the ratio of the Auger signals of 1 ML C_{60} on Co(001) we were thus able to calibrate the thickness scale in the spin-motion experiments. We note that the above thickness calibration is consistent with the calibration based on the reflectivity maxima.

The thickness of the carbon layers (interlayer distance is 0.34 nm) have been calibrated in the same way as explained already for the organic molecules. Like for the organic molecules reflectivity maxima appear in the spin-motion experiments. By combining measurements of the electron reflectivity and of the Auger signal we obtain IMFP values of 0.8 ± 0.1 nm and 2.5 ± 0.4 nm for electrons with kinetic energies of 277 eV and 782 eV, respectively. These values are close to those found in a combined theoretical and experimental work [64]

for graphite, namely 0.8 nm and 2 nm for electrons of 277 eV and 782 eV kinetic energy, respectively. Again, the calibration via the reflectivity maxima allow

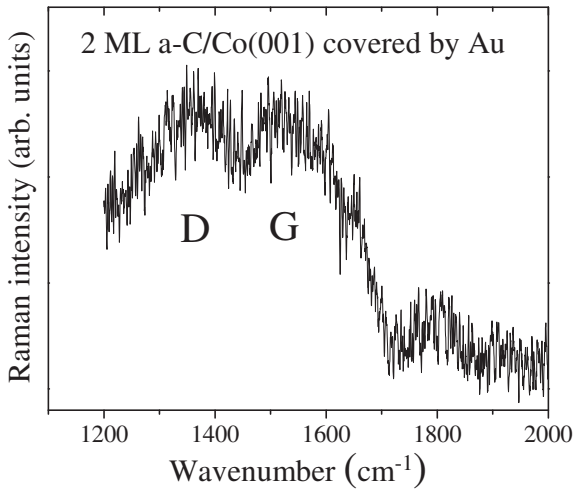

Figure 3.8: Raman spectrum of a Au-covered 2 ML a-C film on Co(001). The presence of both peaks "G" ("graphite") and "D" ("disorder") is typical of amorphous carbon films.

us to determine the thickness in the spin-motion experiments. We note that deposition of thicker carbon films (of a few ML) lead to amorphous carbon (a-C) as evidenced by Raman measurements in which both the G (graphite)- and the D (disorder)-peak have comparable intensities (see Fig. 3.8). The G-peak is close to the position of the single Raman line found at 1575 cm^{-1} on single crystals of graphite. This Raman line is present in all graphitic samples. The D-peak at 1350 cm^{-1}, on the other hand, can be attributed to the strong disorder of the carbon film.

3.3.2 For the synchrotron and inverse photoemission experiments

In the case of spin-polarized photoemission (SPARPES) and spin-polarized inverse photoemission (SPIPES) experiments, we also used a Cu(100) single crystal as substrate which was prepared as explained in the previous section. In these experiments MnPc and H_2Pc molecules were deposited onto thin Co films grown epitaxially on the Cu(001) substrate.

Part II

Results and discussion

Chapter 4

Electron-spin motion experiments

Contents

4.1 Spin-motion experiments with CoPc layers on Co(001)

In order to study the spin motion of the reflected electrons from organic films, we have started by measuring both the spin-integrated electron reflectivity and the electron-spin motion angles ε and ϕ as a function of CoPc film thickness.

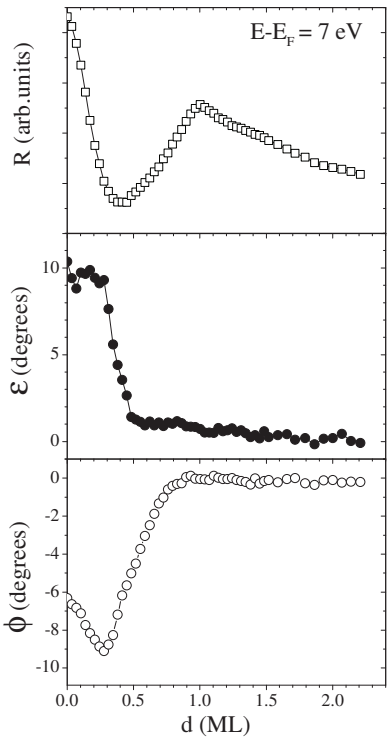

Figure 4.1: For the system CoPc/Co/Cu(001), the following quantities are shown as a function of CoPc film thickness: the spin-averaged electron reflectivity R (top), the precession angle ε (middle), and the rotation angle ϕ (bottom). The primary electron energy is 7 eV

Figure 4.1(top) shows the reflectivity as a function of CoPc thickness at a primary electron energy $E - E_F$=7 eV. After a sharp decay of the intensity it increases again and exhibits a maximum around a thickness of one ML. As explained in chapter "Samples" we attribute this behavior to the variation of the CoPc film morphology during deposition, evolving from an incompletely filled to a filled layer for a thickness of one ML. The behavior of the spin-motion angles, on the other hand, is quite different. In fact, in the case of ε (Fig. 4.1 (middle)) we can identify three different thickness regimes. The first

regime extends from zero to 0.28 ML. Here, ε exhibits only very little changes. From 0.28 ML on, a second regime up to about 0.5 ML, in which ε breaks down very rapidly, is seen. For larger coverages the strongly reduced ε shows only a very slow decrease and disappears completely for thicknesses above 1 ML. Interestingly, the behavior of ϕ (Fig. 4.1 (bottom)) is not identical to that of ε. In the first thickness regime (0-0.28 ML) it shows a significant increase of its absolute value. Although the absolute value of ϕ decreases above 0.28 ML also quite rapidly, the second thickness regime extends now up to about 0.75 ML. For larger coverages ϕ is zero.

The most peculiar feature of the thickness dependence is surely the fact that both spin-motion angles change very abruptly above 0.28 ML and that they become zero for thicknesses as small as 1 ML. It seems that there exists a sort of threshold value above which the system changes completely its behavior with respect to the reflection of electrons. In the following we will try to find out how general this breakdown-phenomenon is. In this way we will also see which explanations can be excluded.

4.2 Does the breakdown depend on the energy of the primary electrons?

In order to study the effect of the electron energy on the behavior of the reflected electrons, we measured the reflectivity R as well as the the electron-spin motion angles ε and ϕ as a function of CoPc film thickness for different electron energies (see Fig. 4.2 and Fig. 4.3).

Although some details differ with energy (slightly different threshold values, different behavior for thicknesses below the threshold value, additional features at around 0.5 ML, slightly different thickness values for which the spin-motion angles disappear), we see that the general behavior as a function of thickness is quite similar for all energies studied:

(1) The existence of a threshold value d_1, above which the absolute values of both spin-motion angles change very strongly. We note at this point that the determination of the small d_1 value is accompanied by a relatively large error. There are two systematic errors which are responsible for it. Beside a certain drift of the evaporation rate during the measurements, the most important source of error is the fact that even if the shutter of the evaporator is closed,

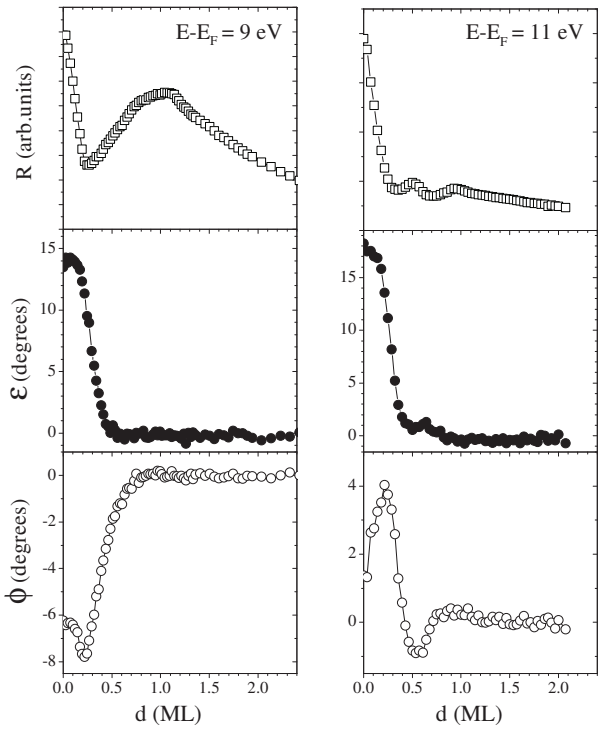

Figure 4.2: Spin-averaged electron reflectivity R, precession angle ε, and rotation angle ϕ as a function of CoPc film thickness for two different electron energies: 9 eV (left) and 11 eV (right).

molecules always diffuse in the vacuum chamber and lead thus to a very small but non-negligible evaporation rate on the sample surface (verified by Auger spectroscopy). This is the reason why we missed the threshold in our very first measurements with Pc (not shown). In order to reduce this disturbing effect, one has to start the measurement of the thickness dependence as rapidly as possible.

(2) A very strong change of the spin-motion angles above d_1 up to a thickness of about 0.5 ML is observed. This latter thickness will be called in the following d_2. A further observation is that this change between d_1 and d_2 is quite linear.

(3) For thicknesses above d_2 two behaviors are observed, depending on the ε- or ϕ-value which is reached at d_2. If the value is zero (see for instance ϕ in Fig. 4.3 (left)) the measured quantity remains zero. If the value is nonzero (see for instance ϕ in Fig. 4.3 (right)) a decrease of its absolute value, but now on a larger thickness scale, is observed.

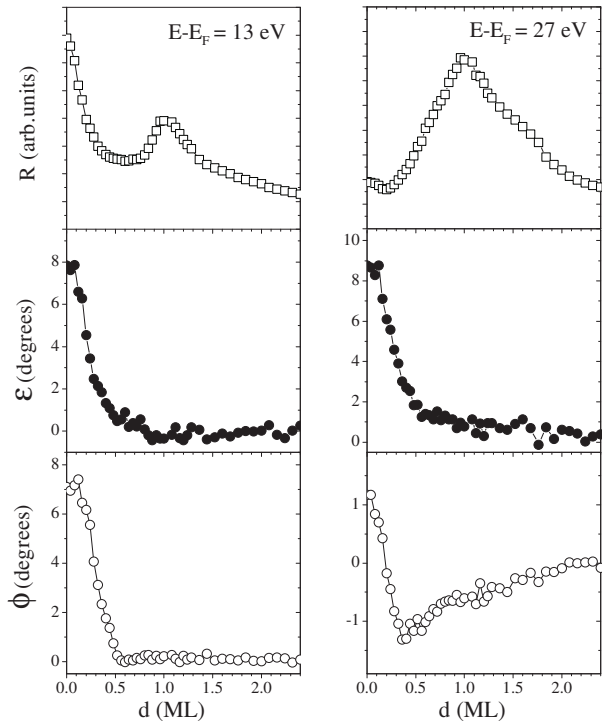

Figure 4.3: As Fig. 4.2, but for other two different electron energies: 13 eV (left) and 27 eV (right).

Figure 4.4 shows the three quantities R, ε, and ϕ as a function of the primary electron energy for several CoPc thicknesses. Although it is of course very difficult, if not impossible to evidence for all energies a threshold value, it is clear that both spin-motion angles approach zero very rapidly. This is an important result as it shows the independence of the breakdown-phenomenon on the energy of the primary electrons. This excludes any explanation which is based on the particular electronic band structure of the CoPc molecules.

We emphasize that while the spin-motion angles break down in the thickness regime between about 0.2 and 0.5 ML the degree of spin polarization of the reflected electron beam remains unchanged for all thicknesses studied (see for instance Figure 4.5 for electrons with a primary energy of 8 eV). Thus, any depolarization of the electron beam during interaction with the CoPc-covered Co surface, for instance by spin-flip scattering, is excluded.

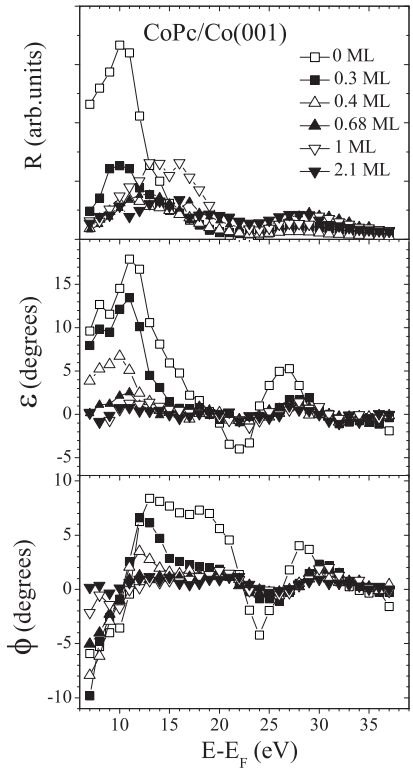

Figure 4.4: For the system CoPc/Co/Cu(001), the following quantities as a function of electron energy for different CoPc coverages are shown: spin-averaged electron reflectivity R (top), precession angle ε (middle), and rotation angle ϕ (bottom).

4.3 Is the breakdown due to a change of the surface magnetization?

To exclude a possible effect of the CoPc molecules on the surface magnetization of Co, we measured the polarization of secondary electrons as a function of CoPc thickness. As the spin polarization of the secondary electrons reflect the magnetization state of the ferromagnetic surface, they are an ideal probe for this type of study. Figure 4.6 shows the spin polarization of secondary electrons created by primary electrons of 132 eV energy. We emphasize that the exponential decay of the signal is as expected. Because of the limited IMFP of the secondary electrons less and less of them are created in the ferromagnetic substrate while more and more secondaries are created in the nonmagnetic

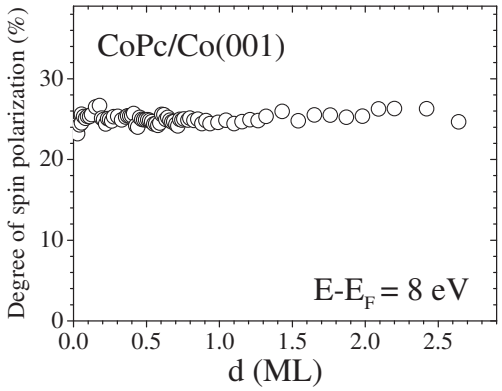

Figure 4.5: For the system CoPc/Co/Cu(001) the degree of spin polarization of the reflected electron beam as a function of CoPc thickness is shown. The primary energy of the electrons is 8 eV.

CoPc layer with increasing CoPc thickness. For thick CoPc coverages we indeed expect to observe zero spin polarization. The essential point of Fig. 4.6 is that the secondary spin polarization does not exhibit any particular change in the thickness regime where the breakdown of the spin-motion angles exists (between around 0.25 ML and 0.5 ML). If there were a strong decrease in the magnetization in this thickness regime we would see a corresponding drop in the secondary electron spin polarization. As this is not the case, a significant change of the Co surface magnetization due to deposition of CoPc can be excluded. We note that measurements of the x-ray magnetic circular dichroism as well as first-principle calculations give no indication of a significant reduction of the Co magnetic moment due to Pc coverage [65]. Finally, we note that both a change of the magnetic anisotropy leading to a switching of the easy axis of magnetization and a dramatic increase of the coercive field to values above the applied magnetic field strength can be excluded as well. In both cases the measured secondary electron spin polarization would be zero.

4.4 Is the breakdown due to a "mirror"-effect?

As phthalocyanine is a semi-conductor, it is possible that it leads to an electrical surface charge during the measurement with electrons. In this case, the charging could lead to a "mirror"-effect, i.e. the primary electrons are reflected by the CoPc layer without reaching the Co substrate. Therefore,

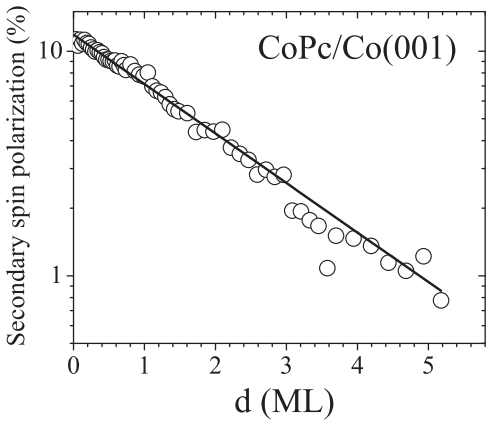

Figure 4.6: Spin polarization of secondary electrons as a function of CoPc thickness. The energy of the primary electrons is 132 eV. The full line is a fit to the data based on an exponential decay. Note the logarithmic polarization scale.

one would not expect any electron-spin motion signal. However, this scenario can be excluded. If there were such an effect, the primary electrons would not be able to create secondary electrons in the Co substrate. Consequently, the polarization of secondary electrons would be zero, which is not the case (see Fig. 4.6).

Another fact which excludes the possibility of a "mirror"-effect, is that the two spin-motion angles ε and ϕ do not behave in the same manner in several cases (see for instance Figures 4.1 (middle) and (bottom)). While ε is already zero, ϕ is still far from zero. However, in the case of a "mirror"-effect one would expect that both spin-motion angles disappear simultaneously.

In this context we have also studied the work function changes of Co(001) and Cu(001) when covered by Pc by measuring the energy position of the cutoff of the secondary electron distribution. Work function changes upon molecular adsorption on metal surfaces are caused by a charge transfer between the molecules and the metal substrate, leading to the formation of an interface dipole. Figure 4.7 shows the work function changes of Co(001) covered by CoPc (top) and Cu(001) covered by MnPc (bottom). In both cases an exponential-like behavior, as expected, with a saturation for coverages above 1 ML is observed. There is no indication at all that something particular happens with the interface dipole in the thickness regime from 0.25 to 0.5 ML.

We note that the work function changes obtained for thick Pc films (-1.1 eV for CoPc/Co(001), -0.9 eV for MnPc/Cu(001)) are in good agreement with measurements on similar systems which all show values around -1 eV [66–68].

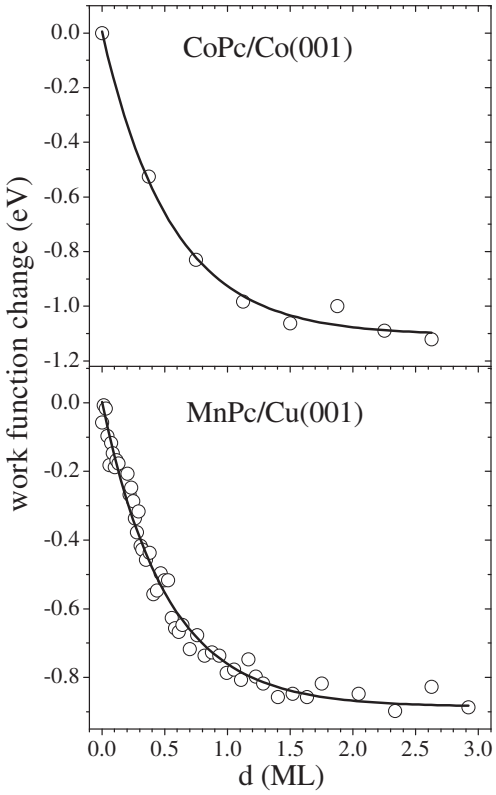

Figure 4.7: The work function changes as a function of CoPc thickness on Co(001) (top) and MnPc thickness on Cu(001) (bottom).

4.5 Does the breakdown depend on the choice of the ferromagnetic substrate?

To continue to seek for an explanation of this phenomenon, we decided to vary the ferromagnetic substrate using Fe(001) instead of Co(001). In this study we prepared Fe(001) films in two different ways, namely by depositing Fe onto a Ag(001) or onto a Pt(001) single crystal. Figure 4.8 shows both the spin-averaged electron reflectivity and the spin-motion angles as a function of the CoPc thickness on Fe/Ag(001) (left column) and on Fe/Pt(001) (right

column). The strong similarity of the thickness-dependent behavior with that of CoPc films on Co(001) let us immediately conclude that the choice of the ferromagnetic substrate has no importance for the existence of the breakdown-phenomenon.

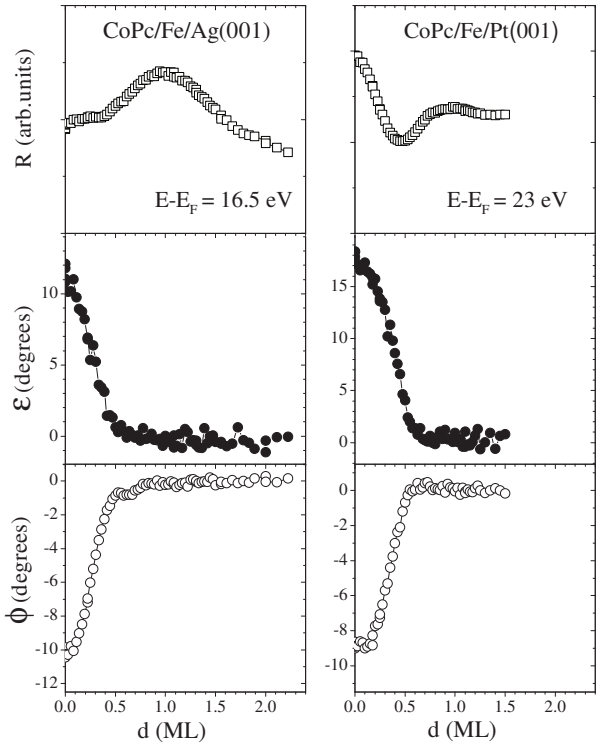

Figure 4.8: For the systems CoPc/Fe/Ag(001) (left column) and CoPc/Fe/Pt(001) (right column), the following quantities as a function of CoPc film thickness are shown: spin-averaged electron reflectivity R (top), precession angle ε (middle), and rotation angle ϕ (bottom). The primary energies are 16.5 eV and 23 eV, respectively.

4.6 Is the interaction of the molecules with the ferromagnetic substrate of any importance?

Even if a significant effect of the CoPc layer on the magnetization of Co can be excluded, an influence on the spin-dependent electronic band structure of Co due to an interaction between the molecules and the substrate cannot. The latter can in principle lead to strong changes of the spin-dependent reflection

properties of the Co surface and therefore of the spin-motion angles. However, very recent spin-resolved photoemission experiments as well as calculations performed on MnPc and H_2Pc layers deposited onto Co(001) show, while strongly spin-polarized molecule-induced interface states could be evidenced, no indications of a significantly changed electronic band structure of Co [65].

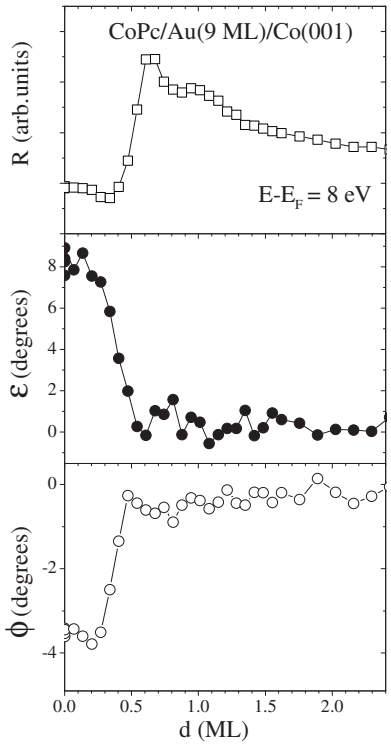

Figure 4.9: For the system CoPc/Au(9ML)/Co/Cu(001), the following quantities as a function of CoPc coverage are shown: spin-averaged electron reflectivity R (top), precession angle ε (middle), and rotation angle ϕ (bottom). The primary energy is 8 eV.

To check whether the contact of CoPc molecules with the surface of Co is crucial for observing the breakdown-phenomenon, we have studied a different system. Instead of putting the molecules directly on the surface of Co, we first deposit a Au film of 9 ML thickness on top of it as an intermediate layer. We have chosen Au, because the IMFP of electrons at low electron energies in Au is quite large [55] such that a significant portion of the detected primary electrons have "seen" the Co/Au interface and thus have experienced an electron-spin motion within the Co substrate even in the presence of a

relatively thick Au film.

Figure 4.9 shows the reflectivity and the electron-spin motion angles as a function of CoPc thickness for primary electrons of 8 eV energy. We observe again the same type of behavior as a function of CoPc thickness: a breakdown of the spin-motion angles above a threshold thickness and the disappearance of both spin-motion angles for thicknesses above 0.5 ML. Moreover, the values of d_1 and d_2 are very close to those obtained with CoPc being in direct contact with Co. Further experiments with an even thicker intermediate Au layer of 15 ML give a similar result (see Fig. 4.10). The fact that it is not necessary at all to have any contact of the molecules with the ferromagnetic substrate to obtain the breakdown of the spin-motion signal is surely the most surprising result. We note that only Au in immediate contact with a ferromagnetic substrate, i.e. the first Au layer, can be polarized. But, even in this case the induced magnetization in Au is ridiculous small (0.03 μ_B/atom [69]). Consequently, the non-magnetic molecules cannot possess any induced magnetization when they are separated from the ferromagnetic substrate by an intermediate Au layer as thick as 15 ML.

We note for the sake of completeness that molecules deposited directly onto the nonmagnetic Cu(001) substrate surface do not exhibit any spin-motion signal.

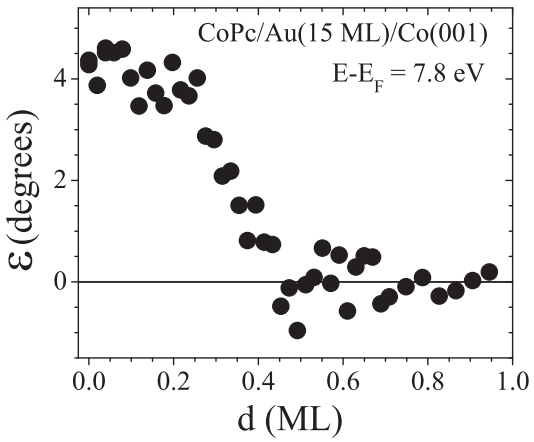

Figure 4.10: For the system CoPc/Au(15ML)/Co/Cu(001), the precession angle ε as a function of CoPc coverage is shown. The primary energy is 7.8 eV.

4.7 Does the breakdown depend on the choice of the organic molecule?

To see how general the breakdown-phenomenon is we studied different types of organic molecules:

(1) Different phthalocyanines with a varying central metal ion in order to test the possible role of the latter: CoPc, FePc, MnPc, and H_2Pc.

(2) Other aromatic molecules such as PTCDA (containing beside carbon and hydrogen also oxygen) and coronene (containing only carbon and hydrogen).

(3) The non-planar molecule C_{60}. As C-H bondings are not existing in C_{60}, their possible role can be tested.

(4) The alkane pentacontane, in which the carbon atoms are exclusively bonded by single bonds, in order to test the possible role of the aromaticity of the organic molecules in (1)-(3).

(5) And finally pure amorphous carbon.

As in the first considered case, namely CoPc, we deposited several molecule species not only directly onto a ferromagnetic substrate but also onto an intermediate Au layer in order to decouple the molecules from the ferromagnetic substrate. In all cases, i.e. for all molecules as well as amorphous carbon (see Fig. 4.11) in direct contact or not to the ferromagnetic substrate, a very similar behavior as a function of thickness is observed. In particular, the presence of three coverage regimes determined by the thicknesses d_1 and d_2 is found for any choice of the molecule species. Therefore, it can be concluded that the existence of the breakdown-phenomenon does not depend at all on the precise structure and composition of the organic molecule. It seems to be the mere presence of carbon atoms (independent of their state of hybridization) that is the essential ingredient to obtain the breakdown-phenomenon.

Figure 4.12 shows for instance the rotation angle ϕ as well as the secondary electron spin polarization as a function of the pentacontane thickness. This is one of the nicest examples we have, because it shows both the begin (at d_1) and the end of the breakdown (at d_2) of ϕ in a very clear manner. In fact, from this logarithmic plot it becomes clear that after the strong decay that ends at about 0.45 ML the further decrease of ϕ follows an usual exponential behavior. We note that the decrease is roughly two times faster than that

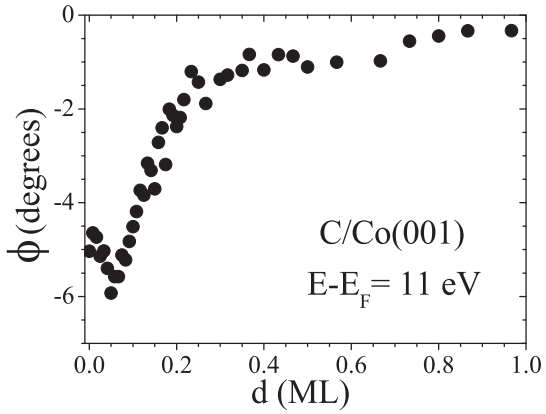

Figure 4.11: For the system C/Co/Cu(001) the rotation angle ϕ as a function of C coverage is shown. The primary energy is 11 eV.

of the secondary electron spin polarization. This is not astonishing. In fact, the primary electrons - before being detected - cross two times the organic layer while the secondary electrons which are created within the sample are crossing only once the organic layer, such that the secondary spin polarization should decrease less rapidly by a factor of 2.

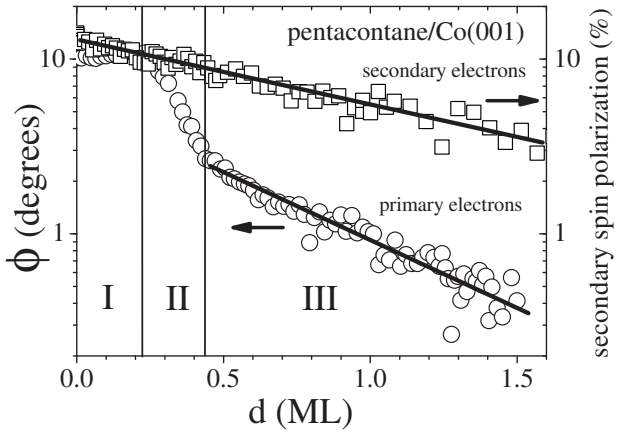

Figure 4.12: For the system pentacontane/Co/Cu(001) the rotation angle ϕ as a function of the pentacontane thickness is shown. The primary energy is 7 eV. The three thickness regimes are indicated. Note the logarithmic ϕ- and spin polarization- scale.

Figures 4.13 and 4.14 show the thicknesses d_1 and d_2 for all systems and

energies studied. We note that the determination of the thickness d_1, apart from the problems mentioned in chapter "Does the breakdown depend on the energy of the primary electrons?", is particular difficult in certain cases. Whether its determination is easy or difficult depends on the manner the measured quantity (ε or ϕ) varies at the beginning. If the absolute value of the quantity decreases as a function of thickness it becomes very difficult or even impossible to identify a threshold. Particularly easy is the situation when the absolute value of the quantity remains constant or even increases. In these cases the existence of a threshold value d_1 becomes obvious.

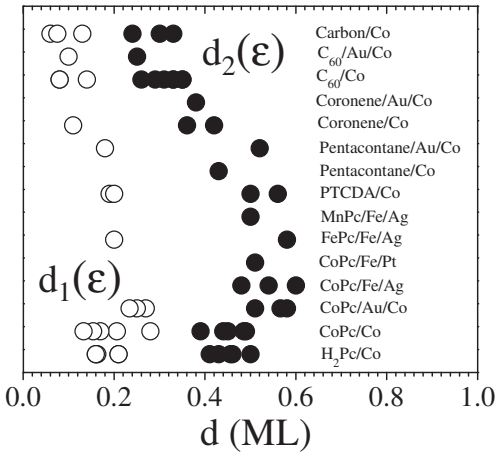

Figure 4.13: The thicknesses d_1 and d_2 obtained from measurements of the precession angle ε.

In the following we suggest the hypothesis that the appearance of the breakdown phenomenon depends on the average carbon surface density in each system. In order to see whether this hypothesis is consistent with our data we have to know the average carbon surface density σ_C^{ML} for a completed ML (see table 4.1). In the case where data are not available in the literature for a system the σ_C^{ML}-value of a similar system has been taken. For instance no data are available for molecules on Co(001) such that we take data for systems with Cu(001) as substrate.

By multiplying the average carbon surface density σ_C^{ML} for a completed ML with the thickness d_2 expressed in units of ML we obtain directly the average carbon surface density that is obtained at the end of the breakdown (see Fig. 4.15). For the planar molecules Pc, PTCDA, pentacontane, and

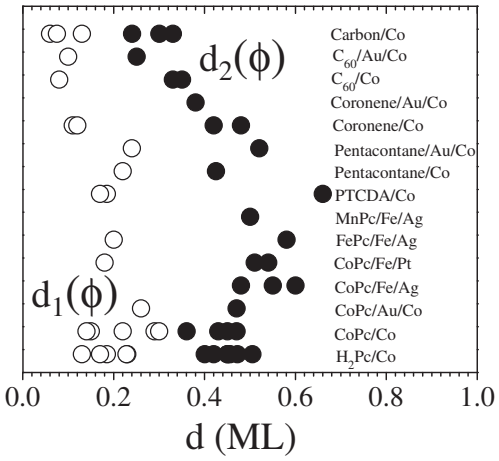

Figure 4.14: The thicknesses d_1 and d_2 obtained from measurements of the rotation angle ϕ.

coronene, be it on Co(001) or on Au(111), we obtain very similar values, $d_2 \cdot \sigma_C^{ML} = 8 \pm 2$ nm^{-2}. The situation is quite different for C_{60} and carbon for which $d_2 \cdot \sigma_C^{ML}$ is about two times and four times larger than for the planar molecules, respectively. This discrepancy between the planar molecules on the one hand and C_{60} and carbon, on the other hand, let us conclude that it is not the value of the average carbon surface density which determines the d_2-value. We nevertheless emphasize that a minimum average carbon surface density might be necessary to obtain the breakdown effect. However, this point cannot be verified as we do not have molecules with much lower average carbon surface density.

Further analysis of the problem shows us that it seems to be rather the by the molecules or carbon occupied sample surface (occupancy) which determines the values of d_2. By inspection of STM images in the literature rough values for the occupancy values can be obtained: 0.54 for PTCDA [77], 0.64 for Pc [70], 0.68 for pentacontane [73], 0.8 for coronene [74], 0.92 for C_{60} [76] and 1 for carbon. Interestingly, the product of the occupancy- and the d2-values is now approximately the same for all systems studied, namely about 0.3 ML (see Fig. 4.16). This is a quite astonishing result. Should we not expect to have a saturation of any type of effect rather for a completed ML? One could understand such a low saturation value if we hypothesize that the molecules or the carbon islands appear much larger for the reflected electrons,

system	σ_C^{ML}
Pc/Cu(001)	17 (Ref. [56])
Pc/Au(111)	14 (Ref. [70])
PTCDA/Cu(001)	18 (Ref. [71])
$C_{44}H_{90}$/Cu(001)	15 (Ref. [72])
$C_{30}H_{62}$/Au(111)	15 (Ref. [73])
coronene/Cu(001)	26 (Ref. [71])
coronene/Ag(111)	21 (Ref. [74])
C_{60}/Cu(001)	60 (Ref. [75])
C_{60}/Au(111)	69 (Ref. [76])
graphite	115

Table 4.1: The average carbon surface density σ_C^{ML} of a completed ML in number of carbon atoms per nm^2.

i.e. they have a cross-section which is larger than the "actual" size of the molecules or carbon islands. As we said before, one might expect a saturation of the effect for a completed ML. If we apply this to the (hypothetical) enlarged cross-section of the molecules we must conclude that the cross-section has to be about three times larger than the "actual" size of the molecules.

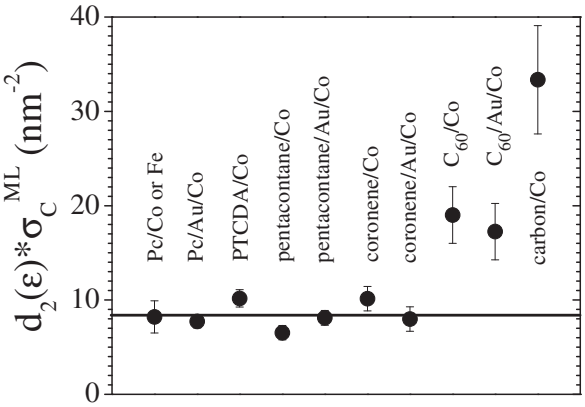

Figure 4.15: The product of d_2 and the average carbon surface density σ_C^{ML} of a completed ML is shown for all systems studied. In the case of C_{60} it is the onto surface projected average carbon density.

Another interesting information might be obtained from the fact that the

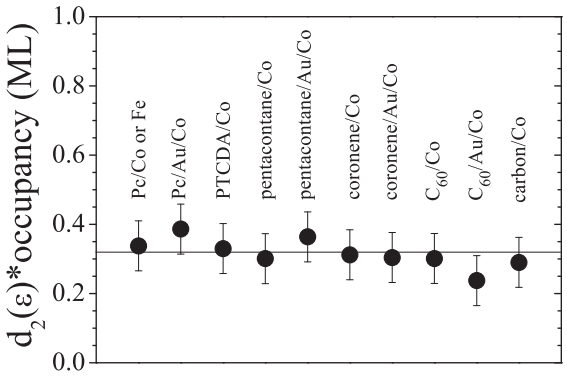

Figure 4.16: The product of d_2 and the occupancy is shown for all systems studied.

breakdown phenomenon presents a threshold thickness d_1. The presence of a threshold is very often typical of an onset of some percolation process, i.e. one needs to have the formation of long-range connectivity. This could mean that the occurrence of the breakdown phenomenon requires the long-range connectivity of the (hypothetical) enlarged cross-sections of the molecules. Figure 4.17 shows the ratio of the threshold and the saturation value d_1/d_2. Surely, the values of d_2 and particularly of d_1 are affected by a relatively large margin of error. Consequently, the scatter of the ratio d_1/d_2 is very significant.

One might wonder now if any other element than carbon is able to induce the same type of breakdown of the spin-motion angles. Of course, we are not able to make a systematic study of the whole periodic system. However, certain experiments which have been performed in the past by several of us as well as by other groups indicate that the following elements do not show this behavior: Au [55], Cu [57], Ag [78], Pd [78], Mn [79], Cr [80], V [81], Pb [82], Mg [82], and O [83]. In these experiments either the spin-motion angles or the exchange asymmetry, being closely related to the rotation angle ϕ, have been measured. Experiments with Si, a neighbour of C in the periodic system, have not been performed but could be very difficult to be conclusive because of the strong tendency of Si to alloy with the ferromagnetic transition metals at least at room temperature. Experiments at low temperatures, which are not possible with the present set-up, might be interesting. We speculate, however,

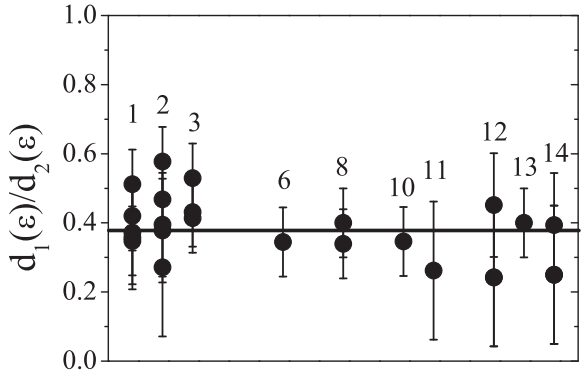

Figure 4.17: The ratio d_1/d_2 for 1: H_2Pc/Co, 2: CoPc/Co, 3: CoPc/Au/Co, 4: CoPc/Fe/Ag, 5: CoPc/Fe/Pt, 6: FePc/Fe/Ag, 7: MnPc/Fe/Ag, 8: PTCDA/Co, 9: pentacontane/Co, 10: pentacontane/Au/Co, 11: coronene/Co, 12: C_{60}/Co, 13: C_{60}/Au/Co, 14: C/Co.

that the compound boron nitride (BN), which is isoelectronic to carbon, might be a possible candidate.

4.8 Does the breakdown depend on the orientation of the initial spin polarization?

In all experiments presented up to now we studied the spin-motion angles for which the initial spin polarization $\vec{P}_0$ was aligned perpendicularly with respect to the magnetization $\vec{M}$. Furthermore, in all cases $\vec{P}_0$ was also oriented perpendicularly with respect to the scattering plane. In order to test whether the orientation of $\vec{P}_0$ with respect to the scattering plane has any importance for the breakdown-effect, we performed an experiment in which $\vec{P}_0$ lied in the scattering plane (see inset in Fig. 4.18). Figure 4.18 shows for the case of PTCDA/Co(001) ε as a function of the PTCDA thickness for both orientations of $\vec{P}_0$. As the thickness dependencies are very similar, in particular with the same values for d_1 and d_2, the orientation of $\vec{P}_0$ has obviously no influence on the breakdown-effect.

What happens if we orient $\vec{P}_0$ not perpendicularly with respect to the magnetization direction, but parallel or antiparallel to it? In this case, of

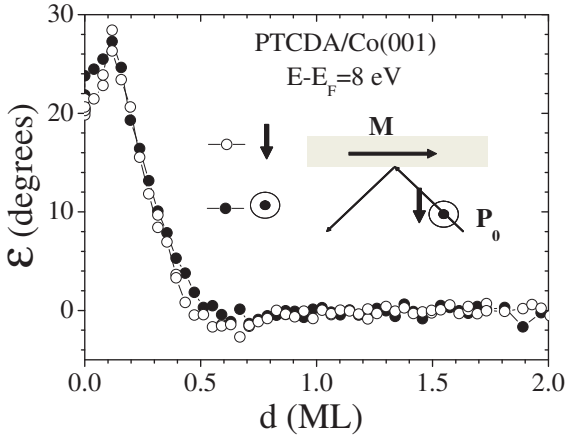

Figure 4.18: For the system PTCDA/Co/Cu(001) the precession angle ε as a function of PTCDA thickness is shown for two different orientations of the initial spin polarization $\vec{P}_0$. The primary energy of the electrons is 8 eV.

course, we will not be able to measure any spin motion. However, we can measure the so-called exchange asymmetry

$$A_{ex} = \frac{R^{\uparrow\uparrow} - R^{\uparrow\downarrow}}{R^{\uparrow\uparrow} + R^{\uparrow\downarrow}}$$

where $R^{\uparrow\uparrow}$ and $R^{\uparrow\downarrow}$ are the reflected electron intensities with $\vec{P}_0$ parallel and antiparallel to $\vec{M}$, respectively. If we take into account that the intensities $R^{\uparrow\uparrow}$ and $R^{\uparrow\downarrow}$ are proportional to the quantities $|r^{\uparrow}|^2$ and $|r^{\downarrow}|^2$, respectively, which we introduced in chapter "Electron-spin motion", we can directly identify the asymmetry

$$A = \frac{|r^{\uparrow}|^2 - |r^{\downarrow}|^2}{|r^{\uparrow}|^2 + |r^{\downarrow}|^2}$$

with the exchange asymmetry A_{ex}. As A and the rotation angle ϕ are closely related, we thus expect the same type of breakdown-phenomenon also for A_{ex}. Figure 4.19 shows the exchange asymmetry A_{ex}, which is normalized to an initial spin polarization of 100%, as a function of FePc thickness on Fe(001). Indeed, A_{ex} behaves as expected and exhibits the breakdown-effect.

Finally, we consider the configuration for which $\vec{P}_0$ is zero. The only quantity which we can measure in this case is the spin polarization which is created due to the spin-dependent reflection of the electrons at the surface of the ferromagnetic substrate. As elastic exchange scattering, responsible for spin flips, is of negligible importance [84], the spin polarization P created with

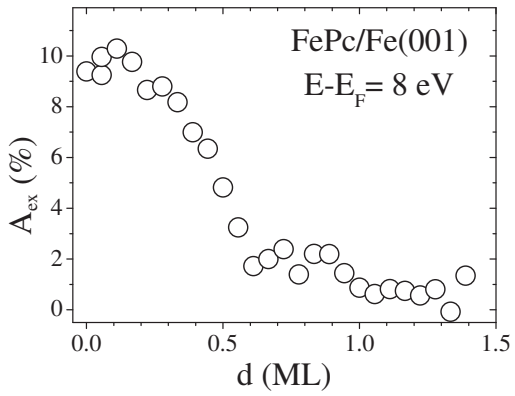

Figure 4.19: For the system FePc/Fe(001) the exchange asymmetry A_{ex} as a function of FePc thickness is shown. The primary energy of the electrons is 8 eV.

an unpolarized electron beam should be identical to the exchange asymmetry A_{ex} created with a (completely) polarized electron beam, $P = A_{ex}$. As A_{ex} exhibits the breakdown-phenomenon, we expect the same behavior for P. In fact, this is exactly what we observe for instance for the system C_{60}/Co(001) in Fig. 4.20.

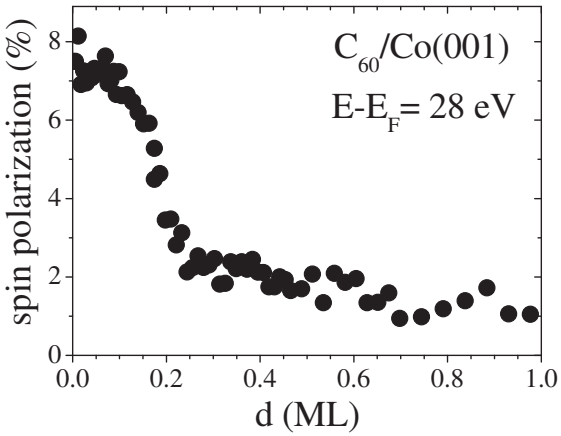

Figure 4.20: For the system C_{60}/Co/Cu(001) the degree of spin polarization of the reflected electron beam as a function of C_{60} thickness is shown. The initial spin polarization is zero. The primary energy of the electrons is 28 eV.

4.9 Does the breakdown only concern elastically scattered electrons?

Up to now we have studied the breakdown-effect on elastically scattered primary electrons. In order to find out whether all primary electrons, being elastically or inelastically scattered, are subject to this effect, we performed two types of measurements. In the first experiment electrons leaving the sample are detected in the spin detector. For this experiment the retardation grid of the energy analyzer was set to zero such that all electrons scattered within the angular acceptance angle of the energy analyzer of a few degrees, independent of their loss in energy, are detected. Figure 4.21 shows the spin polarization of the detected electrons as a function of the CoPc thickness on Co(001) for two different primary energies, 132 and 26.5 eV. In the case of 132 eV the spin polarization shows a nice exponential decay, while that at 26.5 eV exhibits a change of slope around 0.5 ML.

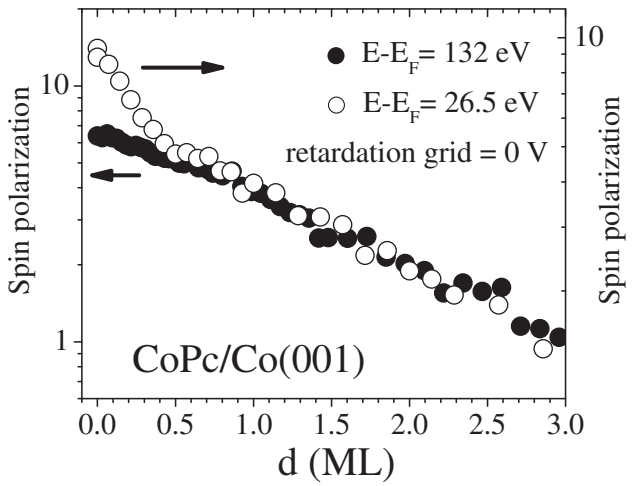

Figure 4.21: For the system CoPc/Co/Cu(001) the degree of spin polarization of inelastic electrons (both inelastically scattered primaries and secondaries) as a function of CoPc thickness is shown. The primary energies of the electrons are 26.5 and 132 eV.

In order to understand this difference between these two primary energies, we have to know which electronic distributions are formed during interaction of the incoming electron beam with the sample. There are three contributions: (1) elastically scattered primary electrons, (2) inelastically scattered primary

electrons, and (3) secondary electrons. As we have detected the scattered electrons in off-specular geometry (by 5o off), the contribution of elastically scattered primaries is very small. Thus, the spin polarization in Fig. 4.21 consists of only two contributions, namely that of inelastically scattered primaries and of secondaries. The key to understand the difference between the signals for 132 and 26.5 eV is the fact that the number of secondaries increases dramatically with increasing primary energy and can be much higher than the number of the incoming primaries, while the number of inelastically scattered primaries can never be larger than that of the incoming primaries. Consequently, for 132 eV the contribution of secondary electrons is dominating the signal, such that the contribution of inelastically scattered primary electrons can be neglected. The situation is quite different at 26.5 eV. As the energy of the incoming primaries is now much smaller the number of secondaries is dramatically reduced with respect to the situation at 132 eV (by one order of magnitude) and becomes comparable to the number of inelastically scattered primaries. The change in slope for 26.5 eV can now simply be explained if we assume that the inelastically scattered primary electrons are subject to the breakdown-effect, leading to the same d_2 value (of about 0.5 ML) as for the elastically scattered primaries. For thicknesses larger than d_2 the inelastically scattered primaries are still contributing to the total intensity, but as their spin polarization is now zero or at least strongly reduced, the total spin polarization is significantly smaller.

In a second experiment the absorbed sample currents $I_a^{\uparrow\uparrow}$ and $I_a^{\uparrow\downarrow}$ with $\vec{P}_0$ parallel and antiparallel to $\vec{M}$, respectively, are measured. In this way we obtain the spin asymmetry of the absorbed sample current:

$$A_a = \frac{I_a^{\uparrow\uparrow} - I_a^{\uparrow\downarrow}}{I_a^{\uparrow\uparrow} + I_a^{\uparrow\downarrow}}$$

We note that the absorbed current I_a is complementary to the total reflected current I_r, i.e. $I_a = I_0 - I_r$ with I_0 the from the electron source arriving current. By measuring A_a we have access to the spin asymmetry of the total reflected current, which is a simple sum of the elastic reflected current, being the sum of the LEED beam intensities (not only of the (00)-beam), and the inelastic reflected current which accounts for all electrons reflected with energies inferior to the primary energy and at arbitrary angles. This becomes clear when we consider that the requirement of charge conservation has to be

fulfilled. Thus, any change in the spin asymmetry of the total reflected current must lead to a complementary change of A_a. The magnitudes of these two asymmetries are simply related by the ratio of the coefficients for reflection and absorption [85]. Figure 4.22 shows the negative spin asymmetry of the absorbed sample current $-A_a$ and for comparison the spin asymmetry of the (00)-beam $A_{(00)}$ as a function of CoPc thickness for the system CoPc/Co(001). We note that a relatively low primary energy of 13 eV has been chosen in order to keep the contribution of secondary electrons to the current leaving the sample small. The essential point is that $-A_a$ and $A_{(00)}$ exhibit a very similar behavior. This proves that the breakdown-phenomenon which is observed for the (00)-beam is also present when we consider the total reflected current. We emphasize that the (00)-beam is only a small part of the total reflected current.

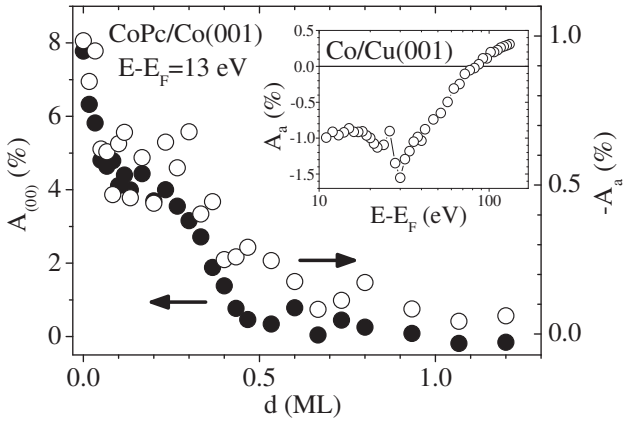

Figure 4.22: For the system CoPc/Co/Cu(001) both the asymmetry of the (00)-beam $A_{(00)}$ and the negative asymmetry of the absorbed sample current $-A_a$ as a function of CoPc thickness are shown. The primary energy of the electrons is 13 eV. The inset shows the asymmetry A_a of an uncovered Co film as a function of the electron energy. Note the logarithmic energy scale.

4.10 Does the breakdown influence the spin-filtering within the ferromagnetic film?

While studying the effect on the absorbed sample current, we realized that this type of experiment might also give a response to another question, namely

whether the breakdown phenomenon influences the spin-filtering within the ferromagnetic film. For this we have first to look at the inset in Fig. 4.22. It shows the asymmetry A_a for a pure uncovered Co(001) film as a function of the electron energy. By going to much higher electron energies (up to 130 eV) we see that the asymmetry changes sign at around 80 eV and remains positive for higher energies. To understand this behavior we have to remind that the total reflected current which is complementary to the absorbed current consists in general in elastically and inelastically scattered primary electrons as well as secondary electrons. However, at the high electron energies the contribution of secondary electrons is dominating such that the contribution of primary electrons can be neglected. The change in sign of A_a is now understood in the following way. Because of the spin asymmetry of the IMFP of the electrons in the ferromagnetic Co film, i.e. the spin filtering effect, the primary electrons are subject to a different number of collisions across the ferromagnetic layer depending on whether the spin is a majority-spin or a minority-spin. Consequently, majority-spin and minority-spin primary electrons create different number of secondary electrons. As majority-spin electrons have a longer IMFP than minority-spin electrons [86], the latter create more secondary electrons and lead therefore to a smaller I_a-value, i.e. a positive value of A_a. We therefore understood that measuring the absorbed current at high electron energies could be a way to see whether the spin-filter effect within the ferromagnetic film is influenced or not by the deposition of organic molecules.

The same type of experiment as described before has therefore been performed at a much higher primary electron energy of 132 eV. Figure 4.23 shows the asymmetry A_a and for comparison the asymmetry of the (00)-beam $A_{(00)}$ as a function of CoPc thickness for the system CoPc/Co(001). While $A_{(00)}$ exhibits a clear breakdown as also observed for much lower electron energies (see Fig. 4.22), A_a behaves quite differently as it is only little varying and does not show a breakdown of the signal in the thickness range where this is observed for the elastic electrons. The essential point is that the presence of the organic layer has obviously no particular effect on the spin filtering properties within the ferromagnetic film, while the spin-dependent reflection properties are strongly influenced. The exponential decrease of A_a with increasing CoPc thickness, which is observed for coverages above 0.5 ML, on the other hand, is as expected, as CoPc does not exhibit a spin-dependence of the IMFP such that the production of the secondary electrons becomes spin-independent for

large CoPc thicknesses.

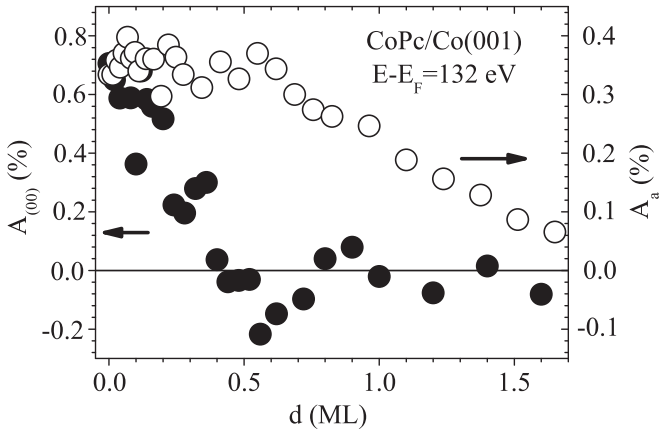

Figure 4.23: For the system CoPc/Co/Cu(001) both the asymmetry of the (00)-beam $A_{(00)}$ and the asymmetry of the absorbed sample current A_a as a function of CoPc thickness are shown. The primary energy of the electrons is 132 eV.

4.11 Does the breakdown depend on the quality of the substrate surface?

In order to see whether the surface quality has any influence on the breakdown-phenomenon we performed the following experiment. In a first step we prepared a substrate consisting of a Au and a Co layer on top of a Cu(001) single crystal. From our studies of this system we know that it possesses a narrow height distribution [55]. On this substrate we evaporated CoPc until the breakdown of the ε-signal at about 0.5 ML was completed. In a second step we sputtered (without (!) subsequent annealing) the CoPc-covered surface slightly until an ε-signal was again measurable. The idea was to introduce a significant roughness into the surface. Then, we started the redeposition of CoPc and stopped again after completion of the breakdown. In a third step the whole procedure was again repeated. Most importantly, the breakdown-phenomenon always appears and moreover results always in the same d_2 value of about 0.5 ML whatever the state of the surface is. We note that, on the

other hand, the initial ε-signal (before CoPc deposition) is clearly influenced by this procedure, as it is reduced by 40% from 14 to 8°.

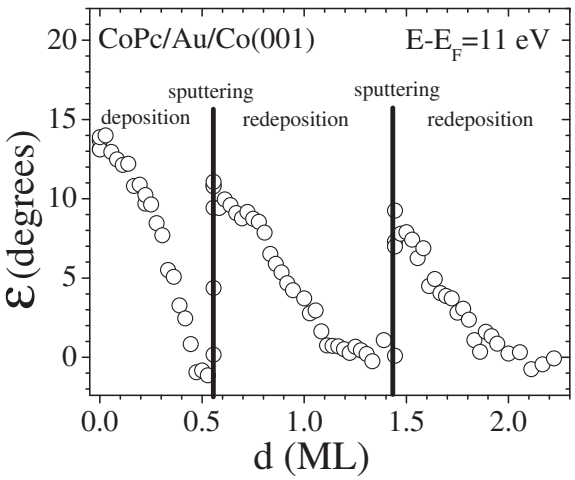

Figure 4.24: For the system CoPc/Au/Co(001) precession angle ε as a function of CoPc thickness is shown. The deposition process is interrupted two times by sputtering. The primary energy of the electrons is 11 eV.

4.12 Is the breakdown due to an interference effect?

An explanation of the breakdown-phenomenon based on a possible interference of electrons can be excluded for two reasons:

1) in the case of an interference the three quantities R, ε, and ϕ should behave in a particular way, because they are not at all independent of each other. One expects for instance a strong relationship between the spin motion angles and the reflectivity [55]. However, by considering all data no clear relationship between reflectivity and the spin motion angles is found. In fact, in the interesting thickness range between d_1 and d_2 the reflectivity shows all sort of behavior: weak or strong increase, weak or strong decrease or even non-monotonous behavior. In order to express these different behaviors by a single quantity we have calculated the ratio $R(d_2)/R(d_1)$ of the reflectivities for the coverages d_2 and d_1. The ratio is plotted in Fig. 4.25 and shows ratios between 0.2 and 4. Of particular importance is the fact that some data exist

which have a ratio close to 1, i.e. the reflected intensity in these cases does not vary much between d_2 and d_1, while the spin-motion angles do.

2) Our measurements of the secondary spin polarization at two different primary energies (26.5 and 132 eV, Fig. 4.21) showed us that inelastically scattered primary electrons exhibit also this breakdown-phenomenon. As no coherence exists between the inelastically scattered electrons, interference - only possible with coherent electrons - cannot be at the origin of this phenomenon.

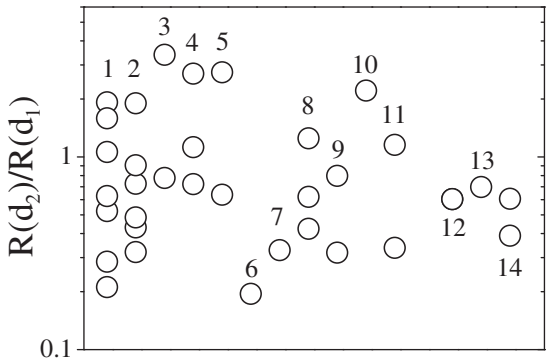

Figure 4.25: The ratio $R(d_2)/R(d_1)$ for 1: H_2Pc/Co, 2: CoPc/Co, 3: CoPc/Au/Co, 6: FePc/Fe/Ag, 8: PTCDA/Co, 10: pentacontane/Au/Co, 11: coronene/Co, 12: C_{60}/Co, 13: C_{60}/Au/Co, 14: C/Co. Note the logarithmic scale of the ordinate.

4.13 Does a buried organic film behave differently?

We have seen in the preceding chapters that the deposition of organic molecules or carbon has a dramatic effect on the spin-motion angles as well as on related quantities. The fact that the breakdown-phenomenon appears even in film systems in which the ferromagnetic substrate and the organic layer are well separated from each other, let us suppose that the behavior of the interface vacuum/organic layer is of crucial importance for an understanding of the breakdown-phenomenon. One might wonder therefore whether a modification of this interface could lead to a different behavior. In this vein we studied the spin-motion angles as a function of Au deposition on top of a Co(001) film

covered by 0.7 ML of carbon (see Fig. 4.26). Because of the breakdown-phenomenon the ε-signal after deposition of 0.7 ML carbon is only 0.5^o while the starting signal before C-deposition was 16^o. In a second step Au has been deposited on this system. We obtain thus a buried carbon film. Interestingly, deposition of Au, which leads to reflection conditions at the Au/C interface that are quite different from those at the vacuum/C interface, does not result in a "recovery" of the ε-signal. Instead the small signal is only modulated by the Au deposition in a way similar to Au deposition on Co(001) (see inset in Fig. 4.26). In the past these oscillations have been explained in terms of quantum-well states within the Au(111) layer [55].

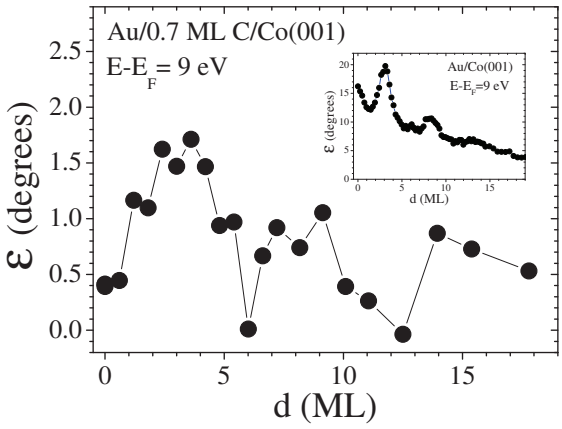

Figure 4.26: For the system Au/0.7 ML C/Co(001), the precession angle ε as a function of Au coverage is shown. The primary energy is 9 eV. The inset shows ε as a function of Au coverage on top of Co(001).

4.14 Do spin-motion first principle calculations predict the breakdown-phenomenon?

In order to unravel the physical origin behind the molecule-induced breakdown-phenomenon we performed spin-motion first principle calculations on carbon-covered Fe(001) films using linear muffin-tin orbital (LMTO) [87,88] and layered Korringa-Kohn-Rostoker (LKKR) methods [89,90]. We note that the same type of calculations performed recently by our group on MgO films on Fe(001) [91] and Fe(001) films on Ag(001) [92] showed reasonable agreement

with the experimental results and allowed them to understand the particular behavior they observed in these experiments.

Two systems are investigated: 9 ML of Fe(001) and 1 ML C on 9 ML Fe(001). As 1 ML is much larger than the thickness d_2 of C (about 0.25 ML), which we found in our experiments, we expect a complete disappearance of the spin-motion angles for Fe covered by 1 ML of C and this independent of the electron energy. The calculations are performed in three steps. First, structural relaxation of the film system is performed until the forces become smaller than 0.001 eV/ in order to determine the most stable geometry. Second, the electronic band structure is calculated using the LMTO method to find out the potential and charge distribution of the system's ground state. Finally, using the LKKR method and the converged potential the electron spin-motion angles of electrons reflected from Fe(001) and from 1 ML C/Fe(001) are obtained. We emphasize that the geometry of the spin-motion calculations is chosen identical to the experimental one.

Figure 4.27 shows the effect of carbon coverage on the calculated spin-motion angles ε and ϕ as a function of the electron primary energy. We can immediately conclude that 1 ML of carbon does not result in a breakdown of the spin-motion angles. Instead it rather leads to more pronounced structures at certain energies compared to the Fe(001) case.

At this point we should emphasize that in the spin-motion calculations the electrons are scattered by a potential which is not supposed to be changed by the presence of the incident electrons. Thus, one might speculate that a possible modification of the scattering potential due to the incident electrons could be at the origin of the breakdown-effect. On the other hand, in this case the effect should depend on the incident electron intensity. However, we varied the incident current over several orders of magnitude, but did not find any modification of the breakdown-phenomenon.

4.15 Conclusion

By performing spin-polarized electron scattering experiments on very different spinterfaces, consisting of different ferromagnetic metals as well as of different organic layers, we observe a completely unexpected behavior of the spin-polarized reflection properties of these spinterfaces. Submonolayer coverages

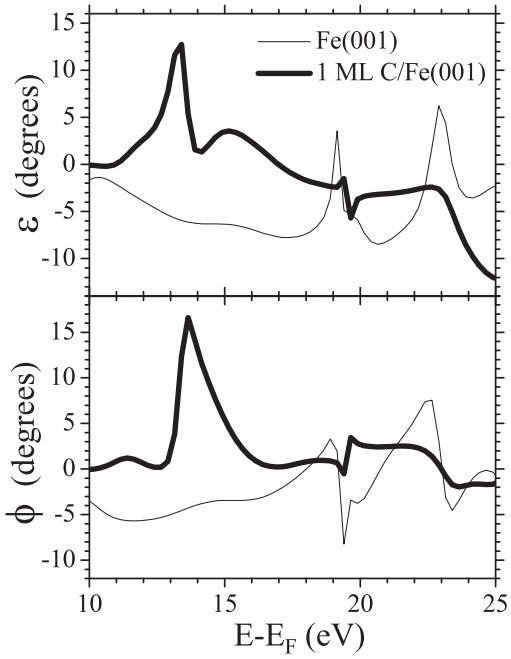

Figure 4.27: Calculated ε (top panel) and ϕ (bottom panel) as a function of the electron energy for 9 ML of Fe(001) (thin line) and 1 ML of carbon on 9 ML Fe(001) (thick line) .

of organic molecules or pure carbon make the electron reflection amplitude independent of the spin, i.e. both the reflectivity and the reflection phase become independent of the spin orientation of the incident electrons. The spin-motion angles are subject to a breakdown if a threshold value d_1 (between 0.1 and 0.25 ML dependent on the system) is exceeded. For thicknesses larger than d_2 (between 0.3 and 0.5 ML dependent on the system) the spin-motion angles are zero or at least very small compared to their initial values without coverage. We have shown that this behavior is a very general phenomenon and it is independent of

- the energy of the primary electrons,
- the choice of the ferromagnetic substrate,
- the choice of the organic molecule,
- the orientation of the initial spin polarization,

- the quality of the substrate surface.

It is not due to

- a change of the surface magnetization,
- a depolarization of the primary electrons,
- a "mirror"-effect,
- a direct interaction of the molecules with the ferromagnetic substrate,
- an interference effect.

Furthermore, the breakdown-phenomenon is not limited to elastically scattered electrons, does not appear in transmission, and is not predicted by first-principle calculations.

Despite this wide range of results we are not able at the moment to identify the cause of this breakdown-phenomenon. We suggest to study this effect by an experimental method which combines spatial resolution at least in the nm-range with the sensitivity to the spin-dependent reflection amplitude: spin-polarized low-energy electron microscopy. By sending polarized electrons with their spin parallel or antiparallel to the sample magnetization, it allows to measure the exchange asymmetry A_{ex}, which has been shown to exhibit the breakdown-phenomenon. Such spatially resolved experiments could be of interest to elucidate the processes which are behind this unexplained phenomenon.

Chapter 5

Spin-resolved photoemission experiments

Contents

5.1 Spin-polarized interface states in Phthalocyanine films on ferromagnetic Co(001)

To single out the spintronic properties of manganese phthalocyanine ($MnC_{32}N_8H_{16}$: MnPc) interface with Co(001), we performed spin-polarized photoemission experiments at the beamline Cassiopée at the synchrotron SOLEIL. The Cu(001) substrate was cleaned through cycles of argon-ion etching and annealing in the preparation chamber. The clean Cu(001) surface was then covered with 15 ML of Co. MnPc was thermally evaporated to form the MnPc/Co(001) interface. Auger electron spectroscopy was used to confirm that the Cu(001)-, Co(001)- and MnPc-surfaces are devoid of contaminants.

Samples were then transferred to the spin-polarized photoemission chamber. The photons impinge on the sample under an angle of 45° with a horizontal linear polarization. The experiment is thus sensitive to the hybridization of Co surface sites with MnPc molecular orbitals (MO) that are both in-plane (σ-MO) and out-of-plane (π-MO). The photoelectrons were in turn energy-analyzed by a hemispherical energy analyzer and collected in a spin detector for spin sensitivity. The energy resolution is 130 meV.

Figure 5.1 shows the direct photoemission data for both spin channels, as well as the resulting spin polarization P, for the system Cu(001)//Co(15ML)/MnPc(xML) (x=0, 1.3, 2.6, 3.9, and 5.2). The absolute intensities can be compared as all measurements were performed under the same conditions, in particular with the same incoming photon intensity. We notice that in the case of the uncovered Co(001) (Fig. 5.1 a), the majority spin spectrum shows a clear broad peak around -1 eV, whereas the minority spin spectrum shows only a peak at about -0.25 eV around the Fermi energy. When we compare our results with perviously reported studies on the same surface electronic structure of Co(001), we expect in our case to see another spin-down future around -0.36 eV which was called minority-spin surface resonance state [93]. In our measurements, we never saw this peak, this is understandable if we assume that the samples were slightly contaminated during the transfer to the measurement chamber. This explanation is justified because a similar work was already studied by Miyamoto and his coworkers [93]. By going to higher thicknesses of MnPc molecules, the two peaks decrease which means that we are dealing with interface states.

For uncovered Co(001) the spin polarization is strongly negative at E_F. This is understandable since the 3d-bands of ferromagnetic Co are exchange split and therefore the DOS for the minority-spin channel is much higher at E_F as compared to that of the majority-spin channel. As MnPc thickness increases, there appears near E_F, against the strong backdrop of Co-induced negative P, a relative decrease in this negative P. Since this MnPc-induced upturn in fact leads to a switchover in sign, we infer that additional MnPc is not merely suppressing the negative P of Co, but is in fact contributing a net positive P. Given the much larger density of states on the Co sites relative to that of the single Mn site, the N and the C sites, this positive P contribution must be substantial and be weighed more heavily within the overall signal since it is at the sample surface. This proves already that there is some

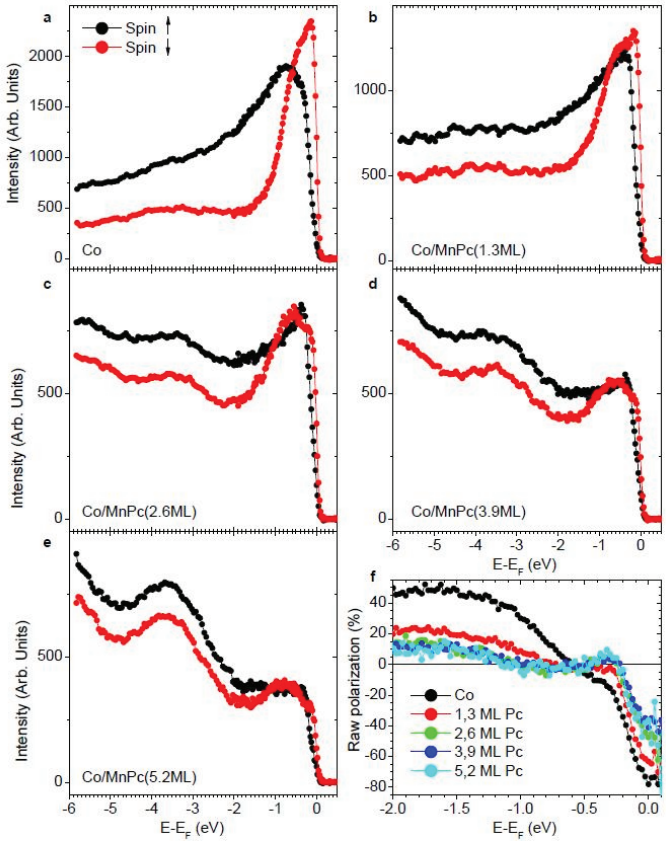

Figure 5.1: Spin-polarized photoemission spectra (spin up: black symbols, spin down: red symbols) of Co(001)/MnPc for five different MnPc thicknesses and the spin polarization as a function of binding energy. The photon energy is 20 eV.

molecule-induced contribution which is significantly (positively) polarized.

For the sake of comparison R. Bertacco and coworkers from Milan, Italy, performed within the framework of a collaboration spin-resolved inverse photoemission experiments on the same system. These experiments were performed using a collimated and transversely polarized electron beam of 25% polarization from a GaAs photocathode. The spectra were taken in the isochromatic mode by collecting photons at a fixed photon energy of 9.3 eV, while varying the incident-beam energy [94]. The energy of the incident electrons was varied between 9 and 17 eV. Data were collected at room temperature and at normal incidence. The energy resolution is 750 meV.

Figure 5.2 shows the spin-resolved inverse photoemission data obtained for pure Co and two different MnPc thicknesses of 1 and 2 ML. Unfortunately,

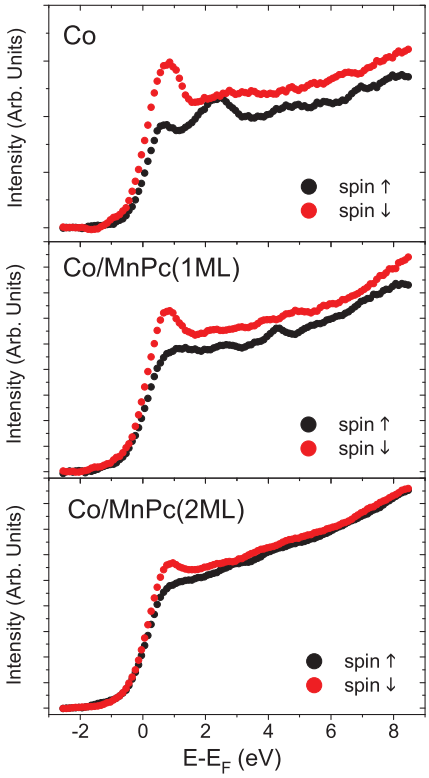

Figure 5.2: Spin-polarized inverse photoemission spectra (spin up: black symbols, spin down: red symbols) of Co(001)/MnPc for three different MnPc thicknesses (0, 1, and 2 ML) as a function of binding energy. Photons with an energy of 9.3 eV are detected.

an analysis of the spin polarization (not shown) exhibits a decrease of the absolute value of the spin polarization with increasing MnPc thickness without a sign change as seen in the direct photoemission data. The situation is therefore not as clear as in the case of the photoemission data and needs further consideration.

We thus need a procedure which allows us to extract the spin polarization of only the molecular sites. Such a procedure is presented and explained in its very details in the following.

To extract the spin polarization P of only the molecular sites, we adopt a subtraction procedure that takes into account the attenuation of the signal arising from ever deeper atomic sites away from the sample surface. Since our

theory shows that the spin-hybridized interface states occur within only a few eV from the Fermi level, one element of this procedure is to ensure that, once the molecular signal is extracted, the spin polarization far from E_F is zero.

The following subtraction procedure is described regarding spin-polarized direct photoemission data. A similar procedure is applied regarding spin-polarized inverse photoemission data (see Fig. 5.2). Our methodology supposes that the spin-resolved photoemission signal arising from Co sites remains essentially unchanged when the Co film is covered by MnPc (see section 5.1.3). It also rests upon the observation that molecular adsorption onto Co clearly has a strong impact on photoemission, even in the raw spectra, implying substantial, not just second-order, changes. Several aspects support this supposition. 1) Supposing an inelastic mean free path in Co of about 0.8 nm, only 20% of the Co photoemission signal is coming from the topmost layer while 80% are coming from the lower Co layers. Thus, the strong changes that we witness are not likely to arise from modifications of the topmost Co layer upon Pc adsorption. 2) Spin-resolved spectra at much higher photon energy (100 eV), which are dominated by Co 3d structures due to the strong photon-energy dependence of the photoionization cross section, show strong similarity for the uncovered and the 2.6 ML MnPc covered Co film. 3) To check how the magnetic properties of Co are affected by the adsorption of MnPc, another group performed x-ray magnetic circular dichroism measurements at the Co L edges at room temperature. Using the so-called sum rules, we find 1.73 μ B/at for the average spin moment per Co atom for 3 Co ML/Cu(001). Upon adsorption of 1 ML MnPc, the Co average spin moment is reduced to 1.67 μ B/at. If we assume that this reduction is borne only on the interface sites, then these sites carry a spin moment of at least 1.55 μ B/at. This minor reduction in spin moment is confirmed by ab-initio DFT calculations including spin-orbit coupling. This clearly excludes the possibility of a Co magnetic dead layer, and shows that modifications to the Co surface sites are a secondary effect. Such a small loss of magnetization cannot account for the large changes in spin-polarized photoemission that we observe in the raw data. We therefore assert that, from our complementary photoemission, XAS experiments, and with theoretical support, that any reduction in the magnetic moment of Co sites that hybridize with molecular sites cannot account for the large signal that we witness in the subtracted photoemission data.

In order to obtain the spin-resolved molecule-induced photoemission spec-

tra $f_{\uparrow,\downarrow}$(xML MnPc), the pure Co spectra $f_{\uparrow,\downarrow}$(Co) have therefore to be subtracted from the xML MnPc/Co spectra $f_{\uparrow,\downarrow}$(xML MnPc/Co) by taking into account the attenuation of the Co signal due to the presence of xML MnPc:

$f_{\uparrow,\downarrow}$(xML MnPc)=$f_{\uparrow,\downarrow}$(xML MnPc/Co) - $e^{(\frac{-x}{\lambda})}f_{\uparrow,\downarrow}$(Co) with λ the inelastic mean free path of the electrons in MnPc. Unfortunately, this "straightforward"-procedure has the great disadvantage that both the MnPc thickness and λ have to be known with sufficient accuracy. However, in particular the values of λ reported in the literature for low kinetic energies are significantly scattering such that a reliable determination of for instance the interfacial spin polarization becomes difficult. Moreover, the knowledge of the absolute MnPc thickness is necessary. We nevertheless try in a first step to determine the difference spectra by taking the absolute MnPc thicknesses as granted and by supposing a "reasonable" range of λ values (between 1 and 1.6 nm). Application of this method to both direct and inverse spin-resolved photoemission reveals that the intensity of the difference spectra around E_F is significantly positively polarized.

In a second step, we try to obtain the above attenuation factor without being obliged to know neither the absolute MnPc thickness nor the value of λ. The following procedure is only based on the fact, that the relative MnPc thicknesses are known and that the experiments are performed under the same conditions (same photon intensity). We emphasize that the relative thicknesses could be determined with great accuracy, while the absolute thicknesses are affected by a larger margin of error.

First, we plot the spin-resolved intensity as a function of MnPc thickness for several binding energies (see Fig. 5.3). For the spin-up intensity an exponential decrease is seen for energies below -0.4 eV. For lower binding energies down to the Fermi level clear deviations from the exponential behavior are observed indicating the presence of a spin-up hybridized interface state in this energy range. For higher binding energies of several eV (not shown), on the other hand, the intensity is rather increasing with thickness indicating the appearance of molecular (bulk) states. For the spin-down intensity an exponential decrease is found for energies between 0 and -0.5 eV, while strong deviations from this behavior are seen for higher binding energies. This indicates the presence of a spin-down hybridized interface state in this higher binding energy range. In fact, theory expects that only the first ML contributes to the DOS by the creation of interface states within this energy

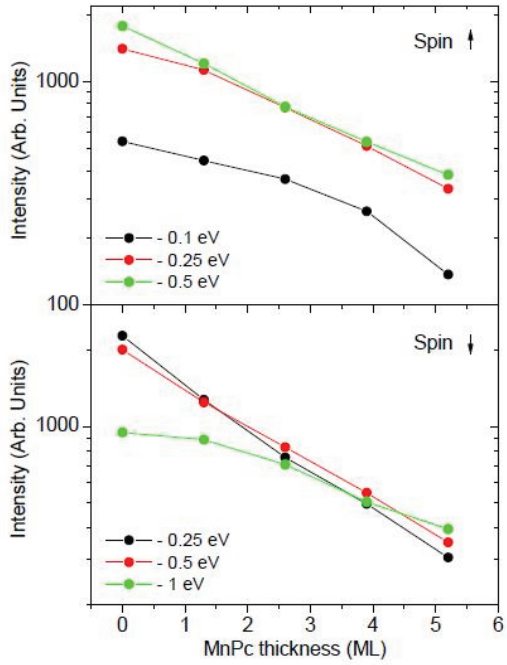

Figure 5.3: The photoemission intensity in the spin-up (top) and the spin-down channel (bottom) for different binding energy positions as a function of MnPc thickness. The photon energy is 20 eV. The attenuation factor used to calculate the difference spectra $f_{\uparrow,\downarrow}$(1.3 ML MnPc), for instance, is obtained by taking the ratio of the intensities for 1.3 ML MnPc and pure Co in the spin-down channel at low binding energies (-0.25 eV): $\alpha = 1274/2270 = 0.56$. Note the logarithmic intensity scale.

range while all other layers contribute only very little. For a given binding energy, we may extract the attenuation factor by taking the ratio of intensity before and after deposition of MnPc. For which binding energy and spin direction should this ratio be calculated?. From the above discussion of the spin-polarized intensity as a function of MnPc thickness for several binding energies it is clear that we have to take the spin-down intensity in the energy region close to the Fermi level. In fact, in this energy region the spin-down intensity shows no or at least very weak MnPc-induced intensity, such that only spin-down Co features are seen which are attenuated by the MnPc layers. Thus the ratio of the spin-down intensities close to E_F yields directly the attenuation factor necessary for the subtraction procedure. So, the attenuation factor used to calculate the difference spectra $f_{\uparrow,\downarrow}$(1.3 ML MnPc) is obtained by taking the ratio of the intensities for 1.3 ML MnPc and pure Co in the spin-down channel at low binding energies (-0.25 eV): $\alpha = 1274/2270 = 0.56$.

To ensure that the attenuation factor is valid, we slightly varied it to see how it influences the spin polarization of the difference spectra at higher binding energies (from -4.5 to -6 eV). For the difference spectra $f_{\uparrow,\downarrow}$(1.3 ML MnPc), for example, zero polarization is found for the same factor which we find also from the exponential intensity decrease, $\alpha = 0.56$ (see Fig. 5.4).

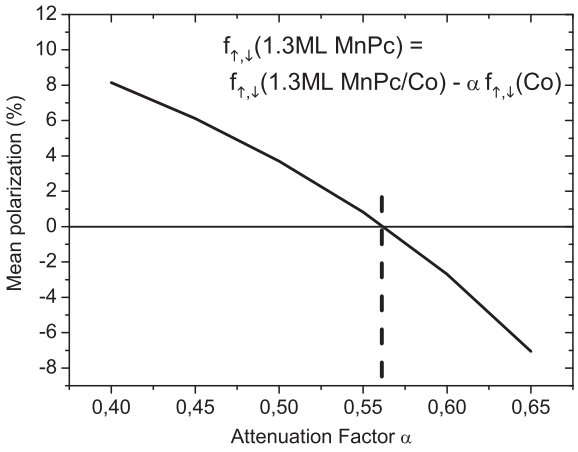

Figure 5.4: The mean spin polarization in the binding energy range from -4.5 to -6 eV of the difference spectra $f_{\uparrow,\downarrow}$(1.3 ML MnPc) as a function of the attenuation factor α. Zero polarization is obtained for $\alpha = 0.56$.

By applying the above described subtraction procedure the molecule-induced spectral contributions both for direct and for inverse spin-resolved photoemission can be obtained. We present in Fig. 5.5 the spin-resolved difference spectra of direct and inverse PE spectroscopy of Co/MnPc at RT (2.6 ML MnPc for direct and 2 ML MnPc for inverse PE) that are obtained by this subtraction procedure. Both direct and inverse PE experiments reveal a significant (nearly no) spin $\uparrow(\downarrow)$ intensity at/near E_F, which indicates a high P of the Pc-induced states in the vicinity of E_F. Assuming that the spin asymmetry of spectra is directly related to P, we can safely state that the P at room temperature and at E_F of the first two layers of MnPc adsorbed on Co(001) reaches $+80\% \pm 10\%$, i.e, is opposite in sign to that of bare Co.

By performing the above spin-polarized photoemission experiments on MnPc deposited on a ferromagnetic Co(001) surface, we were able to evidence the spin-polarized properties of the MnPc/Co(001) spinterface. Several

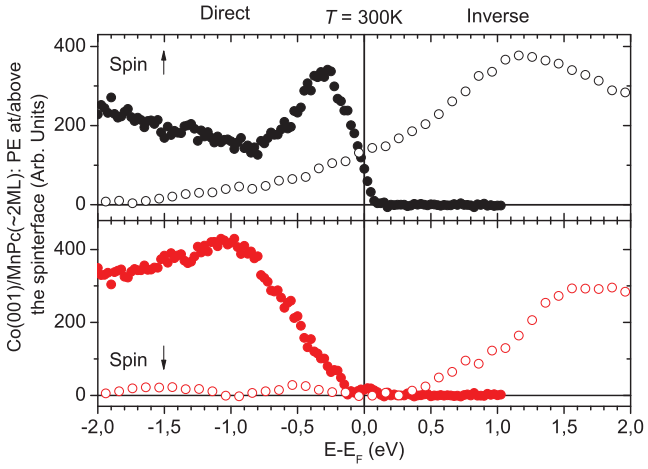

Figure 5.5: Spin-resolved difference spectra of direct (closed symbols; $h\upsilon$=20 eV) and inverse (open symbols) photoemission (PE) spectroscopy at room temperature of Co/MnPc (2.6(2.0) ML for direct(inverse) PE) reveal a P $\sim +80\%$ at E_F.

questions were raised by these observations and prompted us to perform additional experiments on MnPc as well as on a very similar system, namely H_2Pc/Co(001).

5.1.1 Are the Pc-induced states really interface states?

A test of the interface-state character of a spectroscopic feature is provided by studies of its dispersion with the electron wave vector perpendicular to the surface. This can easily be checked by varying the photon energy in the experiment. Our results show that the spin-up feature at -0.3 eV binding energy, which is clearly present at all photon energies studied, does not exhibit any dispersion (see Fig. 5.6). We confirm the interfacial nature of P by examining the impact of additional Pc coverage. Upon appropriately subtracting the spin-resolved spectra of 1 ML H_2Pc/Co from those of 2 ML H_2Pc/Co, the intensity of the interface states is strongly reduced (see Fig. 5.7 (left)). From the bar graph: Fig. 5.7 (right), we see that the second Pc layer contributes only 20% to the total intensity of the interface states of Fig. 5.5, which could reflect deviations from perfect layer-by-layer growth. The third ML does not contribute at all to the interface states intensity.

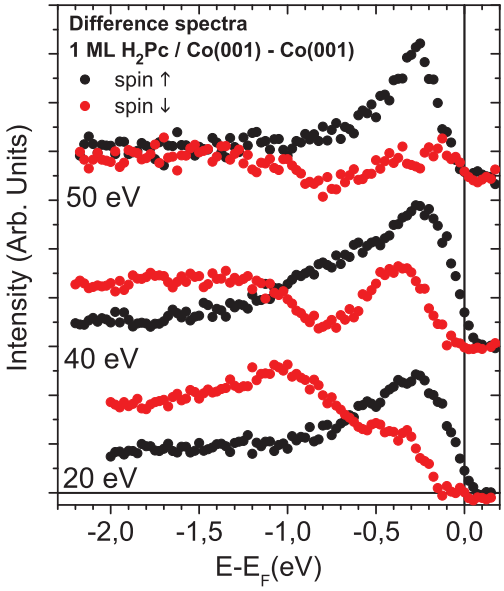

Figure 5.6: Spin-polarized difference spectra (spin up: black symbols, spin down: red symbols) of H_2Pc/Co(001) for three different photon energies (20, 40, and 50 eV).

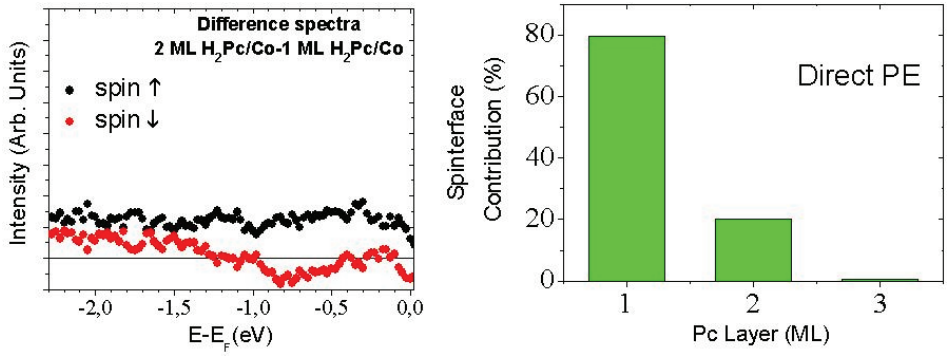

Figure 5.7: (Left) spin-polarized difference spectra (spin up: black symbols, spin down: red symbols) of 2ML H_2Pc/Co(001)-1ML H_2Pc/Co(001) obtained at a photon energy of 40 eV. (Right) the Pc thickness dependence of the direct PE signal ($h\upsilon$=20eV) reveals that Pc-induced intensity at low binding energies is essentially confined to the interface.

5.1.2 Are the features in the two spin channels related?

Measurements at three different photon energies (see Fig. 5.6) allow us to identify four features: (I) a spin-up interface state at -0.3 eV whose intensity

is quite similar for all three energies; (II) a spin-down interface state at -0.4 eV which seems to exhibit a resonant behavior around 40 eV, and whose origin is still unknown; (III) a spin-up feature around -0.65 eV, which appears as a shoulder in the spectrum and seems to follow the same photon energy dependence as the spin-down state at -0.4 eV. The fact that the two features at -0.4 and -0.65 eV are behaving in the same manner as a function of photon energy let us believe that we are dealing here with a spin-split pair. Consequently, a "positive" exchange splitting (spin-up state is lower in binding energy than the spin-down state) of -0.3 eV can be deduced from it; and (IV) a much broader structure in the spin-down channel for energies above -1 eV, which exhibits a different photon energy dependence than the other structures at lower binding energies, as it decreases dramatically by going from 20 to 50 eV photon energy. From this it is immediately clear that this feature cannot be considered as the spin-split counterpart of the spin-up interface state at -0.3 eV.

5.1.3 What is the electronic character of the interface states?

Given the presence of interface states, we wish to determine to what extent they are associated with the Co substrate or the Pc-overlayer. The photon-energy dependence of the photoionization cross section for the various states involved gives us the possibility to determine their character, i.e., to decide if the interface states are assignable to Co (3d) or to C (2p) and N (2p), or if they are intrinsically of mixed character. Calculated atomic photoionization cross sections show that by going from 20 to 100 eV photon energy the cross sections of the 2p states (of C and N) are decreasing by more than one order of magnitude while 3d states (of Co as well as of Mn) does not vary much [95]. We expect that such a large effect for free atoms shall trend similarly in solid-state systems. Consequently, if the interface states were mainly of Co 3d character, they should also be present at 100 eV photon energy. However, spin-resolved photoemission measurements at this photon energy do not reveal any sign of the Pc-induced interface state (see Fig. 5.8). The behavior of the spin polarization as a function of the binding energy is very similar for both uncovered and MnPc-covered Co (3 ML). We conclude that the interface states are mainly of C or N 2p character.

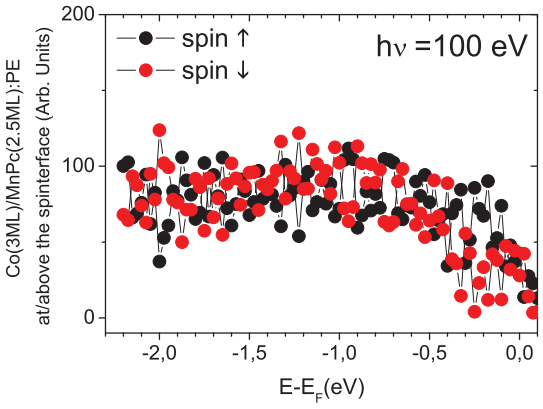

Figure 5.8: Spin-resolved difference spectra of direct PE spectroscopy at room temperature of Co(3 ML)/MnPc(2.6 ML) for $h\upsilon$=100 eV show no sign of any Pc-induced interface state, indicating that the interface states are mainly of C or N 2p character.

5.1.4 Does the central transition metal ion Mn^{2+} play a role in the creation of the spin-polarized interface states

The comparison of the data obtained with MnPc and H_2Pc at the photon energy of 20 eV (the only photon energy where a comparison can be made; see Fig. 5.5 and Fig. 5.6) shows that there are no significant differences between the spin-resolved difference spectra. In particular, the most prominent feature in the spin-up channel has in both cases similar intensity, the same binding energy position and the same width. This observation clearly proves that the central ion does not play an important role in the formation of the spin-polarized interface states.

5.2 What does theory predict?

In collaboration with a theoretical group at the IPCMS, we were able to understand the strong positive spin polarization of the interface states close to the Fermi level. The calculations were performed by Fatima Ali-Ibrahim as part of her PhD thesis. All density functional theory (DFT) calculations were carried out by means of the VASP package [96] and the generalized gradient

approximation for exchange-correlation potential as parametrized by Perdew, Burke, and Ernzerhof [97]. They used the projector augmented wave (PAW) pseudopotentials as provided by VASP [98]. The weak van-der-Waals (vdW) interaction was computed within the so-called GGA-D2 approach developed by Grimme [99] and later implemented in the VASP package [100]. This formalism can correctly reproduce the experimentally determined atomic distances between molecular sites and metallic sites [101]. Fcc Co(001) and fcc Cu(001) surfaces were modeled by using a supercell of 3 atomic ML of 8×8 atoms separated by a vacuum region. The lattice vector perpendicular to the surface is 3 nm. This results in a supercell of 249 atoms, including the 57 atoms of the MnPc molecule. Since experiments used cobalt films epitaxially grown on Cu(001), a fcc lattice parameter of 0.36 nm for both cobalt and copper was used in the calculations. It was found that additional MLs will not change significantly the results [102]. A kinetic energy cutoff of 450 eV has been used for the plane-wave basis set. For the study of a single molecule on a metallic surface, only the Γ-point was used to sample the first Brillouin zone. DOS were calculated using a 1 meV energy mesh and a Gaussian broadening of 20 meV FWHM. Spin-orbit interaction was included pertubatively in the augmentation region at each atomic site.

Earlier calculations performed on Co/Pc interfaces with unrelaxed atomic positions predicted a spin polarization of -25% [24], rather than the $+80\%$ now measured experimentally. To more realistically describe the interface, the new formalism used by Fatima Ali-Ibrahim relaxes atomic positions and includes van-der-Waals forces so as to quantitatively reproduce the crucially important molecule-substrate distance inferred from x-ray standing wave measurements [101]. This leads to a final distance Δz between Co and the adsorbed molecule of 2.1 A°.

To unravel the formation of the spinterface, we first examine the states of the two systems "molecule-Co" with common Fermi level in the absence of interactions between them (see Fig. 5.9(a)). The Co d-spin $\downarrow$ band crosses E_F, while the d spin $\uparrow$ band ends at E-E$_F$ = -0.7eV. Above this energy level, the spin $\uparrow$ sub-band exhibits only small DOS spikes that correspond to surface states. The molecule exhibits a MO only in the spin $\downarrow$ channel near E$_F$. Adsorption-induced displacements of the molecule's atoms overall promote a slight energy shift ($\sim$ 30 meV) of the MOs.

We now turn on interactions between the molecule and the Co surface by

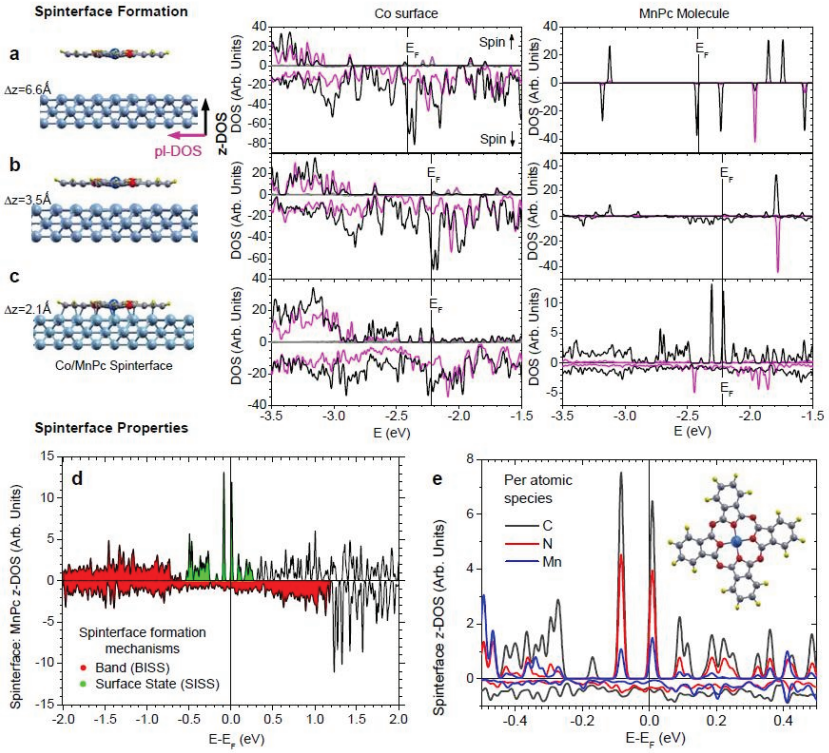

Figure 5.9: As the distance between molecule and the Co surface is reduced from (a) 6.6 A° to (b) 3.5 A° and to (c) the final position of 2.1 A°, p-d hybridization with the Co spin $\downarrow$ band causes energetically sharp, spin $\downarrow$ MOs in the z-DOS to disperse (red area of panel d), leading to a monotonous spin-$\downarrow$ z-DOS (black) at/near E_F (right-hand graph of panel c). In the spin $\uparrow$ channel at the vicinity of E_F, there are neither Co d band states nor MOs but simply Co surface states (panel a) that begin to hybridize as the molecule is brought closer in (panel b) and lead, at the final molecular position (panel c), to energetically sharp peaks that cross E_F. These surface induced spinterface states (SISS) carry virtually no Co s-character (gray datasets in panels a,b,c) and involve all atomic species of the molecule (panel e). The spinterface's planar DOS (pl-DOS; magenta) near E_F is mostly featureless and adopts the spin polarization of Co (right and left-hand graphs of panel c).

reducing Δz to 3.5 A° (Fig. 5.9(b)). At this distance, π-orbitals that spatially extend perpendicularly to the nascent interface promote wavefunction overlap between the molecule and Co surface sites, causing E_F to shift from E=-2.4 eV to E=-2.2 eV. At the vicinity of E_F, the Co spin $\downarrow$ states and spin $\uparrow$ surface states are little affected. In contrast, the interaction strongly modifies the molecule's states: while planar states remain mostly unaffected, perpendicular states experience the onset of hybridization. We emphasize here that there are no spin $\uparrow$ MO at/near E_F (right-hand panel of Fig. 5.9(b)).

At the final $\Delta z = 2.1\ A°$ (Fig. 5.9(c)), the molecule and Co surface sites may fully hybridize to form the spinterface. More precisely, all combinations of s-p,p-d and s-d hybridization may occur. Because fcc Co(001) is obviously not half-metallic [17, 103], the Co/MnPc spinterface shall strongly transmit the highly spin-polarized d-component of the Co DOS and attenuate the s- and p- components. Thus, the important question is: How is the Co d-band DOS transmitted onto the molecule in each spin channel?

Prior to adsorption and in the spin ↓ channel, the Co d band z-DOS intersects E_F and the z-DOS of the free molecule also exhibits a MO at/near E_F. Hybridization is therefore governed by the wellknown spinterface mechanism of spin-dependent broadening of MOs due to band hybridization [25, 26, 110]. The resulting BISS (band-induced spinterface states) are shaded in red in Fig. 5.9(d). These BISS exhibit a flat, continuous energy dependence across E_F.

However, the molecule does not exhibit any sizeable, preexisting spin ↑ z-DOS at the vicinity of E_F to hybridize with, and the Co surface's d-band does not cross E_F. Another spinterface formation mechanism must therefore account for the appearance of entirely new, hybrid states in the spin ↑ channel within -2.7 eV <E< -1.9 eV, i.e. at the vicinity of E_F (see right-hand panel of Fig. 5.9(c) and the segment of the spinterface z-DOS shaded in green in Fig. 5.9(d)). Due to the Pauli exclusion principle, these newly formed SISS (surface-induced spinterface states) which lie at the vicinity of E_F cannot occupy the spin ↓ states since they are already occupied by Co,and hence appear only in the spin ↑ channel. The presence of two sharp, tall peaks near E_F reflects a lifting of degeneracy induced by upward (downward) buckling of the benzene rings below (at) E_F along each of the two orthogonal axes that define the free molecule's 4-fold symmetry. This underscores how crucial it is to fully relax the interface structure if one wishes to study SISS.

Focusing now on the DOS that contributes to transport at RT, we present in Fig. 5.10(c-d) spinpolarised spatial maps, taken along the dashed line of Fig. 5.10(a), of the Co/MnPc interface DOS within $E_F - 25meV < E < E_F + 25meV$ (see Fig. 5.10(b)). Aside from the central Mn site, the remaining N and C sites exhibit very large positive spin polarization at E_F thanks to electronic states that are clearly hybridized with the Co interface atoms. In fact, these interface states are present on all atomic species of the molecule (Fig. 5.9(e)) and their amplitude trends with the number of molecular nearest-neighbors for a given Co spinterface site.

At E_F, both the energetically smooth BISS in the spin $\downarrow$ channel and the energetically sharp SISS in the spin $\uparrow$ channel define the sign and amplitude of the spinterface's spin polarization. Due in large part to the energetically sharp SISS that crosses E_F, we find that $P = 80\%$. Thus, considering the limitations of the comparison, we find that both theory and the direct/inverse PE experiments yield the same sign and high amplitude of the spin polarization at E_F (see Fig. 5.5 and Fig. 5.9(e)). Furthermore, peaks in the spin $\uparrow$ ($\downarrow$) PE (see Fig. 5.5) and DOS spectra (see Fig. 5.9(d)) at $\sim E - E_F = -0.3(-1.0)eV$ underscore a reasonably good agreement between theory and the direct PE experiment thanks to its good energy resolution (130 meV), while a qualitative agreement is found with inverse PE.

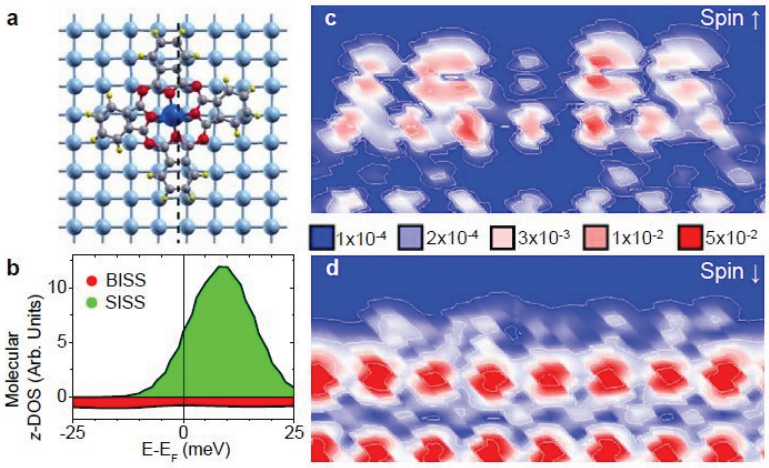

Figure 5.10: (a) Adsorption geometry of MnPc on Co(001). The spin $\uparrow$ and $\downarrow$ z-DOS within $E_F - 25meV < E < E_F + 25meV$: (b) SISS (BISS) lead to a sharp (monotonous) energy dependence at E_F; and (c-d) spatial charge density maps, taken along the dashed line of panel (a), show how the numerous C and N sites of MnPc exhibit a highly spin-polarized density of states at E_F that, furthermore, are hybridized with Co states and thus contribute to conduction.

5.3 Instead of a conclusion: Spintronics prospects for Co/Pc spinterfaces

We now discuss spintronics prospects for these Co/Pc spinterfaces. Indeed, an ideal spin-polarized current source (IspCS) should 1) exhibit a very high degree of spin polarization P that 2) endures well above room temperature (RT) for technological applications; 3) be both cheap and straightforward to synthesize considering existing industrial capabilities; 4) be compatible with miniaturization challenges at the nanoscale; and 5) provide an easy integration path with a semiconductor so as to enable transport of, and operations on, the highly spin-polarized current.

Candidates toward an IspCS include half-metallic ferromagnets, which ideally conduct electrons of only one spin direction [103] and could, using merely a band hybridization mechanism of spinterface formation [25, 26] lead to efficient spinterfaces. Such materials have been studied using direct PE [104] and been integrated into devices with sizeable P, not only at low temperature [17] but also at RT [105]. However, this track fails criteria 3 and 4 for an IspCS because such materials are sensitive to disorder. Dilute magnetic semiconductors offer an interesting solution to criterion 5, but lose their half-metallic property well below RT [106]. Another track is to resistively filter the current so as to spin-polarize it. Fe/MgO-based IspCS accomplish this [107] through tunneling across MgO [108] and can reach $P = 85\%$ [109], but this resistive solution to spinfiltering a) must involve several dielectric monolayers that b) must be of finite lateral extent in order to promote $k_{//}$ conservation. This resistive solution is therefore not as practical toward nanoscale applications (criterion 4) as a conductive one involving merely an interface that can scale down laterally to the individual molecule [110].

In contrast, the Co/Pc interface involves differing spinterface formation mechanism in each spin channel to yield a high P (criterion 1). Since both mechanisms are driven by direct rather than indirect [20] hybridization, the resulting current source is spin-filtered across a conductive [23, 24] interface (criterion 4) and inherits the large temperature resiliency of the Co interface magnetization (criterion 2). Such spinterfaces utilize cheap, abundant materials that can be straightforwardly deposited and will not degrade when processed appropriately into devices [111] even at typically large process tem-

peratures [112](criterion 3). Finally, with its spin-polarized molecular plane, this IspCS candidate elegantly mitigates the conductivity mismatch problem [113] associated with interfaces between metals and semiconductors, which is promising toward satisfying criterion 5. Indeed, the hybridization of wavefunctions from the interfacial molecular plane of high P with those of subsequent molecular layers away from the interface is intrinsically favored. Furthermore, referring to Fig. 5.10, conductivity is substantially lowered when going from Co to the Pc spinterface due to a strongly attenuated spin $\downarrow$ channel. These attributes of the Co/Pc spinterface represent important pre-requisites toward a future room temperature demonstration of sizeable spin transport in the diffusive regime.

Appendix A

Appendix

In this appendix I will show as further illustration of the generality of the breakdown-phenomenon additional measurements of the electron-spin motion as a function of molecule film thickness which are not presented in the main manuscript.

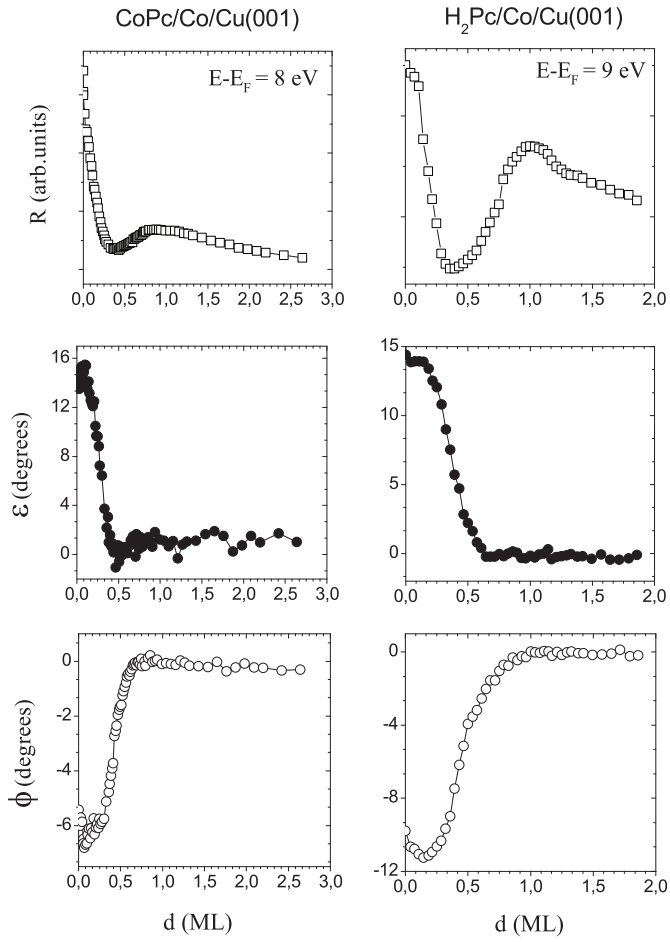

Figure A.1: Spin-averaged electron reflectivity R (top), precession angle ε (middle), and rotation angle ϕ (bottom) are shown as a function of CoPc (left column) and H_2Pc (right column) thickness on Co(001). The primary energies are 8 and 9 eV, respectively.

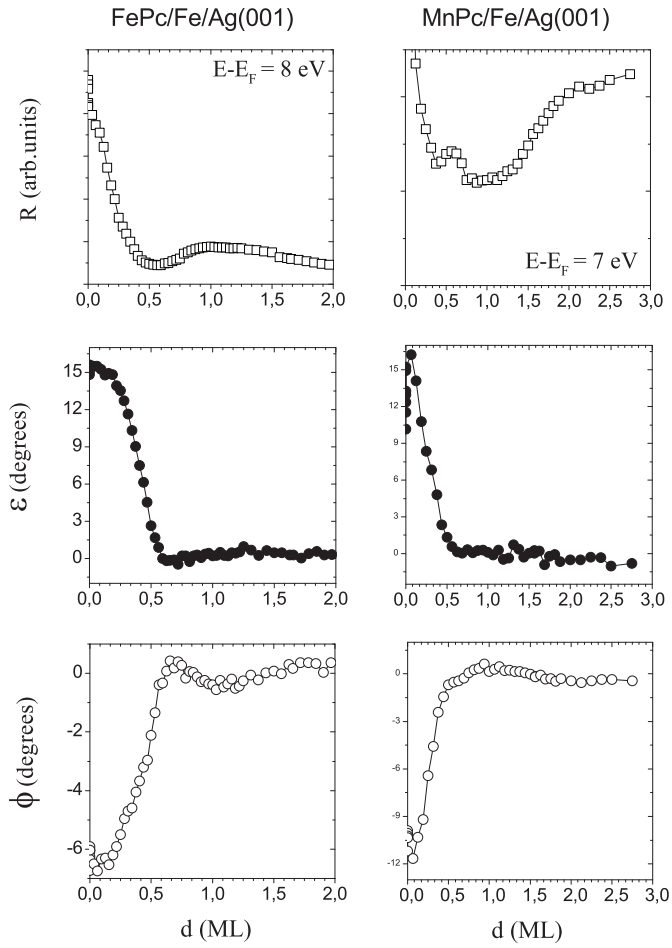

Figure A.2: As in Fig. A.1, but as a function of FePc (left column) and MnPc (right column) thickness on Fe(001). The primary energies are 8 and 7 eV, respectively

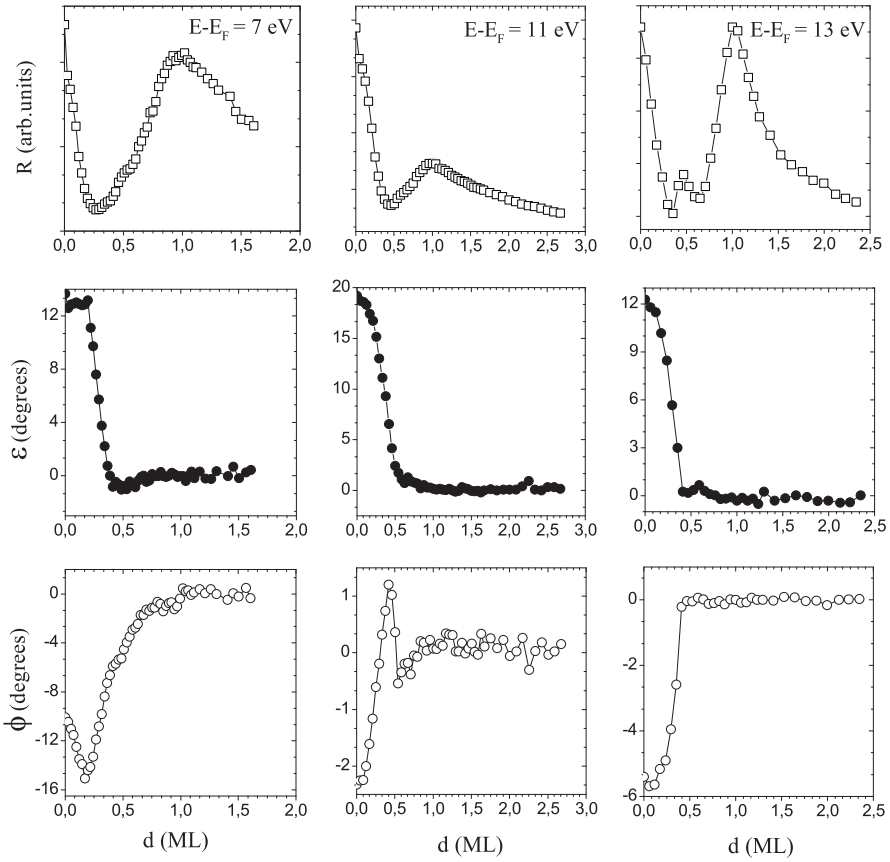

Figure A.3: As in Fig. A.1, but as a function of H_2Pc for different electron energies: 7 eV (left column), 11 eV (middle column) and 13 eV (right column).

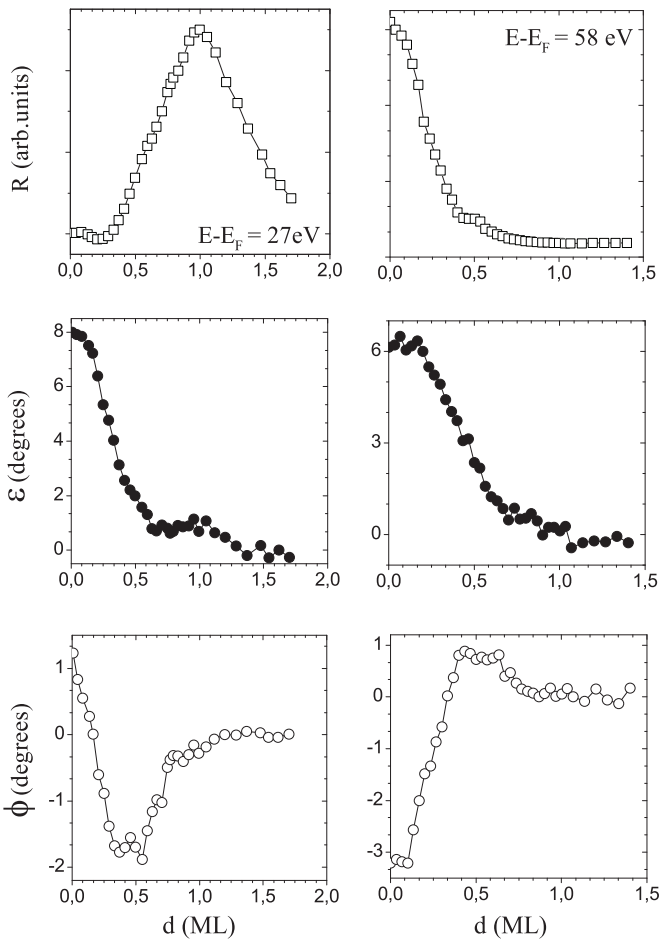

Figure A.4: As in Fig. A.1, but as a function of H_2Pc for different electron energies: 27 eV (left column) and 58 eV (right column).

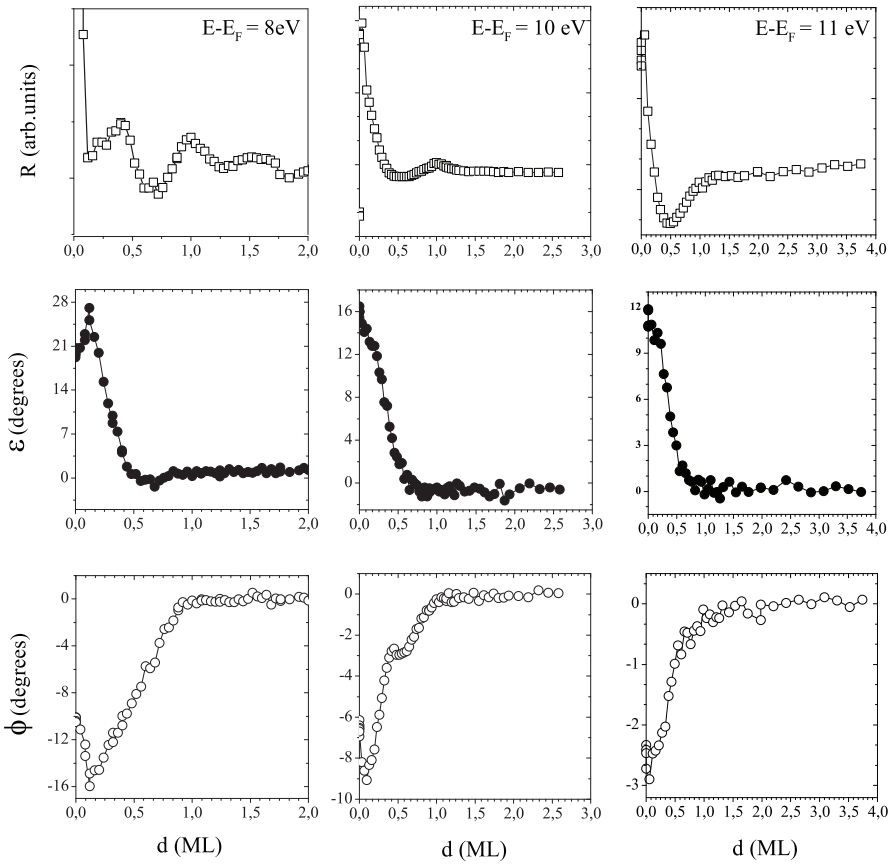

Figure A.5: As in Fig. A.1, but as a function of PTCDA thickness for different electron energies: 8 eV (left column), 10 eV (middle column) and 11 eV (right column).

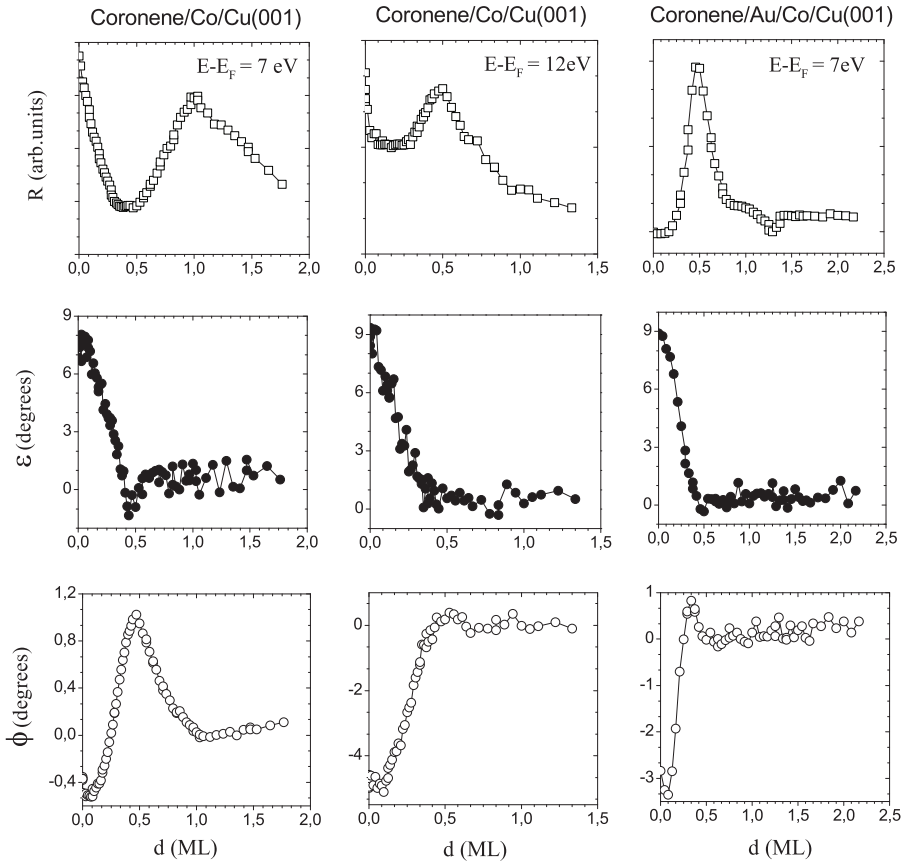

Figure A.6: As in Fig. A.1, but as a function of Coronene thickness for two systems: Coronene/Co/Cu(001) at two energies: 7 eV (left column) and 12 eV (middle column) and Coronene/Au/Co/Cu(001) at 7 eV (right column).

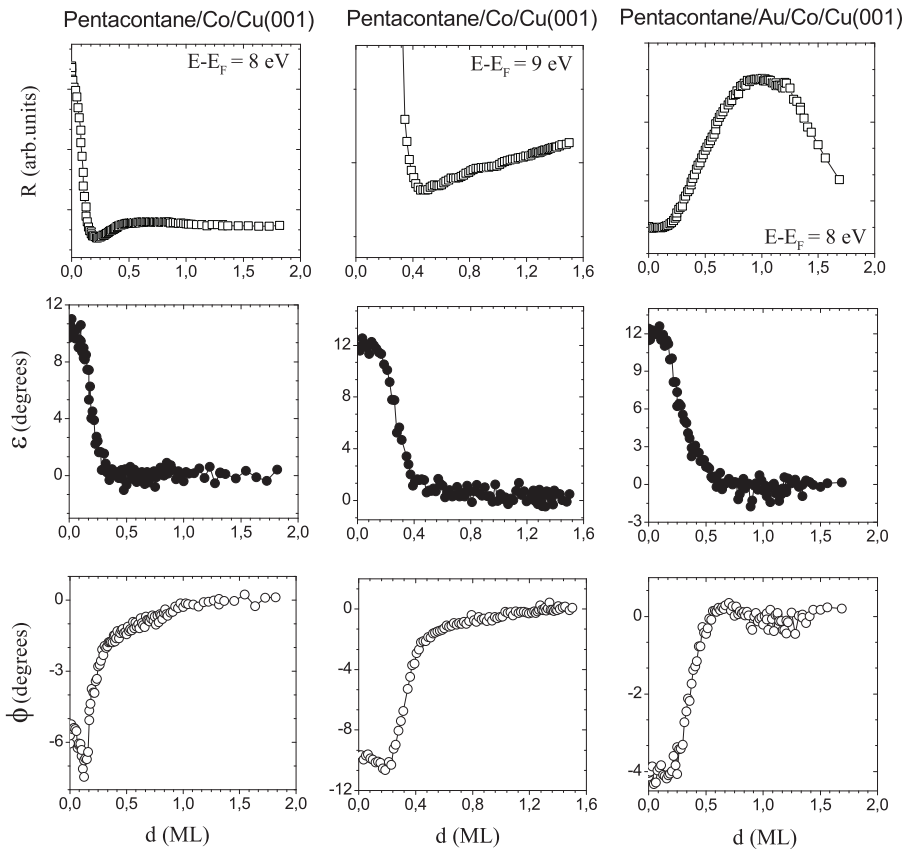

Figure A.7: As in Fig. A.1, but as a function of Pentacontane thickness for two systems: pentacontane/Co/Cu(001) at two energies: 8 eV (left column) and 9 eV (middle column), and pentacontane/Au/Co/Cu(001) at 8 eV (right column).

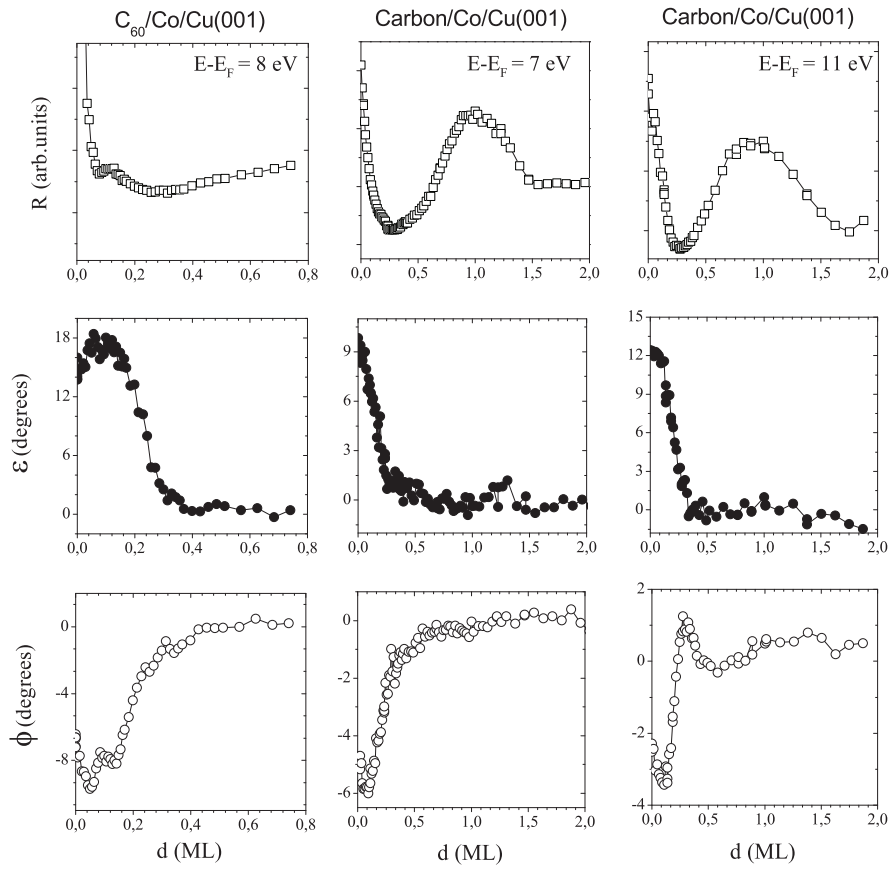

Figure A.8: As in Fig. A.1, but as a function of C_{60} film thickness on Co(001) at 8 eV (left column) and as function of carbon film thickness on Co(001) for two energies: 7 eV (middle column) and 11 eV (right column).

Bibliography

[1] V. A. Dediu, L. E. Hueso, I. Bergenti, C. Taliani. Nat. Mat. **8**, 707 (2009). II, 2

[2] W. Weber, S. Riesen, H. C. Siegmann, Science **291**, 1015 (2001). II

[3] L. Joly, J. K. Ha, M. Alouani, J. Kortus, W. Weber, Phys. Rev. Lett. **96**, 137206 (2006). II

[4] S. Lach, A. Altenhof, K. Tarafder, F. Schmitt, M. E. Ali, M. Vogel, J. Sauther, P. M. Oppeneer, C. Ziegler, Adv. Funct. Mat. **22**, 989 (2012). V

[5] T. Methfessel, S. Steil, N. Baadji, N. Großmann, K. Koffler, S. Sanvito, M. Aeschlimann, M. Cinchetti, H. J. Elmers, Phys. Rev. B **84**, 224403 (2011). V

[6] S. A. Wolf, D. D. Awschalom, R. A. Buhrman, J. M. Daughton, S. Von Molanar, M. L. Roukes, A. Y. Chtchlkanova, D. M. Terger, Science **294**, 1488 (2001). 1

[7] A. Fert, Angew. Chem. Int. Ed **47**, 5956 (2008). 1

[8] P. Grünberg, R. Schreiber, Y. Pang, M. B. Brodsky, H. Sowers, Phys. Rev. Lett. **57**, 2442 (1986). 1

[9] G. Binasch, P. Grünberg, F. Saurenbach, W. Zinn, Phys. Rev. B. **39**, 4828 (1989). 1

[10] M. N. Baibich, J. M. Broto, A. Fert, A. F. Nguyen Van Dau, F. Petroff, P. Etienne, G. Creuzet, A. Friederich, J. Chazelas, Phys. Rev. Lett. **61**, 2472 (1989). 1

[11] M. Julliere, Phys. Lett. A **54**, 225 (1975). 1

[12] J. S. Moodera , L. R. Kinder, M. Wong, R. Meservey, Phys. Rev. Lett. **74**, 3273 (1995). 1

[13] T. Miyzaki, N. Tezuka , J. Magn. Magn. Mat **139**, L231 (1995). 1

[14] S. Yuasa, T. Nagahama, A. Fukushima, Y. Suzuki, K. Ando, Nat. Mat. **3**, 868 (2004). 2

[15] S. S. P. Parkin, C. Kaiser, A. Panchula, P. M. Rice, B. Hughes, M. Samant, S.-H. Yang, Nat. Mat. **3**, 862 (2004). 2

[16] S. Ikeda, J. Hayakawa, Y. Ashizawa, Y. M. Lee, K. Miura, H. Hasegawa, M. Tsunoda, F. Matsukura, H. Ohno, Appl. Phys. Lett. **93**, 082508 (2008). 2

[17] M. Bowen, J.-L. Maurice, A. Barthélémy, M. Bibes, D. Imhoff, V. Bellini, R. Bertacco, D. Wortmann, P. Seneor, E. Jacquet, A. Vaurès, J. Humbert, J.-P. Contour, C. Colliex, S. Blügel, P. H. Dederichs, J. Phys. Condens. Mat. **19**, 315208 (2007). 2, 77, 79

[18] N. Atodiresei, J. Brede, P. Lazic, V. Caciuc, G. Hoffmann, R. Wiesendanger, S. Blügel, Phys. Rev. Lett. **105**, 066601 (2010). 2

[19] C. Iacovita, M. V. Rastei, B. W. Heinrich, T. Brumme, J. Kortus, L. Limot, J. P. Bucher, Phys. Rev. Lett. **101**, 116602 (2008). 2

[20] H. Wende, M. Bernien, J. Luo, C. Sorg, N. Ponpandian, J. Kurde, J. Miguel, M. Piantek, X. Xu, Ph. Eckhold, W. Kuch, K. Baberschke, P. M. Panchmatia, B. Sanyal, P. M. Oppeneer, O. Eriksson, Nat. Mat. **6**, 516 (2007). 2, 79

[21] S. Sanvito, Chem. Soc. Rev. **40**, 3336 (2011). 2

[22] T. Miyamachi, M. Gruber, V. Davesne, M. Bowen, S. Boukari, L. Joly, F. Scheurer, G. Rogez, T. K. Yamada, P. Ohresser, E. Beaurepaire, W. Wulfhekel, Nat. Comm. **3**, 938 (2012) 2

[23] A. F. Takacs, F. Witt, S. Schmaus, T. Balashov, M. Bowen, E. Beaurepaire, W. Wulfhekel, Phys. Rev. B. **78**, 233404 (2008). 2, 79

[24] S. Javaid, M. Bowen, S. Boukari, L. Joly, J.-B. Beaufrand, X. Chen, Y. J. Dappe, F. Scheurer, J.-P. Kappler, J. Arabski, W. Wulfhekel, M. Alouani, E. Beaurepaire, Phys. Rev. Lett. **105**, 077201 (2010). 2, 75, 79

[25] S. Sanvito, Nat. Phys. **6**, 562 (2010). 2, 77, 79

[26] C. Barraud, P. Seneor, R. Mattana, S. Fusil, K. Bouzehouane, C. Deranlot, P. Graziosi, L. Hueso, I. Bergenti, V. Dediu, F. Petroff, A. Fert, Nat. Phys. **6**, 615 (2010). 2, 77, 79

[27] W. Gerlach, O. Stern, Zeitschrift für Physik **9**, 353(1922). 5

[28] J. Stöhr, H. C. Siegmann, *Magnetism from fundamentals to nanoscale dynamics*, Springer (2006). 5, 13

[29] S. Goudsmit, G. E. Uhlenbeck, Physica **6**, 273 (1926). 5

[30] C. Cohen-Tannoudji, B. Diu, F. Laloe, *Mécaninque quantique*, Tome I and II, Paris: Herman (1996). 6

[31] J. P. Kessler, *Polarized electrons*, Springer Series on Atoms and Plasmas, Second edition, Berlin (1985). XV, 7, 19

[32] M. Cardona, L. Ley, *Photoemission in Solids I*, Topics in Applied Physics vol. 26, Berlin: Springer (1978). 11

[33] S. Hüfner, *Photoelectron Spectroscopy, Principles and Applications*, 3rd edition, Berlin: Springer (2003). 11

[34] C. N. Berglund, W. E. Spicer, Phys. Rev. **136**, A1030 (1964). 11

[35] P. D. Johnson, Rep. Prog. Phys. **60**, 1217 (1997). 13

[36] E. Beaurepaire, H. Bulou, F. Scheurer, J.-P. Kappler, *Magnetism: A synchrotron radiation approach*, Springer (2006). 13

[37] A. Damascelli, Z. Hussain, Z.-X. Shen, Rev. Mod. Phys. **75**, 473 (2003). 14

[38] F. Reinert, S. Hüfner, New. J. Phys. **7**, 97 (2005). 14

[39] L. Joly, *Étude de mouvement du spin d'électrons dans des systèmes ferromagnétique mesuré en géométrie de réflexion par spectroscopie électronique résolue en spin*, Thèse de doctorat, Université Louis Pasteur, Strasbourg (2006). 16

[40] L. Tati Bismaths, *Étude de movement du spin d'électrons dans les puits quantique dépendant du spin*, Thèse de doctorat, Université Louis Pasteur, Strasbourg (2008). 16, 22

[41] D. T. Pierce, F. Meier, Phys. Rev. B. **13**, 5484 (1976). XV, 16, 18

[42] D. T. Pierce, R. J. Gelotta, G. C. Wang, W. N. Unterl, A. Galejs, C. E. Kuyatt, S. R. Mielczarek, Rev. Sci. Instrum. **51**, 478 (1980). 16, 17

[43] R. Cun-Jun, Chin. Phys **12**, 483 (2003). 17

[44] A. Clarke, G. Jennings, R. F. Willis, P. J. Rous, J. B. Pendry, Surf. Sci. **187**, 327 (1987). 24

[45] P. Krams, F. Lauks, R. L. Stamps, B. Hillebrands, G. Güntherodt, Phys. Rev. Lett. **69**, 3674 (1992). 24

[46] O. Hackmann, H. Magnan, P. Le Fevre, D. Chandesris, J. J. Rehr, Surf. Sci. **312**, 62 (1994). 24

[47] U. Ramsperger, A. Vaterlaus, P. Pfäffli, U. Maier, D. Pescia, Phys. Rev. B. **53**, 8001 (1996). 24

[48] G. C. Smith, H. A. Padmore, C. Norris, Surf. Sci. **119**, L287 (1982). 24

[49] B. Heinrich, S. T. Purcell, J. R. Dutcher, K. B. Urquhart, J. F. Cochran, A. S. Arrott, Phys. Rev. B. **38**, 12879 (1988). 24

[50] P. Schurer, Z. Celinski, B. Heinrich, Phys. Rev. B. **51**, 2506 (1995) 24

[51] H. Li, Y. S. Li, J. Quinn, D. Tian, J. Sokolov, F. Jona, P. M. Marcus, Phys. Rev. B. **42**, 9195 (1990). 24

[52] S. Rossi, F. Cicacci, Surf. Sci. **307-309**, 406 (1993). 24

[53] K. He, L. J. Zhang, X.C. Ma, J. F. Jia, Q. K. Xue, Z. Q. Qiu, Phys. Rev. B. **72**, 155432 (2005). 24

[54] M. Stampanoni, A. Vaterlaus, M. Aeschlimann, F. Meier, Phys. Rev. Lett. **59**, 2483 (1987). 24

[55] L. Joly, L. Tati-Bismaths, F. Scheurer, W. Weber, Phys. Rev. B. **76**, 104415 (2007). 25, 27, 41, 48, 56, 57, 59

[56] J. C. Buchholz, G. A. Somorjai, J. Chem. Phys. **66**, 573 (1977). 26, 47

[57] L. Joly, L. Tati-Bismaths, W. Weber, Phys. Rev. Lett. **97**, 187404 (2006). 27, 48

[58] S. Tanuma, C. J. Powell, D. R. Penn, Surf. Interface Anal. **21**, 165 (1994). 27

[59] P. E. Laibinis, C. D. Bain, G. M. Whitesides, J. Phys. Chem. **95**, 7017 (1991). 27

[60] S. Modesti, S. Cerasari, P. Rudolf, Phys. Rev. Lett. **71**, 2469 (1993). 28

[61] M. R. C. Hunt, S. Modesti, P. Rudolf, R. E. Palmer, Phys. Rev. B. **51**, 10039 (1995). 28

[62] A. Sellidji, B. E. Koel, J. Phys. Chem. **97**, 10076 (1993). 28

[63] C. Cepek, A. Goldoni, S. Modesti, Phys. Rev. B. **53**, 7466 (1996). 28

[64] S. Tanuma, T. Shiratori, T. Kimura, K. Goto, S. Ichimura, C. J. Powell, Surf. Interface Anal. **37**, 833 (2005). 28

[65] F. Djeghloul,F. Ibrahim, M. Cantoni, M. Bowen, L. Joly, S. Boukari, P. Ohresser, F. Bertran, P. Le Fèvre, P. Thakur, F. Scheurer, T. Miyamachi, R. Mattana, P. Seneor, A. Jaafar, C. Rinaldi, S. Javaid, J. Arabski, J.-P. Kappler, W. Wulfhekel, N. B. Brookes, R. Bertacco, A. Taleb-Ibrahimi, M. Alouani, E. Beaurepaire, W. Weber, Sci. Rep. **3**, 1272 (2013). 37, 41

[66] F. Petraki, S. Kennou, Int. J. Nanotechnol. **6**, 112 (2009). 39

[67] F. Petraki, V. Papaefthimiou, S. Kennou, Organic Electronics **8**, 522 (2007). 39

[68] B. J. Topham, M. Kumarn, Z. G. Soos, Adv. Func. Mat. **21**, 1931 (2011). 39

[69] F. Wilhelm, M. Angelakeris, N. Jaouen, P. Poulopoulos, E.T. Papaioannou, C. Mueller, P. Fumagalli, A. Rogalev, N.K. Flevaris, Phys. Rev. B **69**, 220404 (R) (2004). 42

[70] Z. H. Cheng, L. Gao, Z. T. Deng, N. Jiang, Q. Liu, D. X. Shi, S. X. Du, H. M. Guo, H.-J. Gao, J. Phys. Chem. C **111**, 9240 (2007) 46, 47

[71] S. M. Barlow, R. Raval, Surf. Sci. Rep. **50**, 201 (2003). 47

[72] Y. Hosoi, Y. Sakurai, M. Yamamoto, H. Ishii, Y. Ouchi, K. Seki, Surf. Sci. **515**, 157 (2002). 47

[73] O. Marchenko, J. Cousty, Phys. Rev. Lett. **84**, 5363 (2000). 46, 47

[74] M. Lackinger, S. Griessl, W. M. Heckl, M. Hietschold, J. Phys. Chem. B **106**, 4482 (2002). 46, 47

[75] M. Abel, A. Dmitriev, R. Fasel, N. Lin, J. V. Barth, K. Kern, Phys. Rev. B. **67**, 245407 (2003). 47

[76] J. A. Gardener, G. A. D. Briggs, M. R. Castell, Phys. Rev. B. **80**, 235434 (2009). 46, 47

[77] M. Mura, X. Sun, F. Silly, H. T. Jonkman, G. A. D. Briggs, M. R. Castell, L. N. Kantorovich, Phys. Rev. B **81**, 195412 (2010). 46

[78] W. Weber, D. Kerkmann, D. Pescia, D. A. Wesner, G. Güntherodt, Phys. Rev. Lett. **65**, 2058 (1990). 48

[79] T. G. Walker, H. Hopster, Phys. Rev. B. **48**, 3563 (1993). 48

[80] T. G. Walker, A. W. Pang, H. Hopster, S. F. Alvarado, Phys. Rev. Lett. **69**, 1121 (1992). 48

[81] T. G. Walker, H. Hopster, Phys. Rev. B. **49**, 7687 (1994). 48

[82] unpublished 48

[83] A. Scholl, L. Baumgarten, W. Eberhardt, Phys. Rev. B. **56**, 747 (1997). 48

[84] D. Oberli, R. Burgermeister, S. Riesen, W. Weber, H. C. Siegmann, Phys. Rev. Lett. **81**, 4228 (1998). 50

[85] M. S. Hammond, G. Fahsold, J. Kirschner, Phys. Rev. B. **45**, 6131 (1992). 54

[86] M. Aeschlimann, M. Bauer, S. Pawlik, W. Weber, R. Burgermeister, D. Oberli, H. C. Siegmann, Phys. Rev. Lett. **79**, 5158 (1997). 55

[87] O. K. Andersen, Phys. Rev. Lett. **8**, 149 (1964). 59

[88] http://www.fkf.mpg.de/andersen/LMTODOC /LMTODOC.html. 59

[89] J. Korringa, Physica **13**, 392 (1947). 59

[90] W. Kohn, N. Rostoker, Phys. Rev. **94**, 1111 (1954). 59

[91] T. Berdot, A. Hallal, L. Tati Bismaths, L. Joly, P. Dey, J. Henk, M. Alouani, W. Weber, Phys. Rev. B **82**, 172407 (2010). 59

[92] A. Hallal, T. Berdot, P. Dey, L. Tati Bismaths, L. Joly, A. Bourzami, F. Scheurer, H. Bulou, J. Henk, M. Alouani, W. Weber, Phys. Rev. Lett. **107**, 087203 (2011). 59

[93] K. Miyamoto, K. Iori, K. Sakamoto, H. Narita, A. Kimura, M. Taniguchi, S. Qiao, K. Hasegawa, K. Shimada, H. Namatame, S. Blügel, New. J. Phys. **10**, 125032 (2008). 64

[94] M. Cantoni, R. Bertacco, Rev. Sci. Instrum. **75**, 2387 (2004). 65

[95] J. J. Yeh, I. Lindau, At. Data.and Nucl. Data Tables **32**, 1 (1985). 73

[96] G. Kresse, J. Furthmuller. Phys. Rev. B. **54**, 11169 (1996). 74

[97] J. P. Perdew, K. Burke, M. Ernzerhof, Phys. Rev. Lett. **77**, 3865 (1996). 75

[98] G. Kresse, D. Joubert, Phys. Rev. B. **59**, 1758 (1999). 75

[99] S. Grimme, J. Comput. Chem. **27**, 1787 (2006). 75

[100] T. Bucko, J. Hafner, S. Lebègue, J. G. Ángyán, J. Phys. Chem. A **114**, 11814 (2010). 75

[101] S. Javaid, S. Lebègue, B. Detlefs, F. Ibrahim, F. Djeghloul, M. Bowen, S. Boukari, T. Miyamachi, J. Arabski, D. Spor, J. Zegenhagen, W. Wulfhekel, W. Weber, E. Beaurepaire, M. Alouani, Phys. Rev. B. **87**, 155418 (2013). 75

[102] X. Chen, M. Alouani, Phys. Rev. B. **82**, 094443 (2010). 75

[103] M. Bowen, A. Barthélémy, M. Bibes, E. Jacquet, J. P. Contour, A. Fert, D. Wortmann, S. Blügel, J. Phys. Condens. Matter **17**, L407 (2005). 77, 79

[104] J.-H. Park, E. Vescovo, H.-J. Kim, C. Kwon, R. Ramesh, T. Venkatesan, Nature **392**, 794 (1998). 79

[105] N. Tezuka, N. Ikeda, F. Mitsuhashi, S. Sugimoto, Appl. Phys. Lett. **94**, 162504 (2009). 79

[106] T. Dietl, Nat. Mat. **9**, 965 (2010). 79

[107] M. Bowen, V. Cros, F. Petroff, A. Fert, C. M. Boubeta, J. L. Costa-Krämer, J. V. Anguita, A. Cebollada, F. Briones, J. M. de Teresa, L. Morellón, M. R. Ibarra, F. Güell, F. Peiró , A. Cornet, Appl. Phys. Lett. **79**, 1655 (2001). 79

[108] W. H. Butler, X.-G. Zhang, T. C. Schulthess, J. M. MacLaren, Phys. Rev. B. **63**, 054416 (2001). 79

[109] Y. M. Lee, J. Hayakawa, S. Ikeda, F. Matsukura, H. Ohno, Appl. Phys. Lett. **90**, 212507 (2007). 79

[110] S. Schmaus, A. Bagrets, Y. Nahas, T. K. Yamada, A. Bork, M. Bowen, E. Beaurepaire, F. Evers, W. Wulfhekel, Nat. Nanotech. **6**, 185 (2011). 77, 79

[111] G. Szulczewski, H. Tokuc, K. Oguz, J. M. D. Coey, Appl. Phys. Lett. **95**, 202506 (2009). 79

[112] H. Peisert, T. Schwieger, J. M. Auerhammer, M. Knupfer, M. S. Golden, J. Fink, P. R. Bressler, M. Mast, J. Appl. Phys. **90**, 466 (2001). 80

[113] G. Schmidt, D. Ferrand, L. W. Molenkamp, Phys. Rev. B. **62**, R4790 (2000). 80

Fatima Zohra Djeghloul

Study of organic semiconductor/ferromagnet interfaces by spin-polarized electron scattering and photoemission.

Résumé

J'ai étudié les interfaces semi-conducteur organiques/ferromagnétique par la diffusion des électrons et la photoémission résolue en spin. Dans la première partie, un comportement inattendu de la réflexion d'électrons dépendante de spin à ces interfaces est observé. En fait, une couverture sous-monocouche des molécules organiques rend l'amplitude de réflexion d'électrons indépendante de spin, c.à.d. que la réflectivité ainsi que la phase de réflexion devient indépendante de l'orientation du spin des électrons incidents. Bien que je ne sois pas en mesure d'identifier la cause de ce phénomène, je montre qu'il s'agit d'un phénomène très général qui est indépendante de l'énergie des électrons primaires, du choix du substrat ferromagnétique, du choix de la molécule organique, et de l'orientation de la polarisation initiale. Il n'est pas du à un changement de l'aimantation de surface, à une dépolarisation des électrons primaires, ou à une interaction directe des molécules avec le substrat ferromagnétique. En outre, la théorie ne prédit pas les résultats expérimentaux et d'autres recherches sont donc nécessaires pour dévoiler la physique derrière ces observations. Dans la seconde partie de ma thèse, les expériences de photoémission résolue en spin sont réalisées au synchrotron SOLEIL. Le résultat principal est l'observation d'un état électronique induite par les molécules organiques près du niveau de Fermi qui est hautement polarisé en spin. Des mesures en fonction de l'épaisseur de la couche organique permettent d'identifier le caractère interfacial de cet état électronique. Enfin, ces résultats sont comparés avec des calculs théoriques effectués à l'institut.

Résumé en anglais

I studied organic semiconductor/ferromagnet interfaces by characterizing them by spin-polarized electron scattering and photoemission spectroscopy experiments. In the first part, a completely unexpected behaviour of the spin-dependent electron reflection properties of these interfaces is observed. In fact, sub-monolayer coverage of the organic molecules makes the electron reflection amplitude independent of the spin, i.e. both the reflectivity and the reflection phase become independent of the spin orientation of the incident electrons. Although I am not able at the moment to identify the cause of this phenomenon, I show that it is a very general phenomenon which is independent of the energy of the primary electrons, the choice of the ferromagnetic substrate, the choice of the organic molecule, and of the orientation of the initial spin polarization. It is not due to a change of the surface magnetization, a depolarization of the primary electrons, or a direct interaction of the molecules with the ferromagnetic substrate. Moreover, theory does not predict so far the experimental results and further research is required to unveil the physics behind these observations. In the second part of my thesis, spin-resolved photoemission experiments have been performed at the synchrotron SOLEIL. The main result is the observation of a highly spin-polarized molecule-induced electronic state close to the Fermi level. Measurements as a function of the organic layer thickness allow us to determine the interfacial character of this electronic state. Finally, these results are compared with theoretical calculations performed at the institute.

PROPOSITION DE MOTS-CLÉS:

Electron spin-motion; metal-organic interfaces; spin-resolved photoemission; Spintronics